Host-Targeted Therapies to Treat *Staphylococcus aureus* Skin Infections

By

Nathan Klopfenstein

Dissertation

Submitted to the Faculty of the

Graduate School of Vanderbilt University

in partial fulfillment of the requirements

For the degree of

DOCTOR OF PHILOSOPHY

In

Molecular Pathology and Immunology

September 30, 2021

Nashville, Tennessee

Approved:

Jim Cassat, M.D., Ph.D.

C. Henrique Serezani, Ph.D.

Heather Pua, M.D., Ph.D.

Daniel Moore, M.D., Ph.D.

Maureen Gannon, Ph.D.

Acknowledgements

There are a great many people I need to thank and acknowledge for their help during my graduate school journey. I would first and foremost like to thank my mentor Dr. Henrique Serezani for his guidance and support during this journey, and for always being excited at any new data I had to show him. I also want to extend thanks to my committee Dr. Jim Cassat, Dr. Heather Pua, Dr. Dan Moore, and Dr. Maureen Gannon for their constructive feedback and advice that helped me to grow as a scientist.

This work would not have been possible without the help of my fellow members in the Serezani lab to whom I must also thank for all their help over the years. I would like to especially thank Stephanie Brandt for helping me when I first joined the lab and teaching me everything I know about skin infections. I want to thank Amondrea Blackman for all her help over the years and for being a great person to work with. I would like to thank Julia Bazzano for her great advice in troubleshooting any number of issues and for being a great co-worker. I also need to thank my summer student Sydney Castellanos for being an outstanding scientist and mentee who helped me become a better mentor.

I would also like to thank and acknowledge all of our collaborators here at Vanderbilt University Medical Center. Thanks to Dr. David Aronoff and his lab for being a great group of fellow scientists to provide helpful discussion. In particular I want to thank Lisa Rogers for her advice and lending me various reagents over the years when I realized last minute I was missing something. Special thanks to Dr. Jeff Rathmell and Dr. Amy Major and the entire Immunological

Mechanisms of Disease T32 training group for funding my research and being a great place to share research progress.

Personally, I would like to thank my great group of friends I made here at Vanderbilt for all the tailgates, concerts, celebrations, and overall great times we had outside of lab that made the work in lab enjoyable. Further thanks to my parents Jim and Rhonda and my sister Ashley for their support throughout my time at Vanderbilt, even though they may not fully understand what I do. Finally, my most profound thanks to my girlfriend Angela whose love and support has been critical throughout my time in graduate school. Thank you for your support when I was down on myself and reminding me why it was all worth it. Also, thanks to Callie for providing me with ample distractions while writing this thesis.

TABLE OF CONTENTS

LIST OF TABLES

LIST OF FIGURES

LIST OF ABBREVIATIONS

AA	Arachidonic acid
BMDM	Bone marrow derived macrophage
BLI	Bioluminescence Imaging
BSA	Bovine serum albumin
cAMP	cyclic AMP
cDNA	complementary DNA
CFU	Colony forming unit
COX	Cyclooxygenase
CT	Control/nondiabetic
DAMP	Danger associated molecular pattern
DAPI	4’,6-diamidino-2-phenylindole
DMEM	Dulbecco’s modified Eagle medium
EDTA	Ethylenediaminetetraacetic acid
EGFP	Enhanced green fluorescent protein
EP	E prostanoid receptor
FACS	Fluorescence-activated cell sorting
FBS	Fetal bovine serum
FITC	Fluorescein isothiocyanate
GFP	Green fluorescent protein
H&E	Hematoxylin and eosin
HFD	High-fat diet
IFN	Interferon
IHC	Immunohistochemistry
iNOS	Inducible Nitric Oxide Synthase
i.p.	Intraperitoneal
ISH	In situ hybridization
IL1B(IL-1β)	Interleukin -1 beta
KIR	Kinase inhibitory region

LFD	Low fat diet
Miso	Misoprostol
MRSA	Methicillin-resistant *Staphylococcus aureus*
MyD88	Myeloid differentiation primary response gene 88
NFκB	Nuclear factor kappa b
NLRP3	NACHT, LRR and PYD domains-containing protein 3
NO	Nitric oxide
PAMP	Pathogen associated molecular pattern
PBS	Phosphate buffered saline
PG	Prostanoid
PGE_2	Prostaglandin E2
PLA_2	Phospholipase A2
PTGES	Prostaglandin E synthase
PTGER	Prostaglandin E receptor
PRR	Pattern recognition receptor
qRT-PCR	Quantitative real-time polymerase chain reaction
RNA	Ribonucleic Acid
RNS	Reactive nitrogen species
ROS	Reactive oxygen species
s.c.	Subcutaneous
SOCS-1	Suppressor of cytokine signaling 1
STAT-1	Signal transducer and activator of transcription 1
STZ	Streptozotocin
TLR	Toll-like receptor
TSA	Tryptic Soy Agar
TSB	Tryptic Soy Broth
WT	Wildtype

CHAPTER 1

INTRODUCTION

Inflammation

Inflammation describes a complex process orchestrated by resident immune and nonimmune cells during tissue injury or infection. Upon recognition of inflammatory stimuli, resident immune cells such as macrophages and dendritic cells begin releasing a multitude of mediators to trigger inflammation, including: lipids, chemokines, cytokines, and clotting factors [1,2].

Release of these mediators results in tissue-resident immune and endothelial cell activation that leads to the cardinal signs of inflammation: pain, heat, swelling, redness, and loss of function [1]. Activated immune and endothelial cells produce cytokines (TNF-α, IL-6, and IL-1α) as well as other mediators (prostaglandins and platelet-activating factor) that induce vasodilation and increased permeability of the blood vessels, causing pain, heat, and redness of the infected tissue [1,3]. Vasodilation and vascular permeability result in increased blood flow and fluid accumulation as other immune cells are recruited to the inflamed tissue, resulting in tissue swelling [3]. Chemokines such as CXCL1, CXCL2, and CCL2 released during inflammation also promote the recruitment of specific immune cell populations such as neutrophils and monocytes to the site of infection/injury [3]. Depending on the severity and length of inflammation, loss of function of the inflamed tissue/appendage can occur. However, once the infection is cleared, inflammation is resolved through pro-resolution signaling programs, and tissue homeostasis is restored [4].

A balanced inflammatory response is necessary to promote a proper immune response to eliminate pathogens while returning to tissue homeostasis once the pathogen is cleared [5]. Dysregulation of the inflammatory response, either overactive or insufficient, can result in chronic inflammation or immunosuppression, respectively, which can lead to co-morbidities. Chronic inflammation is associated with poor wound healing (e.g. diabetic foot ulcers), autoimmune disease (e.g. diabetes mellitus), and hypersensitivity, while insufficient inflammation can significantly increase the risk of infection for patients [4,5]. Therefore, there is a need to better understand the mechanisms involved in balancing and controlling the inflammatory mediators that drive the process of inflammation so we can develop therapeutic strategies to treat its dysregulation and maintain tissue homeostasis while properly responding to and eliminating invading pathogens.

Chemotaxis

Recruitment of immune cells to the site of infection is a major process during inflammation [6]. Vasodilation and vascular permeability, combined with the release of chemokines such as CXCL1, CXCL2, and CCL2, promote the recruitment of neutrophils and monocytes to the site of infection or injury [3,6–8]. Vasodilation is promoted through the actions of cytokines such as TNFα while vascular permeability is driven through early production of lipid mediators such as prostaglandin E2 (PGE_2) during inflammation [1,9]. Initially, PGE_2 was thought to only act in its role as a vasodilator during inflammation, however, more recent work has demonstrated its ability to promote the release of both pro- and anti-

inflammatory cytokines/chemokines at multiple stages of inflammation, suggesting it may play multiple roles in coordinating cell recruitment during inflammation.

The migration of a cell towards a molecular signal is termed chemotaxis. Neutrophils are one of the first cells to migrate to the inflamed area, followed by monocytes, with neutrophils making up an estimated 50% of cells at the site of inflammation 48 hours post-injury/infection [7,8,10]. Neutrophil recruitment out of the bloodstream has been well studied and involves a series of specific events: rolling, adhesion, and transendothelial migration [6,11]. The first stage of migration, neutrophil rolling, involves the interaction of cell surface molecules, termed selectins, on the surface of neutrophils (P-selectin glycoprotein-1 (PSGL-1)) and endothelial cells (P-selectin) [6,7,11]. The weak interaction between these molecules results in neutrophils rolling along the interior of the vascular endothelium. Chemokine receptor signaling near the site of infection increases neutrophil adhesion to the endothelium through the upregulation of integrins, including intracellular adhesion molecule 1 (ICAM-1) [3,6]. The binding of ICAM-1 on endothelial cells to LFA-1 on neutrophils results in the firm adhesion of neutrophils to the endothelium [3,6]. Neutrophil transendothelial migration then occurs as neutrophils follow chemoattractant gradients to migrate through the tight junctions between endothelial cells toward the site of infection or injury [3,6,10].

Once out of the bloodstream, recruited immune cells must continue to follow a gradient of chemoattractants to reach the specific site of inflammation. These signals include chemokines, cytokines, and lipid mediators released by resident immune cells, but can also include bacterial peptides released during infection [3,6,8,12]. There are two major classes of chemokines, the CC (e.g., CCL2 – MCP-1, CCL3 – MIP-1α, and CCL5 – RANTES) and the CXC (e.g.,

CXCL1 – KC and CXCL2 – MIP-2α) families, named for the configuration of cysteine residues at the amino terminus [13]. These chemokines bind to specific cognate receptors, CCR (e.g. CCR2 and CCR7) for CC chemokines and CXCR (e.g., CXCR1 and CXCR2) for the CXC chemokines [13]. Levels of specific chemokine secretion, combined with levels of receptor expression, create a chemoattractant hierarchy, wherein cells prioritize responses to specific signaling molecules over others as they get closer to the site of injury or infection [3,12,14]. Complement factor C5a and bacterial products such as *N*-formylmethionine-leucyl-phenylalanine (fMLP) represent end-target chemotactic molecules that activate phagocytes as they approach the site of infection and are prioritized over intermediate signals, such as CXC chemokines and lipid mediators [13,14]. This hierarchy allows a more coordinated response from recruited cells as they approach the site of infection and initiate antimicrobial effector functions [3,6,14]. However, how the initial secretion of chemotactic signals may impact the secretion of end-stage molecules and receptor expression as well as dictate the subsequent host immune response remains an active area of study. The regulation of chemokines and their receptors allows for the robust yet coordinated recruitment of immune cells in response to infection or injury and drives the chemotaxis of monocytes and neutrophils during inflammation in multiple organ systems [3,6,8,10,13]. By investigating these chemotactic pathways and their dysregulation in various disease states we can uncover potential therapeutic targets to promote sufficient but not overwhelming chemotaxis during inflammation.

Phagocytes of the innate immune system

Many of the functions of the innate immune response rely on myeloid cell lineage phagocytes; including monocytes, macrophages, neutrophils, and dendritic cells. Macrophages are critical to coordinating the innate immune response due to their resident tissue specificity and their ability to both instigate and resolve the inflammatory response through their spectrum of activation [15–17]. It has been suggested that tissue-resident macrophages often arise during development from the yolk sac or fetal liver and are capable of proliferation to maintain these populations [16]. Tissue residency distinguishes macrophages from monocyte-derived macrophages, which are recruited out of the bloodstream and differentiate at the site of infection/injury. Tissue-resident macrophages serve many different specialized functions depending on the tissue environment and activation signals they receive [15–18].

The “plasticity” of macrophages to change function based on environment and stimuli has long been recognized, with macrophages traditionally being classified as either classically-activated (M1 or “proinflammatory”) or alternatively-activated (M2 or “anti-inflammatory”) [15–17]. However, more recent work in the field has highlighted that not all macrophages can be clearly defined as belonging to one of these two activation states. Rather, macrophages can fall along a spectrum of several different activation/functional states that are less defined. At one end, there are classically activated macrophages that typically function at the site of injury or infection to recognize pathogens; while secreting a number of proinflammatory chemokines and cytokines to promote immune cell recruitment and drive the inflammatory response [11,17–19]. These macrophages are also crucial for the clearance of pathogens through

phagocytosis and the production of reactive oxygen and nitrogen species, along with other antimicrobial peptides [17,19,20].

As pathogens are cleared, however, macrophages begin to move to the other end of the phenotypic spectrum and exhibit a pro-resolution program to resolve inflammation and promote wound healing [17]. These alternatively-activated macrophages first act to clear out apoptotic cells and cell debris through a process termed efferocytosis. During efferocytosis, these macrophages secrete anti-inflammatory and pro-angiogenic mediators such as IL-10 and VEGF to limit inflammation and promote the process of tissue repair, angiogenesis, and revascularization [17,21]. Alternatively-activated macrophages also assist in the final remodeling stage of wound healing by secreting factors to strengthen and rearrange the extracellular matrix within the wound, allowing for granular tissue formation, and eventually scar tissue, at the wound site [21,22]. Chronic non-healing ulcerative wounds, which frequently occur in patients with diabetes, are characterized by a low number of these alternatively-activated macrophages compared to classically activated macrophages within the wound [23]. As these inflammatory macrophages fail to change activation states, they continue to secrete proinflammatory mediators that significantly impair the wound healing process, demonstrating the importance of macrophages and their plasticity [23].

Neutrophils represent one of the first innate immune cells recruited to the site of injury or infection [11], and are one of the most abundant immune cell populations in circulation in both mice (10-25%) and humans (40-60%) [7]. Neutrophils operate during inflammation to remove and eliminate pathogens through several different antimicrobial effector functions. Neutrophils contain granules, or small membrane-bound vesicles, that contain a number of

antimicrobial molecules (e.g., defensins) and enzymes (e.g., myeloperoxidase and lysozyme) that act to eliminate pathogens [24,25]. These granules fuse with the neutrophil cellular membrane to release these contents into the extracellular space, in a process known as neutrophil degranulation, to eliminate extracellular pathogens [24,25]. However, upon phagocytosis, these granules can also fuse with the phagosome to eliminate intracellular pathogens [24,26]. Neutrophils are also capable of producing web-like structures termed "neutrophil extracellular traps", or NETs, in which DNA decorated with histones and other antimicrobial effectors (e.g., neutrophil elastase and LL37) are extruded from the neutrophil to trap and eliminate extracellular pathogens [27]. While neutrophils have long been considered a primarily proinflammatory immune cell that functions mainly in the elimination of pathogen, recent work has demonstrated a role for neutrophils in resolving the inflammatory response at the end stages of infection or injury [13,28,29], suggesting a more prominent role for these cells at multiple stages of inflammation.

Antimicrobial effector functions

Antimicrobial effector functions describe a wide range of processes by which cells remove and kill pathogens. These processes often begin with the chemotaxis of cells to the site of infection followed by the phagocytosis of the pathogen, which leads to the production of antimicrobial peptides, reactive oxygen species (ROS), reactive nitrogen species (RNS), and proinflammatory mediators [19,20,24,26,30]. Cytokines, chemokines, and lipid mediators can

also further enhance or suppress these functions adding another layer of regulation to these processes [3,14].

Phagocytosis is the process by which phagocytes engulf pathogens or other cellular debris into intracellular vesicles termed phagosomes [30]. This process is initiated through the signaling of several receptors on the cell surface. These include C-type lectin receptors which recognize sugars on the cell wall of bacteria and fungi and scavenger receptors MARCO and CD36, which can recognize bacterial lipoproteins to stimulate phagocytosis [30–32]. While some pathogens, such as *Staphylococcus aureus* (*S. aureus*), have evolved strategies to avoid detection by phagocytic receptors, the process of phagocytosis can be enhanced by the presence of opsonins on the surface of the pathogen. These include complement proteins and antibodies that are recognized by complement or Fc receptors (FcR), respectively, which enhance the ingestion of the opsonin-coated pathogen [30]. Phagocytosis can be further promoted through the actions pro-inflammatory cytokines such as the interferons (IFNs), a family of cytokines known as potent macrophage activators [33]. However, other mediators such as IL-10 and PGE_2 have been shown to limit this process [30].

Phagocytosis requires cytoskeletal rearrangements within the cell to surround the pathogen in the phagocytic cup before internalizing the cell membrane to engulf the pathogen. This process is actin-dependent and mediated by F-actin polymerization [30,32]. Once internalized, phagosomes fuse with lysosomes containing several antimicrobial molecules that acidify the phagosome, creating a phagolysosome. Upon acidification of the phagolysosome, lysosomal enzymes are activated to eliminate pathogens and cellular debris [26]. Pathogens within the phagolysosome are also exposed to ROS and RNS. The primary source of phagocyte

ROS comes from NADPH oxidase activity [20]. This oxidase requires the assembly of multiple subunits on the membrane of the phagolysosome and, upon activation, generates superoxide (O_2-), which is thought to eliminate engulfed pathogens through an unknown mechanism. Superoxide can also form hydrogen peroxide (H_2O_2) or hypochlorous acid (HOCl) through a series of reactions to eliminate pathogens [20]. Patients with defects in the NADPH oxidase have a significantly increased susceptibility to infections, particularly to *S. aureus*, due to their inability to eliminate pathogens via ROS generation [34]. This inability to generate proper ROS for pathogen killing can result in pathogen escape from the phagolysosome and allow for intracellular pathogen replication and prolonged infection [19]. Certain pathogens also actively suppress ROS generation to promote their survival and replication within the phagosome. *Salmonella enterica* has been shown to limit ROS generation by promoting PGE_2 production, which limits NADPH oxidase assembly via protein kinase A, increasing pathogen survival and replication [35].

Reactive nitrogen species are also produced in response to infection, with nitric oxide (NO) being the predominant species produced via nitric oxide synthase 2 (NOS2 or iNOS) activation [36]. NO drives immune cell activation and proinflammatory cytokine production outside of its role in pathogen elimination [36]. However, overproduction of NO can be immunosuppressive and limit immune cell effector functions [36]. In a model of *Leishmania spp.* infection, PGE_2 increased NO release and improved parasitic elimination, demonstrating its complex role in potentially enhancing and limiting immune cell effector function [37].

Antimicrobial peptides represent another mechanism of pathogen killing that targets bacterial membranes, DNA and protein synthesis, protein folding, and cell wall synthesis [38].

The amphipathic peptides in particular are critical for skin host defense and include cathelicidins, LL37, and defensins that form pores in bacterial membranes resulting in the leakage of intracellular contents [39]. Neutrophils release these peptides from within intracellular granules through the process of degranulation [24]. During skin infection, as well as at homeostasis, a number of these amphipathic peptides are actively secreted by keratinocytes to control resident skin commensal organisms and potentially infective species [38,40]. Secretion of these peptides, which can act as chemoattractants for phagocytes, can also activate immune cells to enhance phagocytosis and ROS/RNS generation, demonstrating the connection of these antimicrobial programs with one another [38]. Understanding how these molecules impact expression of not only each other but other components in the inflammatory cascade to promote a robust yet non-damaging host immune response will greatly benefit the development of immunotherapeutic strategies to treat infections and diseases resulting from their dysregulation.

PGE_2 synthesis

Eicosanoids are a large family of bioactive lipids that are oxidized derivatives of 20-carbon polyunsaturated fatty acids [41]. Released from cell membrane phospholipids via phospholipase A2 (PLA_2), these polyunsaturated fatty acids are metabolized by either cyclooxygenase (COX), lipoxygenase (LOX), or cytochrome P450 oxidase enzymes [41]. Due to their lipid nature, eicosanoids are not stored within cells. After rapid production, they act locally in response to various stimuli, such as those released during inflammation [42]. The rapid

synthesis and signaling after activation makes these lipids important mediators of instigating the inflammatory response to stimuli [42–44]. However, how these lipids or their dysregulation during metabolic disease impacts inflammation versus cellular immunity and anti-microbial effector functions remains an active area of study.

Prostaglandins (PGs) are part of a subclass of the larger eicosanoid family termed prostanoids that are produced by the cyclooxygenase (COX) pathway [41]. The synthesis of prostaglandins is dependent on several rate-limiting steps, including the activation of phospholipase A2 (PLA_2), which is responsible for the release of arachidonic acid (AA) from phospholipids in the cellular membrane [41,45]. Once released, AA acts as a substrate in the COX pathway that leads to PG synthesis. The first two steps of the pathway are sequential reactions that are both catalyzed by the PG endoperoxidase H synthase (COX) [43,45]. The first reaction in the pathway is a cyclooxygenase reaction that produces PGG_2, followed by a peroxidation reaction that produces PGH_2 [43,45]. These reactions are carried out by one of the two isoforms of COX, COX-1 or -2 (**Fig. 1**) [43,45].

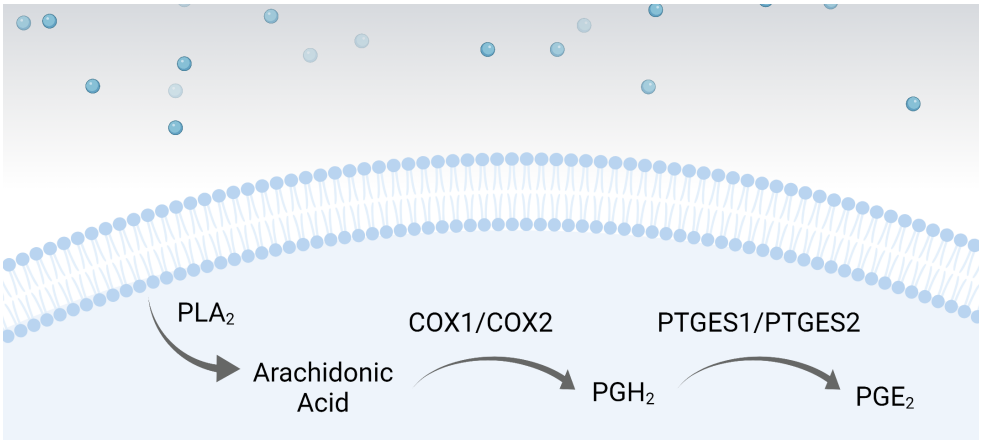

Figure 1. Prostaglandin E2 synthesis. PLA_2 releases AA from cellular membranes. AA is a substrate for COX1 or COX2 to produce PGH_2. PGH_2 is metabolized by PTGES1 or PTGES2 to produce PGE_2. Created with BioRender.com

While both COX-1 and -2 have nearly identical crystal structures and molecular weights, differences in regulation and activity do exist between these two enzymes. The gene that encodes COX-1, *Ptgs1*, lacks a TATA or CAAT box within its promoter region leading to constitutive expression in most mammalian tissues (**Table 1**) [43,46]. The gene that encodes COX-2, *Ptgs2,* however, has multiple transcriptional regulatory sequences within its promoter region, including a TATA box, an NF-IL6 motif, two AP-2 sites, two NF-κB sites, and a CRE motif [43,46,47]. Therefore, *Ptgs2* gene expression is induced by multiple ligands in response to bacterial products or proinflammatory mediators and cytokines in more restricted cell types (**Table 2**). COX-2 is thought to be the primary producer of PGs under inflammatory conditions as COX-2 preferentially oxygenates arachidonic acid over COX-1 when it is present at a concentration >10 μM, which typically only occurs during acute inflammation or cell injury [42,43,45,46]. Therefore, the constitutive expression of COX-1 may produce prostanoids such as PGE_2 during the early stages of inflammation before COX-2 upregulation in response to inflammatory stimuli.

	Brain	Heart	Lung	Liver	Stomach	Bladder/ Kidney	Skin	Testis	Uterus
COX-1	++	++	+	+	++	+	++	++	+++
COX-2	-	+	+	+++	-	++	+	++	++
PTGES-1	-	-	-	-	-	+++	+	+++	+++
PTGES-2	++	+++	++	++	+++	+++	++	+++	+++

Table 1. Expression of PGE_2 synthesis enzymes in various tissues. + indicates relative amounts of EP receptor expression in various tissues. – indicates a lack of expression.

PGH_2 is unstable, and levels do not build up within cells as it is quickly metabolized by one of a series of specific prostanoid synthases to yield PGD_2, PGE_2, $PGF_2\alpha$, PGI_2, or TXA_2 [41,45]. Most of these prostanoid synthases have multiple isozymes with differing levels of expression and tissue distribution [45]. This allows different cell types to have different capabilities and specificity to produce these PGs based on their physiological needs [45] (**Table 1 and 2**). However, the stimuli that drive synthesis of these prostanoids, how the synthesis differs in response to stimuli in different organ systems, and the impact these initial lipid mediators have on the host response is an active area of study. In the case of PGE_2, there are two specific prostaglandin E2 synthases (PTGES), termed PTGES-1 and PTGES-2 [43,47].

PTGES-1 was discovered first and found to be closely linked with COX-2 expression [47]. Both PTGES-1 and COX-2 enzymes were found to be induced by IL-1β stimulation and NF-κB activation with PTGES-1 closely linked with the activation of COX-2 for the production of PGE_2 in myeloid cells during inflammation [42,43]. In cells lacking COX-2, IL-1β stimulation resulted in lower levels of PGE_2 production, suggesting that PTGES-1 is not preferentially coupled with COX-1 to produce PGE_2 during inflammation [43,47]. PTGES-1 can also be induced in response to other inflammatory stimuli and transcription factors NF-κB and AP-1 [42,43]. PTGES-2, unlike PTGES-1, is constitutively expressed and is thought to maintain basal levels of PGE_2 for homeostatic functions. PTGES-2 is found in most tissues and cell types compared to the more restricted expression of PTGES-1 (**Table 1 and 2**) and has been shown to couple with both COX-1 and COX-2 to produce PGE_2 during both acute and chronic inflammation [48]. However, less is known about the regulation of these enzymes compared to the upstream COX enzymes which under most physiological conditions are through to regulate the secretion of PGE_2. Studies into

the regulation of these enzymes could uncover new mechanisms by which they exert another level of control over PGE2 synthesis under various physiological and disease states. After synthesis by either PTGES-1 or -2, PGE_2 can bind to one of its 4 G-protein-coupled receptors (GPCRs) to initiate various intracellular signaling cascades.

Receptor	T Cells	B Cells	Dendritic Cells	Macrophages	Monocytes	Neutrophil	Mast Cells
COX-1	-	+	+	++	++	+	+++
COX-2	-	-	+	+++	+	++	+++
PTGES-1	-	-	-	+	++	+	++
PTGES-2	+	+	-	++	+++	+	+

Table 2. Expression of PGE_2 synthesis enzymes in various immune cell populations. + indicates relative amounts of EP receptor expression in various tissues. – indicates a lack of expression.

PGE_2 is a major prostanoid in human skin and is generally synthesized at low levels during homeostasis. However, skin PGE_2 production significantly increases during inflammatory conditions, such as sunburn, and in diseases like skin squamous cell carcinoma [49]. Increased skin PGE_2 production is also associated with skin aging. Both PTGES-1 and COX-2 expression are increased with aging in human skin and are associated with increased production of PGE_2 by skin fibroblasts [49]. Studies have demonstrated that increased PGE_2 production by skin fibroblasts limits the production of collagen-I by these same fibroblasts [49]. As collagen-I is the main component of the extracellular matrix of the skin, the loss of collagen leaves aging skin thin and fragile, with an increased risk of bruising and delayed wound healing [49]. However,

increased PGE_2 synthesis during skin wound healing also promotes keratinocyte proliferation and migration that is necessary for skin reepithelization and the wound healing process [50]. Overall, PGE_2 synthesis represents a potential therapeutic target for skin maladies given its strong effect on keratinocytes and skin fibroblasts.

EP receptors

There are four distinct G-protein coupled receptors (GPCRs) through which PGE_2 can exert its actions. Termed E prostanoid (EP) receptors, the four designated subtypes are named EP1, EP2, EP3, and EP4, with EP3 the only receptor to have multiple isoforms due to alternative splicing at its C-terminal tail [51]. The four EP receptors have differences in signal transduction, tissue localization, and expression level, allowing for PGE_2 to be one of the most versatile prostanoids [52]. The distribution of EP receptors differs between humans and mice; however, in both, EP4 is the most widely expressed across various tissues followed by EP3, EP2, and EP1 [51,52] (**Table 3**). Of the EP receptors, EP3 and EP4 are considered high-affinity receptors, followed by EP2, with EP1 having the lowest binding affinity for PGE_2 in both mice and humans [53].

	Brain	Thymus	Heart	Lung	Liver	Stomach	Skin	Ileum	Kidney	Uterus
EP1	-	-	-	-	-	+	-	-	+++	-
EP2	-	+	+	-	+	+	+	+	-	++
EP3	+	+	+	-	-	++	++	+	+++	++
EP4	-	++	+	++	-	+	++	++	+	++

Table 3. Expression of EP receptors in various tissues. + indicates relative amounts of EP receptor expression in various tissues. – indicates a lack of expression.

While EP2 and EP4 are $G_{\alpha s}$ coupled receptors and EP3 is $G_{\alpha i}$ coupled, EP1 is the sole $G_{\alpha q}$ receptor and has been shown to increase intracellular Ca^{2+} [52]. However, its actions are dependent on extracellular Ca^{2+}, suggesting it regulates Ca^{2+} channel gating, although the exact mechanism remains an active area of study [51–53]. Both EP4 and EP2 are $G_{\alpha s}$ coupled receptors and activate adenylate cyclase to generate cAMP, and both receptors have been shown to activate similar signaling pathways (**Fig. 2)** [52,53]. Despite these similar functions, EP4 has been shown to also signal via a cAMP-independent PI3K-dependent mechanism through direct PI3K activation that leads to phosphorylation of extracellular signal-related kinases (ERKs), which leads to early growth response factor-1 (EGR-1) expression that is not seen with EP2 signaling [51].

Analysis of receptor expression in the context of inflammation has shown that while EP2 expression is rapidly upregulated in response to proinflammatory signaling or bacterial products such as LPS, EP4 expression is only slightly increased [53,54]. Promoter region analysis for EP2 and EP4 has revealed they contain several putative cis-acting elements such as binding

sites for AP-1, AP-3, NFκB, and NF-IL6 that could drive receptor expression in response to inflammatory stimuli [43,52,55]. Further studies have revealed that while EP4 is quickly desensitized during inflammation, EP2 is rapidly recycled back to the cell surface, suggesting that while EP4 may mediate signaling early on during inflammation, EP2 may have a larger, more significant impact on cAMP during later stages of inflammation [54,55].

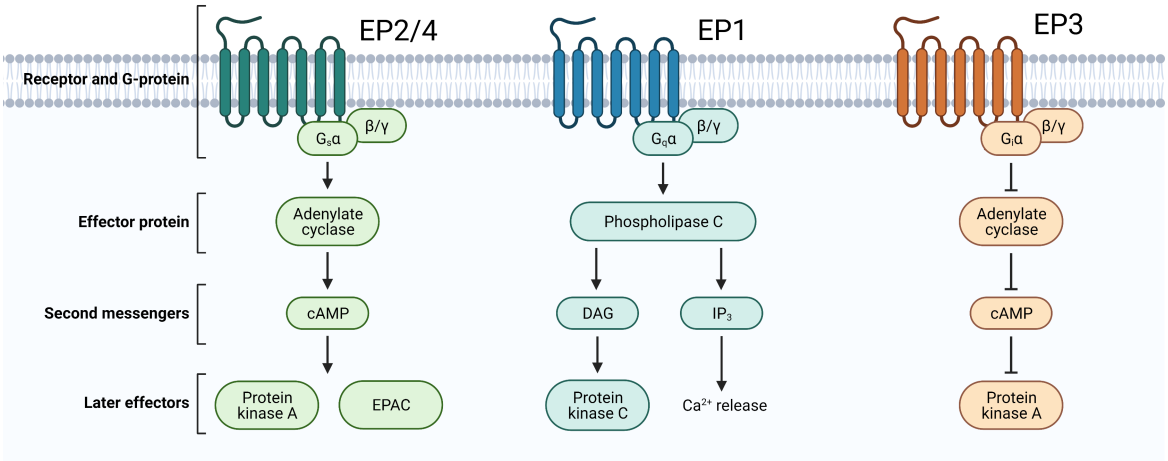

Figure 2. EP receptor signaling pathways. EP2 and EP4 are $G_{\alpha s}$ coupled receptors that activate adenylate cyclase. EP1 is a $G_{\alpha q}$ coupled receptor that increases intracellular calcium. EP3 is a $G_{\alpha i}$ coupled receptor that inhibits adenylate cyclase. Created with BioRender.com

The activation of adenylate cyclase by EP2 or EP4 signaling leads to the increased production of cAMP that in turn activates protein kinase A (PKA) and exchange proteins directly activated by cAMP (EPAC-1 and -2) (**Fig. 2**) [51,52]. While PKA acts to phosphorylate downstream proteins such as the cAMP response element binding protein (CREBP) and the transcription factor CREB, EPAC-1, and -2 are guanine exchange factors which can function as nucleotide exchange factors for the Rap subfamily of RAS-like small GTPases [56,57]. Studies have demonstrated that while CREB activation may play a part in promoting IL-1β secretion by

enhancing pro-IL1β transcription during infection [55,56,58], EPAC activation via EP2 and EP4 signaling has primarily been shown to limit immune cell effector functions. Macrophages treated with PGE_2 have demonstrated diminished phagocytic capabilities due to impaired F-actin polymerization that was shown to be dependent on EPAC-1 activation [57,59]. Furthermore, activation of both PKA and EPAC limits ROS and RNS generation in macrophages, restricting their antimicrobial effector function [57,59]. PKA activation alone limits proinflammatory cytokine release (TNF-α, IL-1β) while increasing the secretion of anti-inflammatory mediators (IL-10, TGF-β) [57]. This creates a paradigm wherein PGE_2 promotes inflammation through driving vasodilation yet suppresses the functions of recruited phagocytes, raising question on whether the level of receptor expression or PGE_2 synthesis dictates its role acting in either a pro- or anti-inflammatory capacity. In the context of skin research, both EP2 and EP4 have been shown to promote VEGF expression and keratinocyte migration and proliferation to increase wound healing and limit inflammation during skin infection and injury, dependent on PKA activation [60].

Unlike EP2 and EP4, EP3 is primarily a $G_{\alpha i}$ coupled receptor that inhibits adenylate cyclase activity and reduces intracellular cAMP (**Fig. 2**) [51,52]. EP3 is unique amongst the EP receptor for having three isoforms in mice, termed EP3α, EP3β, and EP3γ, that are generated by alternative splicing at its C-terminal tail [51,52]. EP3α and EP3β localize to the intracellular compartment while EP3γ is localized at the plasma membrane [61]. All three isoforms display similar ligand binding properties but differ slightly in their signal transduction pathways, which are an active area of study today. While all three isoforms have been shown to lower cAMP levels, differences have been reported between these isoforms in sensitivity to agonist-induced

desensitization, amounts of constitutive activity without stimuli, and coupling to different signal transduction pathways [51,52,62]. In particular, EP3α and EP3γ have been shown to have partial $G_{\alpha i}$ constitutive activity (EP3α > EP3γ) without agonist binding while EP3β has none [52,63]. Furthermore, their binding to and activation of $G_{\alpha i}$ has been shown to differ (EP3γ > EP3α > EP3β), with EP3γ being the sole isoform able to also couple with $G_{\alpha s}$ to increase intracellular cAMP dependent on agonist binding [63]. EP3 activation is closely tied to the role of PGE_2 as a promoter of inflammation, as EP3 agonism promotes pyrogenic fever through vasodilation at the site of injury [64]. Furthermore, studies have shown activation of EP3 can promote phagocytosis and proinflammatory cytokine release from immune cells [54,64]. As EP3 is the receptor through which PGE_2 promotes inflammation more studies are needed into its isoforms and how their distinct activation may impact not only inflammation but also phagocyte effector functions and potentially PGE_2 synthesis. The current research goals primarily focus on EP3, as its role in promoting inflammation and pathogen clearance is of clear relevance in the context of skin infection, although the roles of EP2 and EP4 are also of interest.

PGE_2 in the immune response

PGE_2 is considered both an anti- and pro-inflammatory mediator that modulates the cardinal signs of inflammation: redness, swelling, heat, and pain [9,54,60,65]. It is one of the earliest mediators of inflammation released by resident immune cells in response to infection or injury [44,56,65]. EP receptors are expressed on most immune cells which are thought to produce the majority of PGE_2 during inflammation and quickly respond to PGE_2 in an

autocrine/paracrine manner (**Table 4**). In fact, non-steroidal anti-inflammatory drugs (NSAIDs) specifically target the cyclooxygenase enzymes involved in PGE_2 synthesis as a way to reduce inflammation [9]. Studies in both mice and humans have shown that treatment with PGE_2 drives inflammation through promoting vasodilation to allow for the recruitment of immune cells and serum proteins during inflammation [9,12,54]. PGE_2 can promote inflammation in several ways; the first is by binding to the EP3 receptor on mast cells, resulting in their degranulation, which releases histamine that acts on endothelial cells to drive vasodilation [9,52,54]. The second is by acting directly on endothelial cells themselves via the EP2 or EP4 receptor to increase intracellular cAMP, which relaxes the smooth muscle cells of the endothelium, resulting in vasodilation and inflammation [9,52]. Finally, EP2- and EP3-mediated inflammasome activation has also been shown to drive inflammation through IL-1β production [9,60]. Despite this well-known proinflammatory role, a large body of work highlights a role for PGE_2 in suppressing the innate cellular response to multiple models of infection [56,59].

Receptor	T Cells	B Cells	Dendritic Cells	Macrophages	Eosinophils	Neutrophils	Mast Cells
EP1	+	+	-	+	-	-	+
EP2	+	+	-	+	+	+	+
EP3	+	+	-	+	-	-	+
EP4	+	+	-	+	-	-	+

Table 4. Expression of EP receptors on immune cells. + indicates relative amounts of receptors on various immune cell populations. – indicates no expression detected.

Paradoxically, despite its role in promoting cell recruitment to the site of infection, immune cells and phagocytes treated with PGE_2 demonstrate impaired effector functions [53,56]. In macrophages, PGE_2 weakens microbial phagocytosis and impairs proinflammatory cytokine release [57,59]. Furthermore, in both macrophages and neutrophils, PGE_2 limits ROS generation by inhibiting the assembly of the NADPH oxidase [9,56,57,59]. In a model of peritoneal inflammation, PGE_2/EP2 signaling limits monocyte maturation within the peritoneum via elevated suppressor of cytokine signaling-1 (SOCS-1) expression in a manner dependent on cAMP [66]. In a model of peritoneal infection, the PGE_2/EP2/cAMP pathway also limited the phagocytic capabilities of macrophages and was improved with COX-1 inhibition via treatment with NSAIDs [22]. The role of PGE_2 in limiting immune cell effector function is exploited by several pathogens, including *Salmonella* [35], *Streptococcus pneumoniae* [67], and *Pseudomonas aeruginosa* [68], all of which promote PGE_2 release to impair host defense and allow enhanced pathogen replication and dissemination to occur. Furthermore, elevated PGE_2 serum levels are associated with several immunosuppressed states including HIV infection, organ transplant, and burn trauma [42,44]. Together, this research has led to the concept of PGE_2 as a pro-inflammatory mediator with immunosuppressive activity, where PGE_2 has roles in both promoting and inhibiting the inflammatory response to properly regulate host defense. This dual nature of PGE_2 makes an ideal target for therapeutic intervention in diseases resulting from chronic or impaired inflammation. However, more studies are needed into understanding the regulation of PGE2 synthesis and EP receptor signaling that dictate either its pro- or anti-inflammatory role in various disease states.

Recent studies utilizing PGE_2 have provided more evidence on the pleiotropic nature of this lipid mediator of inflammation. While it was previously known that receptor binding (EP3 vs. EP2 or EP4) could strongly dictate the role of PGE_2 in promoting or resolving the inflammatory response [9,52–54,57], new studies have demonstrated how the level of PGE_2 production can also dictate the downstream response. Studies by several groups have shown that while high levels of PGE_2 can limit inflammasome assembly and IL-1β release [69], low levels of PGE_2 exposure can increase pro-IL-1β transcripts via NF-κB and CREB activation, resulting in increased IL-1β as more pro-IL1β transcripts are processed by the inflammasome upon its activation [58,70,71]. Similar effects have also been noted in regard to phagocytosis and ROS generation as well. Low levels of PGE_2 result in better phagocyte effector function as opposed to higher levels which result in a more immunosuppressed or "anti-inflammatory" phenotype [53,56,57,59]. However, the anti-inflammatory role of PGE_2 is critical to promote wound healing and prevent chronic inflammation that can result in tissue destruction and bacterial spread during infection [50,65,72]. In a diabetic skin wound healing model in mice, COX-1 derived PGE_2 was shown to be critical for driving skin reepithelization and the release of pro-angiogenic and wound healing factors such as VEGF and IL-10 [73,74]. Together, these data suggest PGE_2 may have roles at multiple stages of infection, particularly in the skin where it initially promotes inflammation and phagocyte recruitment but upon pathogen clearance suppresses inflammation to promote wound healing and revascularization. Given the wide variety of effects PGE_2 can have on inflammation, as well as host defense, further studies are needed into its role and regulation in early versus late inflammation to inform its future application as a therapeutic to treat inflammatory conditions and disease states.

SOCS-1 in inflammation/immunity

Proper regulation of the immune system is critical to promoting potent host defense while avoiding chronic inflammation that can be detrimental to the host and lead to several comorbidities. The Suppressor of Cytokine Signaling (SOCS) family of proteins are inducible intracellular proteins that negatively regulate cytokine signaling to prevent chronic inflammation [75,76]. SOCS proteins also regulate several other signaling pathways, including GPCRs, as well as receptor associated tyrosine kinases such as the Janus Kinases (JAKs) and receptor tyrosine kinases, such as the epidermal growth factor (EGF) receptor [77]. Regulation of JAKs is critical for immune homeostasis as they phosphorylate/activate downstream transcription factors called STATs (signal transducer and activator of transcription), which promote cytokine, growth factor, and hormone signaling [75,76]. While there are 8 SOCS proteins, SOCS-1 is one of the most studied for its potent modulation of the immune system and inflammation [77].

SOCS-1 acts mainly through direct inhibition of the JAK tyrosine kinase to prevent STAT-1 phosphorylation and activation in a classical negative feedback loop (**Fig. 3**) [78]. As such, SOCS-1 is well known as a potent inhibitor of interferon signaling driven by STAT-1 activation. The role of SOCS-1 in this pathway is critical as genetic deletion of SOCS-1 in mice results in death 2-3 days post-birth due to intense acute inflammation, driven by interferon gamma signaling-mediated liver damage and necrosis [75,76]. The SOCS-1 protein has three functional domains: a kinase inhibitory region (KIR), an SH2 domain, and a SOCS box. The KIR domain functions as a pseudo-substrate that inhibits JAK2-mediated STAT-1 and STAT-3 phosphorylation and activation [77,78]. The SH2 domain binds directly to the activation loop of

JAK2, which blocks STAT activation (**Fig. 3**) [78,79]. The SOCS box targets proteins such as JAK2 and MyD88-adaptor-like protein (MAL) for degradation by the ubiquitin-proteasome pathway through recruitment of the E3 ubiquitin ligase scaffold Cullin 5 and other components of the E3 ubiquitin ligase complex [80,81].

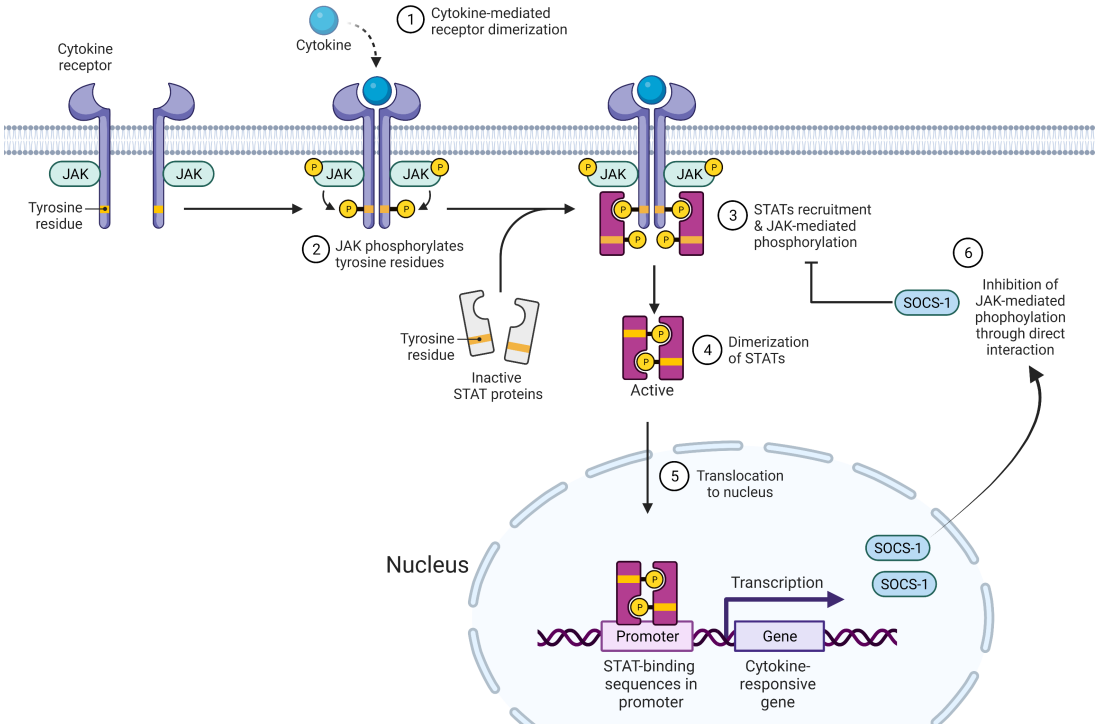

Figure 3. SOCS-1 inhibition of JAK/STAT signaling. Negative feedback loop of STAT1 activation 1.) Cytokine-mediated receptor dimerization 2.) JAK phosphorylation of tyrosine resides. 3.) STATs recruited and phosphorylated by JAK. 4.) Dimerization of phosphorylated STATs. 5.) Translocation of dimerized STATs to nucleus. 6.) Inhibition of JAK-mediated phosphorylation by SOCS-1 through direct interaction with JAKs. Created with BioRender.com

In addition to STAT-1, SOCS-1 also prevents the activation of different transcription factors, such as STAT-3, NF-κB and AP-1 [75,76,82]. SOCS-1 also inhibits phagocyte function via: 1) hampering the TLR-MyD88-dependent activation of NF-κB by targeting MAL [83]; 2) inhibiting IL-1 receptor-associated kinase (IRAK) [80]; 3) preventing MAPK signaling by binding

to apoptosis signal-regulating kinase 1 (ASK-1) [76]. Since SOCS-1 exerts pleiotropic effects in phagocytes, it is expected that SOCS-1 could influence host defense. Indeed, SOCS-1 has demonstrated a detrimental impact in different infections, including viral, fungal, parasitic, and bacterial infections [84–86]. Infections with both gram-positive [87,88] and gram-negative [84] bacteria, as well as *Mycobacterium tuberculosis* [89], and parasites such as *Leishmania major* [90], and the fungus *Candida albicans* [91], promote SOCS-1 expression to actively suppress the immune response, allowing pathogen replication and immune evasion. Expression of SOCS-1 during infection correlates with reduced levels of the proinflammatory cytokines IL-1β, TNF-α, and IL-6, as well as antimicrobial NO and ROS [75,81]. As SOCS proteins are potent negative regulators of inflammation, they also represent potential targets for therapeutic intervention to boost the immune response via their inhibition, however further studies would be needed to fine tune this strategy different pathological conditions to limit potential damaging inflammation.

Dysregulation of SOCS-1 expression is correlated with several diseases, including colitis and neural inflammation. During these conditions impaired expression of SOCS-1 results in damaging levels of inflammation in these immune-privileged tissues [92–94]. Related to our current research goals, in the colitis model, PGE_2 treatment was shown to increase SOCS-1 expression via EP4 in a cAMP and PKA-dependent mechanism, limiting inflammation and restoring tissue homeostasis [94,95]. This points to a potential mechanism by which cAMP levels driven by PGE_2 and EP receptor signaling impact SOCS-1 expression, with potential therapeutic implications to limit or enhance inflammation. Modulation of SOCS-1 activation by mimics or antagonists has been a topic of intense research [79,80]. Since JAK/STAT pathways

are involved in a number of inflammatory diseases, there is an abundance of research focusing on the modulation of SOCS-1 actions in models of diabetes, atherosclerosis, EAE, and dermatological diseases [80,91]. However, whether SOCS protein expression impacts skin host defense against infection remains to be fully elucidated.

Staphylococcus aureus

Staphylococcus aureus is a gram-positive bacterium estimated to asymptomatically colonize ~30% of the human population [96]. Despite this innocuous lifestyle, *S. aureus* is an opportunistic pathogen that is capable of breaching the skin barrier, leading to severe and systemic infections [96–98]. One of the most common presentations of *S. aureus* infections are those of the skin and soft tissues, and it is estimated that *S. aureus* skin infections account for ~12 million outpatient and emergency room visits and 500,000 hospital admissions per year [99–101].

The rise of resistance to multiple antibiotics, particularly methicillin-resistant *S. aureus* (MRSA), has made treatment of these infections particularly difficult [102–104]. This is of particular concern to immune-compromised individuals, including patients with diabetes who frequently suffer from recurrent skin infections caused by MRSA [105–107]. While MRSA infections have traditionally been associated with healthcare settings and immune-compromised patient populations, the recent rise in community-acquired MRSA (CA-MRSA) outside of the healthcare setting has highlighted these infections as a serious public health risk [104,108]. Furthermore, these CA-MRSA strains have acquired not only antibiotic resistance but

a number of potent virulent factors that allow them to infect otherwise healthy individuals and decimate susceptible patient populations [109,110].

The recent identification of *S. aureus* resistant to Vancomycin, considered the last line of defense against antibiotic-resistant bacterial infections, demonstrates that its acquisition of antibiotic resistance is far outpacing the development of new antibiotics [104,109]. Therefore, there is an urgent unmet clinical need to develop new therapies to treat these antibiotic-resistant infections [103,104]. One strategy is to use immunotherapies that rely on boosting the host's immune response to these types of infections with or without the use of antibiotics [111]. Mediators of the innate inflammatory response such as PGE_2 and SOCS-1 represent potential host-centered therapeutic targets to promote or restrain immune activation in various disease states such as during MRSA skin infection. By better understanding these molecular signaling events and mediators that either elicit or control the immune response during MRSA infection, we can develop more host-centered immunostimulatory therapies that improve infection outcomes in healthy and susceptible patient populations.

Skin structure and response to *S. aureus*

The skin is the largest organ in the body and performs several vital functions, such as hormone and vitamin production. However, its primary function is as a barrier between the body and the environment, serving as the first line of defense against infection. It acts primarily as a physical barrier to prevent the entry of invading pathogens into deeper tissues or dissemination via the bloodstream [40]. The skin is composed of two primary layers that make

up this barrier, the upper epidermis and the underlying dermal layer, which are separated by a basement membrane [40].

Keratinocytes (KCs) in various stages of maturation make up the majority of the epidermis, along with Langerhans's cells (LCs) and T cells [40,112]. Together, these cells compose the primary physical layer that prevents entry of harmful environmental substances and invading pathogens. Keratinocytes are also responsible for producing antimicrobial peptides that form the biochemical layer of protection provided by the epidermal layer of skin [38,113]. The inner dermal layer of the skin contains extracellular matrix proteins and connective tissue that provide the structural framework for blood vessels, adipose tissue, fibroblasts, and several skin resident immune cells [40,114]. There are lymphoid and myeloid skin resident immune cells within the dermis such as dermal macrophages, dendritic cells, B and T lymphocytes, NK cells, and innate lymphoid cells [40,114]. Together with the cells of the epidermal layer, these skin resident cells are responsible for mounting and maintaining a coordinated immune response to invading pathogens like *S. aureus* [114–117].

During skin infection, KCs are the first cells to encounter invading microbes and recognize pathogen associated molecular patterns (PAMPs) as they bind to pathogen recognition receptors (PRRs) on the cell surface [113]. KCs express numerous PRRs such as Toll-like receptors (TLRs), nucleotide-binding-oligomerization domain (NOD)-1 and -2 receptors, and the scavenger receptors CD36 and MARCO that have been shown to bind components of *S. aureus* [112,113]. Of the TLRs, TLR1, -2, and -6 on the surface of KCs recognize lipopeptides and peptidoglycan that make up the cell wall of *S. aureus*, while the intracellular NOD-2 recognizes muramyl-dipeptide, a product derived from the breakdown of peptidoglycan [113,117].

Initial recognition of *S. aureus* typically occurs via TLR2 on KCs that utilize the signaling adaptor Myeloid differentiation primary response 88 (MyD88) to initiate signaling and transcriptional events that lead to the inflammatory response [2,115–117]. This results in the production of a number of proinflammatory cytokines (IL-1α, IL-1β, IFNγ, TNF-α, IL-17, and IL-22), chemokines (CXCL1, CXCL2, and CXCL5), lipids (prostaglandins and leukotrienes), and antimicrobial peptides (defensins and cathelicidin LL-37) (**Fig. 4**) [38,40,112,115–117]. TLR2 is also expressed on a number of skin resident immune cells, such as dermal macrophages, which also respond to *S. aureus* recognition by initiating a similar inflammatory cascade [2,114–116]. The production of chemokines (CXCL1, 2, and 5) initiates the recruitment of neutrophils and monocytes to the site of infection through the bloodstream by binding to CXCR2 [8,10]. Recruited phagocytes express PRRs that recognize *S. aureus* and perpetuate the secretion of proinflammatory mediators initially released by skin resident immune cells (**Fig. 4**) [115–117].

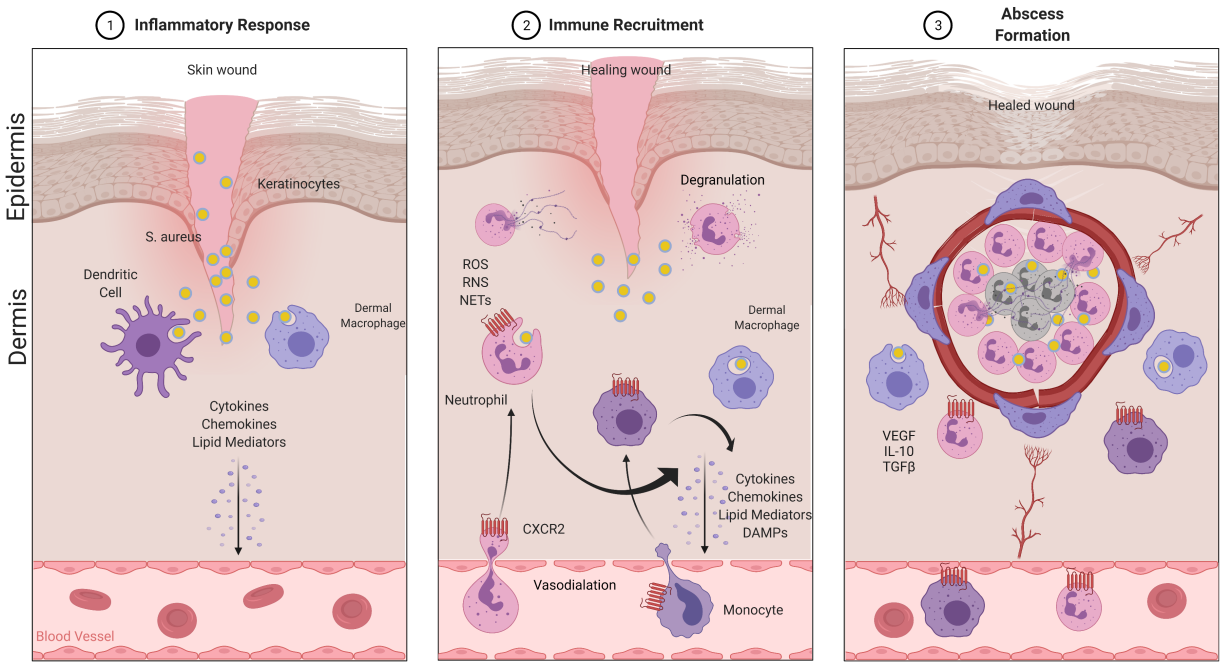

Figure 4. Skin immune response to *S. aureus*. Left Panel: Dermal macrophages and other cells in the skin respond to an injury colonized by *S. aureus* by producing inflammatory mediators. **Middle panel**: Inflammatory mediators promote vasodilation and immune cell recruitment to the site of infection and injury, where they eliminate pathogens and produce more inflammatory mediators. **Right panel**: As the infection progresses, abscess formation occurs. Once the pathogen is eliminated, pro-resolving inflammatory mediators are released and wound healing/ revascularization begins. Created with Biorender.com

The initial inflammatory response to *S. aureus* skin infection is dependent on signaling via TLR2 and IL-1R, both of which utilize the adaptor protein MyD88 and can be negatively regulated by SOCS-1 [114–119]. Mice deficient in TLR2 exhibit significantly worse infection outcomes with lower expression of proinflammatory mediators in multiple *S. aureus* infection models, including in the skin [118]. Furthermore, mice deficient in either MyD88 or IL-1R have significantly worse *S. aureus* infection outcomes than those seen in TLR2 deficient mice [117–119]. In particular, IL-1R is critical for skin host defense against *S. aureus*. IL-1R-/- mice, or irradiated wildtype mice reconstituted with bone marrow from IL-1R-/- mice, have

demonstrated severe impairments in pathogen clearance, chemokine release and subsequent cell recruitment, and abscess formation [118–120]. Restoration of IL-1R signaling via bone marrow transplantation ameliorated these impairments and improved pathogen clearance and abscess formation to that of wildtype mice [118,119]. Together these data point to IL-1β as a critical cytokine in initiating chemokine release, neutrophil recruitment, and abscess formation during *S. aureus* skin infection. Although the importance of IL-1β for optimal skin host against MRSA has been demonstrated by several groups, the role of other mediators of inflammation, in particular lipid mediators, within this skin host defense pathway has yet to be fully investigated.

While skin resident macrophages act in the initial recognition and clearance of *S. aureus,* via phagocytosis and the production of ROS and RNS, they are soon joined by recruited neutrophils that make up to 50% of leukocytes within the infection area as early as 1 day post-infection [114–116]. Neutrophils eliminate pathogens in a similar mechanism via phagocytosis and ROS production, as well as through extruding NETs to further trap bacteria for elimination (**Fig. 4**) [7,121]. As the infection progresses, neutrophils also initiate the formation of a neutrophilic abscess that is the hallmark of *S. aureus* infection [114,122,123]. These abscesses within the skin and soft tissue all have a similar structure, with a necrotic core made up of live and dead neutrophils, bacteria, cell debris, and extracellular DNA, surrounded by a fibrous capsule preventing bacterial dissemination into deeper tissues and limiting adjacent tissue damage [122–124]. Skin resident macrophages and recruited monocyte derived macrophages are often found at the periphery of this abscess structure [114,122,123]. However, while the

anatomy of the abscess has been well characterized, the mediators promoting and driving proper abscess formation during MRSA are still an active area of study.

Once the pathogen is eliminated, the resolution phase of the inflammatory response is initiated, and the wound healing phase of skin infection begins. During resolution, dermal macrophages break down the fibrous capsule of the abscess and remove apoptotic cells via efferocytosis [114,125]. The removal of apoptotic cells and cell debris is critical during the resolution phase of infection to prevent a secondary inflammatory response to danger associated molecular patterns (DAMPs) that may be released by apoptotic cells if they are not appropriately removed and become necrotic [18,126]. This secondary inflammatory response can become recurrent if apoptotic cells are not properly removed, leading to chronic inflammation of the wound that impairs the healing process [127]. During efferocytosis macrophages also release mediators such as IL-10 and PGE_2 to limit inflammation that can impeded the wound healing process [128]. Granular tissue that will eventually form scar tissue is also deposited during this final phase of infection, and while it is thought most of this work is handled by macrophages [23], recent studies have highlighted a role for neutrophils in this process. In particular, CXCR2+ neutrophils recruited via CXCL5 secretion promote angiogenesis and wound reepithelization via expression of VEGF and other pro-angiogenic factors [13,28,29,126]. As the wound healing process continues, macrophages also switch to an M2 or "anti-inflammatory" state to promote further wound healing and angiogenesis through the secretion of factors such as VEGF, IL-10, and TGFβ. The granular tissue is eventually replaced by scar tissue as the wound completely heals, the infection is resolved, and the skin returns to homeostasis.

Diabetes mellitus

Diabetes mellitus is a disease resulting in hyperglycemia or elevated blood glucose due to impairments in insulin production or signaling [129]. Insulin, a hormone produced by pancreatic beta cells, is required to promote the expression of glucose transporters on target tissues such as muscle and adipose tissue to uptake glucose out of circulation to be used [130,131]. Diabetes is classified as one of two major subtypes, type I (insulin deficient) or type II (insulin resistant), depending on the nature of impairment to insulin signaling that drives the hyperglycemia [129].

In type I diabetes, insulin production is impaired after autoreactive B and T cells infiltrate the pancreas and attack the insulin producing beta cells [132]. Patients with type I diabetes are normally diagnosed during childhood and require supplemental insulin for the remainder of their life to properly regulate blood glucose levels [129]. While there is a strong case for a genetic link to type I diabetes, tied to certain MHA alleles promoting susceptibility or resistance to disease, viral infections as well as other environmental factors have been shown to contribute to this autoimmune disease [132]. Type II diabetes, however, is the result of resistance to insulin receptor signaling and is closely associated with obesity [129,133]. During the onset of type II diabetes, insulin resistance contributes to increased glucose production by the liver and decreased glucose uptake by muscle and adipose tissue, resulting in hyperglycemia [133]. While the pancreas will continue to produce increasing insulin levels to maintain blood glucose homeostasis, pancreatic beta cells can eventually become exhausted, resulting in their death and reduced insulin receptor signaling; further increasing blood glucose levels as the patient becomes insulin deficient [133]. Interestingly patients with type II diabetes

have also been shown to have elevated levels of PGE_2 in their blood, with hypotheses suggesting these elevated levels could promote the chronic inflammation in these patients while also contributing to their immunosuppressed state [56]. Individuals with type II diabetes are typically diagnosed later in life and usually have a history of obesity [129,133]. Therapies for type II diabetes include drugs to increase insulin production and sensitivity, insulin itself if the patient has become insulin deficient, and lifestyle changes to reduce excess body weight and glucose levels [129].

Diabetes and risk for infection

Chronic or poorly controlled hyperglycemia can lead to a number of comorbidities such as neuropathy, retinopathy, kidney disease, and a significantly increased risk of infection in different organ systems [132,133]. In patients with type I and type II diabetes, infections of the skin and soft tissues are particularly worrisome [106]. These infections typically happen in the feet, with diabetic foot infections accounting for an estimated 1 out of every 5 diabetes related hospital admissions in the United States [99]. Wounds in the feet of patients with diabetes take significantly longer to heal and can easily become chronic non-healing wounds if not treated properly early on during infection or injury [74,99,127]. If the wound progresses to the point of becoming a chronic non-healing wound, it can act as a portal for infection in these patients, adding the risk of pathogens colonizing these wounds, disseminating to other organs, and leading to life-threatening systemic infections such as sepsis [105,134]. In these cases, a diabetic foot amputation may be required to save the life of the patient. However, diabetic foot

amputations have a five-year mortality rate of nearly 50%, highlighting the need for safe and efficient therapeutic intervention to treat these foot infections before they progress to the point of requiring an amputation [99].

The increased risk of infection in patients with diabetes has long been correlated with impairments in immune cell effector function. Phagocytes isolated from the blood of patients with diabetes display poor chemotaxis in response to stimuli, suggesting poor recruitment to the site of infection is contributing to infection susceptibility [135]. Furthermore, these phagocytes also display impaired respiratory burst and phagocytosis which contributes to impaired host defense against infection during hyperglycemia [135,136]. Despite these impairments in immune cell effector function, however, these phagocytes tend to express exaggerated levels of proinflammatory mediators, such as TNF-α and IL-6, in response to bacterial stimuli [127,137]. This creates the paradigm of a hyperinflammatory response wherein delayed, but overwhelming immune cell recruitment results in tissue destruction rather than proper pathogen clearance, allowing for dissemination of the pathogen and worse infection outcomes [112]. While we have long known that hyperglycemia is closely correlated with these impairments in immune cell effector function, the root cause remains elusive. As diabetes is associated with chronic inflammation, levels of inflammatory mediators are altered even in the absence of infection and may result in immune cell desensitization. However, during infection these mediators are even further dysregulated and their impact of inflammation versus cellular immune functions is not fully understood. This highlights the need to study how phagocytes function under hyperglycemic conditions to allow for the development of new therapeutics to boost the host's own immune system outside of the use of antibiotics to limit infection severity.

Research Goals

A properly regulated inflammatory response is critical for eliciting an effective immune response during infection while returning to homeostasis after pathogen is cleared. However, chronic inflammatory diseases often alter the homeostatic levels of mediators of the inflammatory response, such as PGE_2 and SOCS-1. Diabetes is a chronic inflammatory disease and its dysregulation of the inflammatory response is correlated with a significantly increased risk of infection, particularly within the skin and soft tissues. The hypothesis for this work is that these inflammatory mediators represent potential targets for therapeutic intervention to stimulate the hosts own immune response to better clear pathogen without the use of antibiotics. This hypothesis was tested by investigating the role of PGE_2 and SOCS-1 during MRSA skin infection in both euglycemic and hyperglycemic mice.

Based on previous work in the lab demonstrating a role for PGE_2 in skin host defense, the first research goal was to further investigate its role in coordinating the innate immune response to MRSA skin infection in HFD fed insulin-resistant hyperglycemic mice. For this goal, the aims were to: 1.) determine how hyperglycemia impacted PGE_2 synthesis and 2.) investigate mechanistically how restoration of PGE_2 signaling improved skin host defense in hyperglycemic mice during MRSA infection. Our initially hypothesis was that PGE_2 may be important in driving proper immune cell recruitment to the skin during infection through properly regulating the secretion of pro-inflammatory cytokines/chemokines.

The second research goal was to evaluate the role of SOCS-1 during MRSA skin infections in both euglycemic and STZ-induced insulin-deficient hyperglycemic mice. The aims

of this goal were to: 1.) determine how excessive SOCS-1 expression in the skin of hyperglycemic mice negatively impacted skin host defense during MRSA infection and 2.) evaluate the therapeutic potential of blocking SOCS-1 actions during MRSA skin infection. Our initial hypothesis was that SOCS-1 may negatively impact skin host defense by limiting MyD88 dependent signaling that is critical for skin host defense against MRSA.

This work demonstrates the importance of studying how inflammatory mediators can regulate and impact the overall immune response. Targeting PGE_2 or SOCS-1 has potential for therapeutic intervention to enhance or dampen the inflammatory response as necessary. These therapeutic strategies could benefit both immunocompromised patients and those suffering from chronic inflammatory conditions. They also represent a strategy to improve infection outcomes against a number of antibiotic resistant pathogens.

CHAPTER 2

METHODS

Animals

All experimental procedures were approved by the Institution of Animal Care and Use Committee (IACUC) at Vanderbilt University Medical Center. Mice were purchased from Jackson Laboratory or were donated by other investigators. C57BL/6J breeding pairs were initially obtained from the Jackson Laboratory and maintained by breeding at Vanderbilt University Medical Center (VUMC), Nashville, TN, USA. Lys^{EGFP} mice were donated by Dr. Nadia Carlesso (City of Hope, Duarte, CA, USA). $Catchup^{IVM\text{-}red}$ mice [138] were donated by Dr. Matthias Gunzer (Institute for Experimental Immunology and Imaging, University Hospital, University Duisburg-Essen, Essen, Germany). Wildtype BALB/c and BALB/c IFNAR -/- mice were a gift from Dr. Stokes Peebles (Vanderbilt University Medical Center, Nashville, TN). C57BL/6 *Socs1*^{fl} mice were obtained from Warren Alexander (Walter and Eliza Hall Institute, Parkville, Victoria, Australia) [139]. This strain was crossed with $LysM^{cre/cre}$ mice (Jackson Laboratory) to create $SOCS1^{\Delta myel}$ mice. C57BL/6 *Socs1*^{fl} littermates were used as controls. PTGER3-/- mice were donated by Dr. Richard Breyer (Vanderbilt University Medical Center, Nashville, TN) [62]. MMDTR or *Csfr1*$^{LsL\text{-}DTR\text{-}mCherry}$*_LysM*^{Cre} mice were generated by breeding the *Csf1r*-HBEGF/mCherry) 1Mnz/J plus *LysM*$^{cre/cre}$ mice as previously reported [140] and allowed for the detection of monocytes/macrophages by mCherry fluorescence. Colonies of mice were bred and maintained at Vanderbilt University Medical Center in Nashville, TN.

Streptozotocin (STZ) induced hyperglycemia

6- to 8-week-old male C57BL/6J mice were treated by i.p. injection with 40 mg/kg of STZ (Adipogen) dissolved in 0.1 M sodium citrate buffer (pH 5.0) once daily for 5 consecutive days [141]. Female mice were not used as female mice are more resistant to STZ-induced hyperglycemia [142]. Euglycemic control mice received the vehicle control, citrate buffer. Mice were considered hyperglycemic when blood glucose levels were >250 mg/dL. Blood glucose was measured 10 days after the final dose of STZ and 1 day before infection. Mice were treated with STZ to induce hyperglycemia 30 days before MRSA skin infection.

Diet-induced obese hyperglycemia

For diet-induced obese (DIO) hyperglycemia, 6- to 8-week old male C57BL/6J mice were placed on a diet containing 60% kcal from saturated fats (Research Diets Inc. #D12492), while control mice were fed a nutritionally identical diet containing only 10% kcal from saturated fats (Research Diets Inc. #D12450J). After 3 months of free feeding, mice were examined for body weight and blood glucose levels. Mice were considered hyperglycemic when blood glucose levels were >200 mg/dL. Blood glucose was examined the week prior to infection and confirmed 1 day before infection.

***S. aureus* strains and preparation**

The MRSA USA300 LAC strain was a gift from Bethany Moore (University of Michigan, Ann Arbor, Michigan, USA) [143]. The bioluminescent USA300 (NRS384 lux) strain was a gift

from Roger Plaut (Food and Drug Administration, Silver Spring, Maryland, USA) [144]. The methicillin-susceptible *S. aureus* (MSSA) Newman strain was obtained from Eric Skaar (Vanderbilt University Medical Center, Nashville, TN). The GFP-expressing USA300 LAC strain was a gift from William Nauseef (University of Iowa, Iowa City, Iowa) [121]. MRSA and MSSA stocks were stored at –80°C in 50% glycerol. For culture, frozen aliquots were transferred to a 50 mL conical tube containing 10 mL tryptic soy broth (TSB) and incubated overnight shaking at 200 RPM at 37°C with a loose cap to generate a saturated culture. The next morning, the saturated culture was sub-cultured 1:100 (100 μL of culture into 10 mL of new TSB in a 50 mL conical tube) and place back on the shaker at 200 RPM for 3 hours at 37°C.

To determine bacterial density the sub-culture was diluted 1:10 in TSB and the OD_{600} was measured and compared to a previously generated growth chart for that particular strain. To prepare the inoculum, $6x10^8$ bacteria were centrifuged in a 1.5 mL tube at 12,000g for 10 min at 4°C. The supernatant was carefully removed before bacteria was resuspended in 1 mL PBS and centrifuged as before to "wash" bacteria. This step was repeated twice before bacteria were resuspended in 10 mL of sterile PBS for a concentration of $6x10^7$ CFU/mL. Bacterial preparations used for infection were serially diluted and plated onto TSA plates to determine actual infection inoculum. MRSA and MSSA were cultured as previously described [145].

S. aureus skin infection

The murine skin infection model is outlined in [145]. Male mice between 6 and 12 weeks of age were used for *S. aureus* skin infection. Fur was removed from the back of the mice one day prior to infection using hair clippers. The skin was cleansed with 70% ethanol before

infection with approximately 3×10^6 MRSA or MSSA CFU in 50 μl injected subcutaneously using a 1 mL syringe and 30G ½ inch needle. Biopsies and sample collection were taken at various times after infection, ranging from 6 hours to 9 days. Lesion size was measured every other day via caliper, and the affected area was calculated using the standard equation for the area (length x width) [146]. For biopsy collection, mice were euthanized via CO_2 inhalation. The exterior of the skin was cleaned with 70% ethanol, and an 8mm-diameter biopsy punch was used to collect a sample of infected skin. Biopsy punches were sectioned and processed for analysis via histology, ELISA/multiplex bead assay, Western blot, bacterial burden (CFU), or flow cytometry. Processing methods for some of these samples are described in more detail in the following sections.

Ointment preparation

Ointments were prepared by emulsifying the active compound into 100% petroleum jelly, prepared just before treatment application. Treatments were applied to the infected area using a sterile cotton swab. Mice were treated topically with an ointment containing either the compound or the vehicle control (petroleum jelly) at the indicated time point post-infection and twice daily following initial treatment. Misoprostol ointment (.03%) was made as previously described in petroleum jelly [147]. To antagonize EP3, mice were treated with an ointment containing the EP3 antagonist L-798, 106 (Tocris Cat. #3342) at 0.5 mM emulsified in petroleum jelly.

Antagonist and inhibitor treatments

The iKIR (DTHFRTFRSHSDYRR) and scrambled-KIR peptide control (DTHFARTFARSHSDYRRI) were obtained from GenScript [79,148]. A lipophilic palmitoyl group was added to the N-terminus of both sequences to facilitate cell penetration [79]. Mice were treated intraperitoneally with 50 μg of either the iKIR peptide or the scrambled peptide control [148,149] 1 hour before infection and once daily following infection. Mice were injected intraperitoneally with 40mg/kg of the anti-IFNGR or IFNAR antibody 3 hours before infection, followed by infection for 24 hours. For CXCR2 antagonism, mice were injected intraperitoneally with 5mg/kg of Navarixin (Med Chem Express) resuspended in 10% DMSO 90% corn oil 3 hours prior to infection and once daily during infection.

Histopathology analysis

For histological analysis, 8 mm biopsy punch samples were collected and fixed overnight in 4% paraformaldehyde before being transferred to 70% ethanol before paraffin embedding. Processing and paraffin embedding were performed by the Translation Pathology Shared Resource Core (TPSR) at Vanderbilt University Medical Center. The following tissue stains were performed by the Vanderbilt TPSR core: H&E and gram staining for bacteria. Images of tissue sections were visualized and acquired using the Nikon Eclipse Ci and Nikon Ds-Qi2 (Nikon, Tokyo, Japan).

In situ mRNA hybridization

8 μm tissue sections mounted to unstained slides were provided by the TPSR. To detect *Ptges1 and Ptges2* mRNA expression in FFPE tissues, *in situ hybridization* (ISH) was performed using the RNAScope Multiplex Fluorescent V2 Assay (Advanced Cell Diagnostics (ACD)) with TSA Plus fluorescein (PerkinElmer) according to the manufacturers' instructions. Briefly, ZZ probe pairs with channel C1 targeting the above mRNA targets were designed and synthesized by Advanced Cell Diagnostics (Catalog #497831-PTGES1 and #536661-PTGES2). FFPE tissue sections were co-stained with channel C2 and C3 probes for *Ly6g* (ACD Cat. # 455701-C2) and *CD68* (ACD Cat. # 316611-C3) mRNA as well. Tissue sections were exposed to ISH target probes and incubated at 40°C in a hybridization oven for 2 hours. After rinsing, the ISH signal was amplified using a company-provided preamplifier and amplifier conjugated to fluorescent dyes (Perkin Elmer #NEL744001KT and #NEL745001KT) as described in the figure legends. Sections were counterstained with 4',6-diamidino-2-phenylindole (DAPI) (Advanced Cell Diagnostics), mounted and stored at 4°C until image analysis. Image capture was performed using the BZ-X710 (Keyence, Osaka, Japan), and analysis was performed using HALO Software (Indica Labs). The results presented are the average of 3 different fields of view.

Determination of *in vivo* bacterial burden

8 mm skin biopsy samples were collected, weighed, and homogenized in a 1.5mL tube containing 200 μl of tryptic soy broth (TSB) using a pestle. Undiluted, 1:100, and 1:10,000 serial dilutions of these samples were plated (5 μl) on tryptic soy agar (TSA) plates. Colony-forming

units (CFUs) were counted after incubation overnight at 37 °C and corrected for tissue weight. Results are presented as CFU/g tissue.

RNA isolation and quantitative real-time PCR

Skin biopsy samples for RNA isolation were collected and homogenized in 400 μl of RLT buffer (QIAGEN) + β-mercaptoethanol using a disposable pestle in a 1.5 mL tube. Samples were then centrifuged at 12,000g for 10 minutes at 4°C to pellet tissue debris. After centrifugation, supernatants were moved to a new 1.5 mL tube, and 400 μl of isopropanol was added. Samples were then incubated at room temperature for 10 minutes on a rocker before additional centrifugation at 12,000g for 10 min at 4°C to pellet RNA. Supernatants were discarded and the RNA pellet was washed in 800 μl of 75% ethanol before repeating the previous centrifugation. The supernatant was then discarded, and excess ethanol was allowed to evaporate before the RNA pellet was resuspended in 50 μl of nuclease-free water.

The iScript cDNA Synthesis Kit (Bio-Rad) was used for cDNA synthesis following manufacturers protocol for 1 μg of isolated RNA. Quantitative PCR (qPCR) was performed on a CFX96 Real-Time PCR Detection System (Bio-Rad). Relative gene expression was calculated using the comparative threshold cycle (C_t) and expressed relative to control groups beta-actin (ΔΔCt Method). Primers for both β-actin and *Socs1* were purchased from Integrated DNA Technologies (IDT, Coralville, IA).

Detection of cytokines and chemokines

Biopsy samples (8 mm) were collected, weighed, and homogenized in TNE cell lysis buffer containing phosphatase and protease inhibitors (Sigma) and centrifuged at 12,000g for 5 minutes at 4°C to pellet tissue and cellular debris. Supernatants were then transferred to a new 1.5 mL tube for analysis. Skin biopsy homogenates were then analyzed using the proinflammatory-focused 18-plex Discovery Assay from Eve Technologies (Eve Technologies, Calgary, AB) to detect cytokines and chemokines. Measurement of PGE_2 was performed via ELISA (Cayman Chemical #500141). Levels of IFNγ, IFNα, and IFNβ were measured the time points indicated in the legends by ELISA, (IFNγ -Invitrogen #88-7314) (IFNα-Biolegend #439407) (IFNβ-PBL #42120-1). All assay plates were read and analyzed on a Molecular Devices Spectramax iD3 and SoftMax Pro software. Protein concentration was corrected for tissue weight.

Skin single-cell isolation and staining for flow cytometry

Skin biopsy specimens (8mm) were collected and minced with sterile scissors before digestion in 1 mL of DMEM with 1 mg/mL collagenase D (Roche Diagnostics) for 3 hours at 37°C. Reactions were then quenched with a 10 mM final concentration of EDTA before being passed through a 70 μm cell strainer and washed with PBS. Single-cell suspensions were treated with CD16/32 Fc blocking antibodies (Biolegend; catalog 101310; clone 93) to prevent non-specific antibody binding and stained with fluorescent-labeled antibodies for 20 minutes followed by fixation using 1% paraformaldehyde. The following antibodies were utilized: F4/80-FITC

(Biolegend; catalog 123107; clone BM8), Ly6G-PerCP/Cy5.5 (Biolegend; catalog 127616; clone 1A8) Ly6C-AF647 (Biolegend; catalog 128010; clone HK14), CXCR2-APC (R&D Systems; catalog #FAB2164A), CD11b-PE/Cy7 (Biolegend; catalog 101216; clone M1/70). Analyses were completed using FlowJo software (FlowJo, Ashland, OR).

***In vivo* bioluminescence imaging (BLI) and analysis with IVIS**

An IVIS Spectrum/CT (Perkin Elmer) *in vivo* optical instrument was used to image bacterial bioluminescence and phagocyte fluorescence in the mice. Mice were anesthetized using isoflurane prior to and during image acquisition. For bioluminescent imaging mice were scanned at the appropriate wavelength for an amount of time to allow for bioluminescent signal detection to occur from each mouse. Mice were generally imaged 24 hours post-infection, then every other day throughout the infection. For analysis, Living Image software (Perkin Elmer) was used to draw a region of interest around each bioluminescent infection area, and total flux (photons/second) was measured for the infection site. A background region was also drawn to determine the background signal for each scan. Background-free total flux was calculated by subtracting the total flux of the background region from that of the infected region.

For phagocyte fluorescence imaging of Lys^{EGFP}, $Catchup^{IVM\text{-}red}$, or $Csfr1^{LsL\text{-}DTR\text{-}mCherry}\_\_LysM^{Cre}$ mice wildtype littermates that did not have the fluorescent protein were used at auto fluorescent background controls. Mice were scanned using filter pairs for GFP, mCherry, and tdTomato as indicated in the figure legends. A region of interest was drawn around the

infection area, and total flux was determined after subtracting the total flux of wildtype controls.

Detection of reactive oxygen and nitrogen species

In vivo and *in vitro* nitrate/nitrite levels were measured using a modified Griess assay (Sigma Aldrich #G4410) following the manufacturer's protocol. *In vivo* hydrogen peroxide (H_2O_2) production was measured with the Amplex Red Assay (ThermoFisher #A2218) following the manufacturer's protocol.

Measuring cAMP levels

Biopsy samples were collected, weighed, and flash frozen. Frozen samples were then homogenized in 5-10 volumes (mL solution/gram tissue), based on tissue weight, of 5% TCA. Homogenate was then centrifuged at 1500 x g for 10 minutes and the supernatant was removed and moved to a clean 1.5 mL tube. TCA was then extracted from the sample by mixing with water-saturated ether and discarding the top layer. To remove residual ether, the sample was placed on a heat block at 70℃ for 5 minutes. Samples were then assayed for cAMP concentration using an ELISA (Cayman Chemical #581001) following the manufacturer's protocol.

MALDI-MS imaging

Skin biopsies were sectioned at 12-µm thickness and thaw-mounted onto ITO-coated glass slides. Serial sections were collected for H&E staining. MALDI matrix 9-aminoacridine (9AA) was spray-coated onto the ITO-coated slides via an automatic sprayer (TM Sprayer; HTX Technologies). 9AA was made up as 5 mg/mL in 90% methanol, and four passes were used with a nozzle temperature of 85 °C, a flow rate of 0.15 mL/min, 2-mm track spacing, and a stage velocity of 700 mm/min. Nitrogen was used as the nebulization gas and was set to 10-gauge pressure (psig). Images were acquired with a 15T Fourier transform ion cyclotron resonance mass spectrometer (FTICR MS, SolariX; Bruker Daltonics) equipped with an Apollo II dual ion source and Smartbeam II 2 kHz Nd:YAG laser that was frequency tripled to a 355-nm wavelength. Data were collected in the negative ion mode using 2,000 laser shots per pixel with the laser operating at 2 kHz. The pixel spacing was 100 µm (center-to-center distance) in both x and y dimensions. Data were collected from m/z 200–1,400. Tentative metabolite identifications were made by accurate mass, typically better than 1 ppm.

Immunoblotting

Western blots were performed as previously described [82]. Protein samples were resolved by SDS-PAGE, transferred to a nitrocellulose membrane, and probed with commercially available primary antibodies against PTGES1, PTGES2, SOCS-1, total-STAT-1, phosphorylated STAT-1 (Y701), total- and phosphorylated STAT-3 (S727) (all at 1:1000; Cell signaling), or β-actin (1:10,000; Invitrogen). Membranes were then washed and incubated with appropriate fluorophore-conjugated secondary antibodies (1:10,000, anti-rabbit IgG, IRDye

800CW antibody, #926-32211, Licor). Relative band intensities were quantified using ImageJ software (NIH).

Nanostring and gene enrichment analysis

Global gene expression in infected skin biopsies from wildtype hyperglycemic and euglycemic mice was assessed by the NanoString nCounter gene expression system (Nanostring, Seattle, WA). Mouse Myeloid Innate Immunity panel for 770 genes in 19 different pathways was used for the analysis. Designed CodeSet underwent extensive quality control to avoid cross-hybridization to non-target molecules in samples. RNA was extracted from the infected skin as described in RNA isolation above. The purity and concentration of the RNA were confirmed spectrophotometrically with a Nanodrop (Thermo Scientific, Waltham, MA). 100 ng of RNA (20 ng/µl) was hybridized with probe CodeSet before running samples on NanoString. nSolver 3.0 software was used to assess the quality of the run, followed by the deletion of the low-quality sample from further analysis. Two-sided hypergeometric statistical analysis was performed with the Kappa Score threshold setting of 0.3. Enrichment depletion was calculated based on Benjamini-Hochberg Correlated p-values of <0.05.

Bone marrow-derived macrophage generation

Bone marrow cells were flushed from both tibias and femurs of mice with ice-cold PBS. Cells were centrifuged, and red blood cells were lysed using ACK buffer. Cells were adjusted to

$1x10^6$ cells/mL in DMEM with FBS (5%), M-CSF (20 ng/mL), and GM-CSF (10 ng/mL) and maintained at 37°C with 5% CO_2, and the cell culture media containing M-CSF and GM-CSF was changed every 3 days until day 7 when the cells were fully differentiated and utilized for studies.

Phagocytosis and bacterial killing assays

Bacterial phagocytosis and killing were performed as previously shown [82,148,150,151]. Briefly, BMDMs (2×10^5/well) were plated into two individual 96-well plates with opaque walls and clear bottoms. Cells were pretreated with 10 μM iKIR or scrambled (SCR) KIR peptide for 1 hour before the addition of GFP-MRSA at a multiplicity of infection of 50:1 [150]. Infected cells were incubated for 1 hour to allow for phagocytosis to occur with both plates then washed with warm PBS, and GFP fluorescence measured on the first plate. The second plate was then maintained in PBS with SCR KIR or PBS with iKIR peptide and was incubated for another 2 hours for killing assays. To determine the role of NO in iKIR-mediated microbial killing, cells were treated with 50 μM of the iNOS inhibitor 1400W dihydrochloride (Tocris). To measure the intensity of intracellular GFP fluorescence, extracellular fluorescence was quenched with 500 μg/mL trypan blue, and the GFP fluorescence was quantified using a fluorimeter plate reader. Trypan blue served as a blank. A reduction in GFP fluorescence in the killing plate relative to the phagocytosis plate indicated bacterial killing [150,152]

Statistical analysis

Results are shown as a mean +/- SEM and were analyzed using GraphPad Prism 8.0 software (GraphPad Software, San Diego, CA). For comparisons between two experimental groups, a Mann-Whitney test was used, and for comparisons among three or more experimental groups, one-way ANOVA followed by Bonferroni multiple comparison test was used. Two-way ANOVA with repeated measures followed by Bonferroni multiple comparison test was used to compare infection areas over time between two or more groups. $p<0.05$ was considered significant.

CHAPTER 3

RESULTS

Part I – Role of PGE_2 in hyperglycemic skin host defense

Diet-induced obese and hyperglycemic mice have impaired bacterial clearance and PGE_2 production during skin infection

Previous work in the lab has demonstrated that STZ-induced hyperglycemic mice have impaired skin host defense that correlates with impaired production of PGE_2 [147]. We sought to examine if this same infection phenotype existed in a secondary diet-induced obesity (DIO) model of insulin-resistant hyperglycemia. C57BL6/J mice were placed on either a low fat (LFD) or high fat (HFD) diet for three months in which either 10% (LFD) or 60% (HFD) of calories were derived from saturated fats. After 3 months of feeding, mice on the HFD displayed significantly higher body weight (**Fig. 5A**) and blood glucose levels (**Fig. 5B**) than LFD controls. Next, we infected these mice subcutaneously with 3 million CFU of the USA 300 LAC strain of MRSA. Mice fed the HFD had significantly larger skin lesions over the course of a 9-day infection compared to mice fed the LFD (**Fig. 5C**), which correlated with a significantly higher bacterial burden in the skin on day 9 post-infection (**Fig. 5D**). These data demonstrate that DIO mice with hyperglycemia have impaired skin host defense against MRSA compared to lean euglycemic control animals.

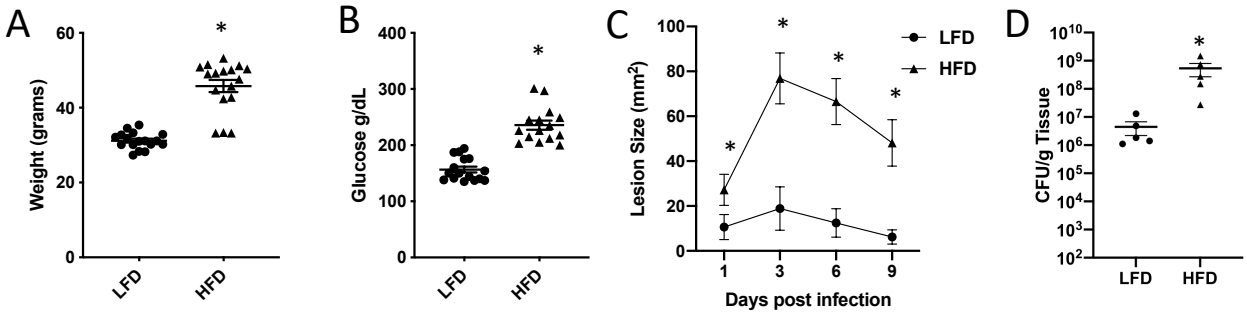

Figure 5. Subcutaneous MRSA skin infection in LFD and HFD mice. A.) Body weight of C57BL6/J mice placed on a low or high fat diet (LFD or HFD) for 3 months. **B.)** Blood glucose readings from mice in **A.** **C.)** Infection area as measured every other day with a caliper in mice from **A** infected subcutaneously (s.c.) with $3x10^6$ CFU of the USA300 strain of MRSA. **D.)** Bacterial burden as measured by CFU in skin biopsy homogenates collected from mice in **C** at day 9 post-infection. Data represent the mean ± SEM from 5-15 mice from 2-3 independent experiments. **A** and **B.)** *p<0.05 vs. LFD (Mann-Whitney test). **C.)** *p<0.05 vs. LFD (Two-way ANOVA followed by Bonferroni multiple comparison test) **D.)** *p<0.05 vs. LFD (Mann-Whitney test).

Next, the levels of PGE_2 in the skin of LFD and HFD fed mice were examined to see if a deficit in PGE_2 production was present in the skin of infected HFD animals. When biopsies from both LFD and HFD fed animals at day 3 and day 9 post-infection were examined for levels of PGE_2, HFD mice had significantly lower levels of PGE_2 at day 3 post-infection but not at day 9 post-infection compared to euglycemic controls (**Fig. 6A**). To examine if HFD mice would benefit from exogenous PGE treatment similar to STZ-induced hyperglycemic mice, we infected both LFD and HFD animals with bioluminescent MRSA and treated them immediately after infection and twice daily during infection with an ointment containing the PGE analog misoprostol or vehicle control alone (petroleum jelly). When HFD mice were treated with misoprostol throughout a 9-day infection, we observed that misoprostol treatment improved infection area (**Fig. 6B**) and bacterial burden (**Fig. 6C**) in the skin at day 9 post-infection. Bioluminescent imaging confirmed that misoprostol treatment reduced bioluminescent bacterial burden at day

9 post-infection and as early as day 1 post-infection (**Fig. 6D and 6E**). To verify this phenotype was not specific to MRSA, we also infected LFD and HFD fed mice with the methicillin-susceptible *S. aureus* (MSSA) Newman strain, followed by treatment with misoprostol or vehicle control. We found that misoprostol treatment also significantly reduced the bacterial burden in HFD mice infected with MSSA (**Fig. 6F**). Overall, these data suggest a role for PGE_2 production during the skin immune response to MRSA and that its impaired production correlates with worse infection outcomes in HFD fed hyperglycemic mice.

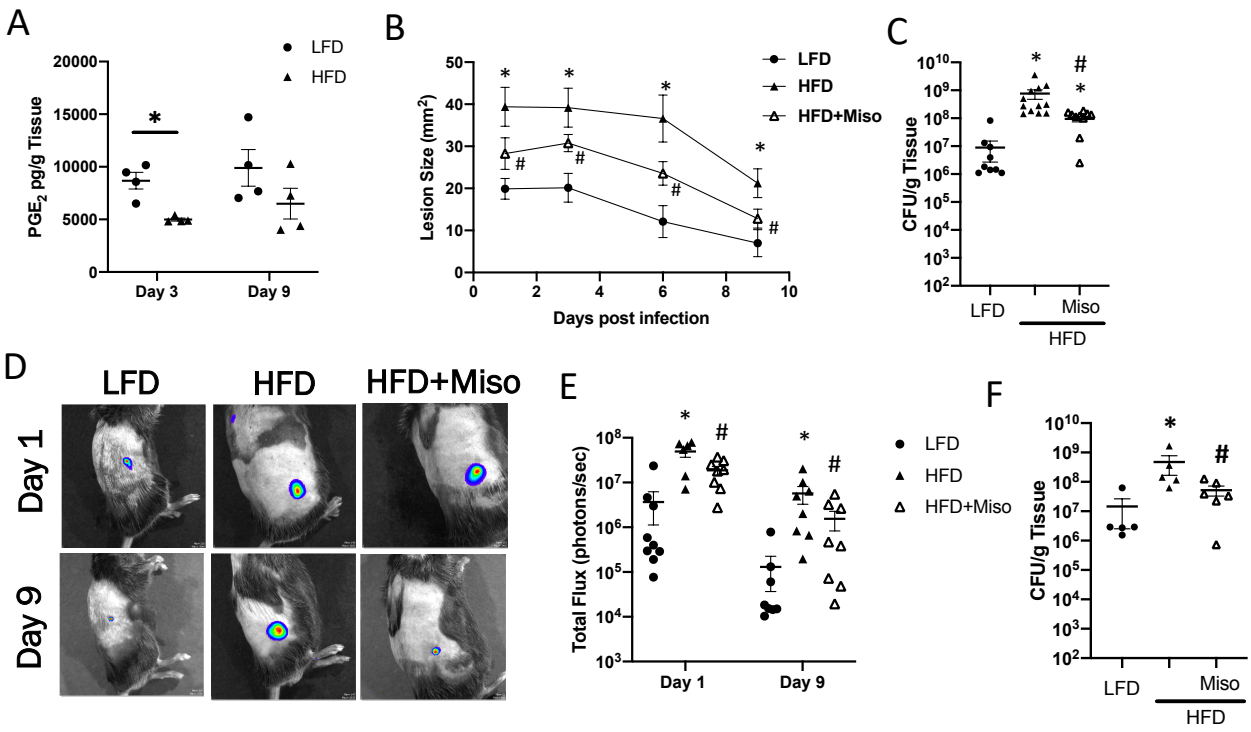

Figure 6. Misoprostol improves bacterial clearance in DIO mice. A.) Levels of PGE_2 as measured via ELISA from skin biopsy homogenates from LFD and HFD fed mice infected s.c. with MRSA at day 3 and day 9 post infection. **B.)** Bioluminescent infection area in LFD and HFD mice infected with bioluminescent MRSA and treated with or without misoprostol as measured using the *in vivo* animal imaging (IVIS Spectrum) detection system. **C.)** Bacterial burden as measured by CFU at day 9 post infection in mice infected and treated as in **B. D.)** Representative images of bioluminescent MRSA in the skin of mice treated as in **B** using planar bioluminescent imaging. **E.)** Total flux (photons/second) quantification of images from **D** using the IVIS Spectrum. **F.)** Bacterial burden as measured via CFU at day 9 post infection in LFD and HFD mice infected with the MSSA Newman strain and treated with or without misoprostol. Data represent the mean ± SEM from 4-12 mice from 2-3 independent experiments. **A.)** *p<0.05 vs. LFD. (Mann-Whitney Test) **B.)** *p<0.05 vs. LFD. #p<0.05 vs. HFD (Two-way ANOVA followed by Bonferroni multiple comparison test). **C-F.)** *p<0.05 vs. LFD. #p<0.05 vs. HFD (One-way ANOVA followed by Bonferroni multiple comparison test).

Misoprostol treatment demonstrates efficacy during a delay in treatment

Based on previous results, misoprostol represents a possible therapeutic strategy to improve skin and soft tissue infections in patients with hyperglycemia outside the use of antibiotics. However, as patients cannot treat themselves at the moment of infection as we have previously done, we sought to examine the efficacy of misoprostol treatment in an

established infection model. Therefore, LFD and HFD mice were infected as had been done previously, however, topical misoprostol ointment was not applied until day 3 post-infection and twice daily thereafter. As early as day 6 post-infection (day 3 post-treatment) a significant reduction in infection area in the skin of the misoprostol treated HFD animals was observed (**Fig. 7A**). Utilizing bioluminescent *in vivo* imaging, these results were confirmed, showing similar bacterial burden between the groups at day 3 post-infection prior to treatment and a reduction in bacterial load at day 9 post-infection with misoprostol treatment (**Fig. 7B and 7C**). Biopsies harvested from these mice at day 9 post-infection also showed a reduction in bacterial burden when plated for CFU (**Fig. 7D**).

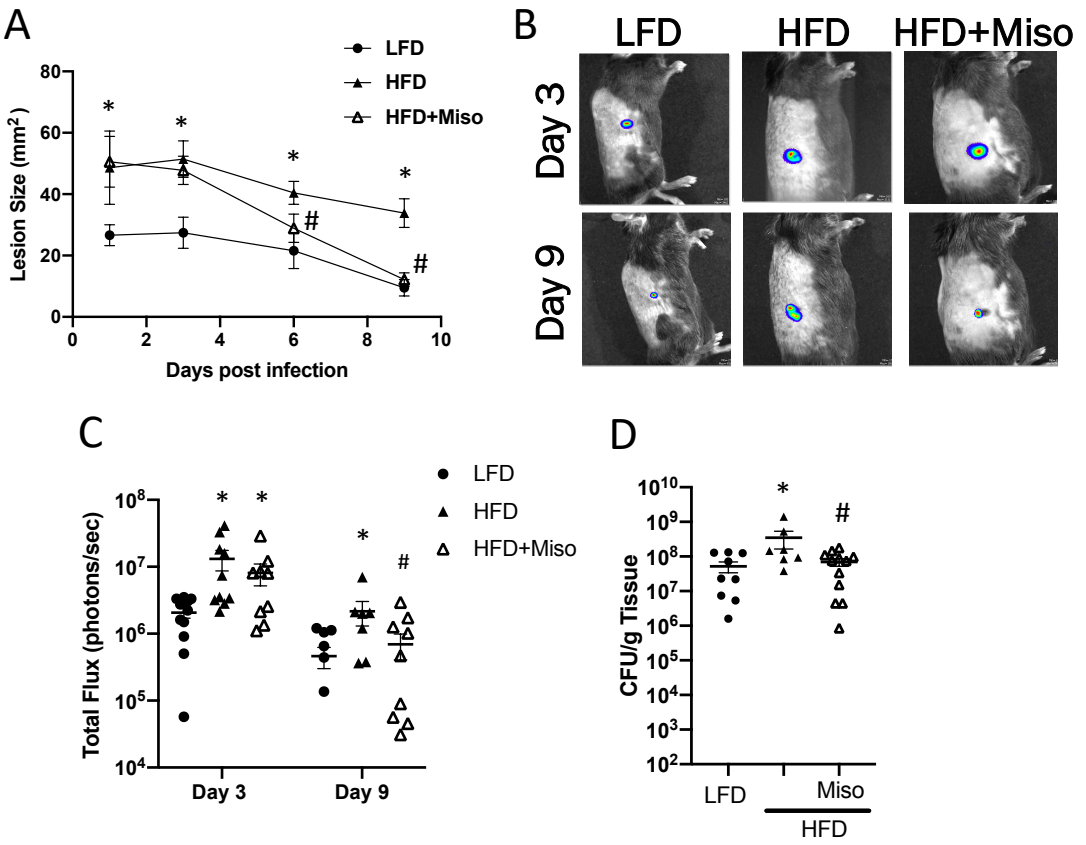

Figure 7. Misoprostol treatment improves bacterial clearance in delayed treatment model. A.) Bioluminescent infection area in LFD and HFD fed mice infected with bioluminescent MRSA treated with misoprostol or vehicle control starting at day 3 post-infection measured using the IVIS Spectrum. **B.)** Representative images of bioluminescent MRSA in mice infected and treated as in **A** taken using the IVIS Spectrum at days 3 and 9 post-infection. **C.)** Quantification of Total Flux from bioluminescent MRSA from mice treated as in **B** using the IVIS Spectrum at day 3 and day 9 post-infection. **D.)** Bacterial burden as measured by CFU from skin biopsy homogenates from mice treated as in **A** at day 9 post-infection. Data represent the mean ± SEM from 7-11 mice from 2-3 independent experiments. **A.)** *p<0.05 vs. LFD. #p<0.05 vs. HFD (Two-way ANOVA followed by Bonferroni multiple comparison test). **C and D.)** *p<0.05 vs. LFD. #p<0.05 vs. HFD (One-way ANOVA followed by Bonferroni multiple comparison test).

To confirm the efficacy of misoprostol in improving infection outcome with delayed treatment was not dependent on the model of insulin-resistant hyperglycemia, we repeated these experiments in STZ-induced hyperglycemic mice. Similar to our results in misoprostol-treated HFD mice, infected STZ mice treated with misoprostol at day 3 post-infection had

significantly reduced surface lesion size starting at day 6 post-infection (day 3 post initial treatment) until day 9 when biopsies were harvested (**Fig. 8A**). Skin biopsy homogenates from these mice plated for CFU also demonstrated significantly reduced bacterial burden in STZ mice treated with misoprostol compared to untreated mice (**Fig. 8B**). When we repeated the infection and treatment with bioluminescent MRSA, these results were further confirmed. Both groups of infected STZ-treated mice had similar levels of bioluminescent bacterial burden at day 3 post-infection, prior to misoprostol treatment, but the misoprostol treated mice had significantly reduced bioluminescent bacterial burden at day 9 post-infection (**Fig. 8C and 8D**). Taken together, these data demonstrate that misoprostol enhanced bacterial clearance during skin infection is not hyperglycemia model dependent and has efficacy in an already established infection, suggesting a potential therapeutic strategy to treat these antibiotic resistant infections.

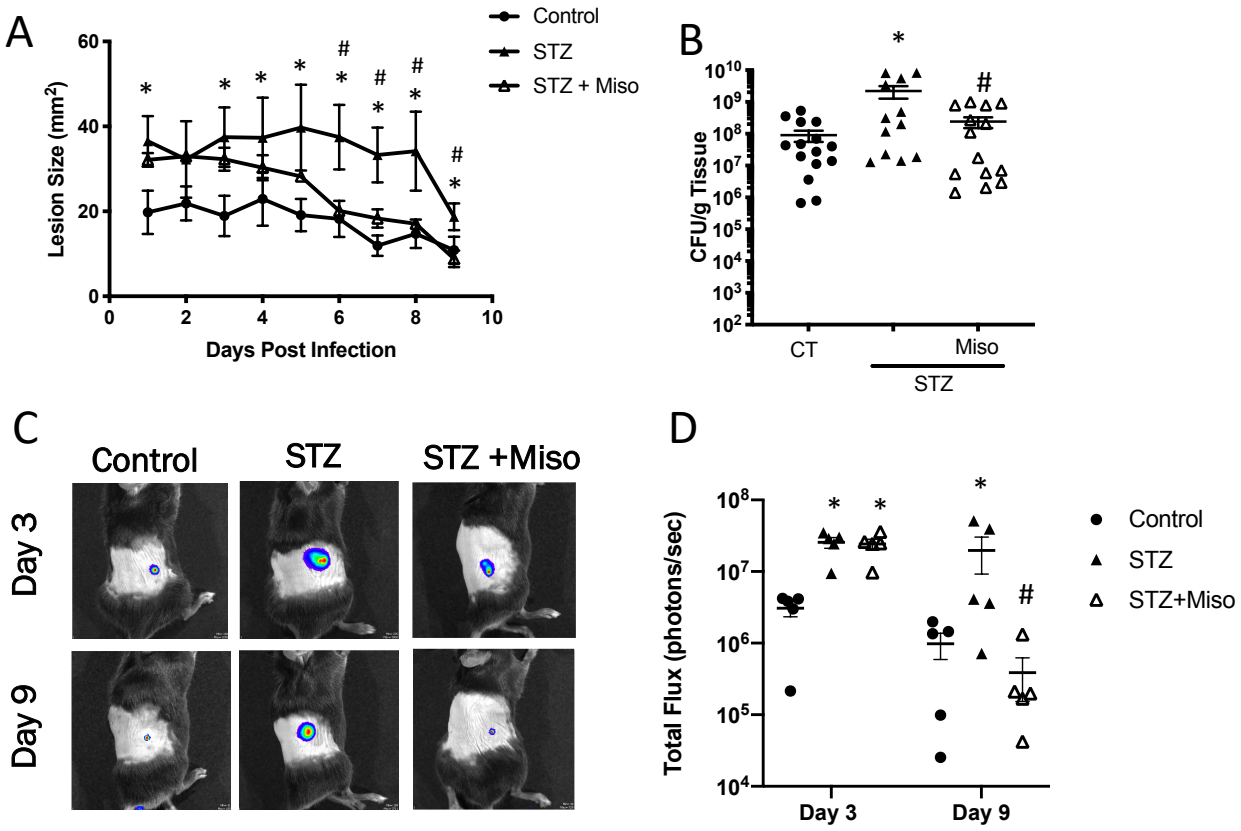

Figure 8. STZ-induced hyperglycemic mice benefit from delayed treatment model. A.) Infection area in control and STZ-induced hyperglycemic mice infected with MRSA and treated with misoprostol or vehicle control starting at day 3 post-infection measured via calipers. **B.)** Bacterial burden as measured by CFU from skin biopsy homogenates from mice treated as in **A** at day 9 post-infection. **C.)** Representative images of bioluminescent MRSA in mice infected and treated as in **A** taken using the IVIS Spectrum at days 3 and 9 post-infection. **D.)** Quantification of Total Flux from bioluminescent MRSA from mice treated as in **A** using the IVIS Spectrum at day 3 and day 9 post-infection. Data represent the mean ± SEM from 4-15 mice from 2-3 independent experiments. **A.)** *p<0.05 vs. Control. #p<0.05 vs. STZ (Two-way ANOVA followed by Bonferroni multiple comparison test). **B** and **D.)** *p<0.05 vs. Control. #p<0.05 vs. STZ (One-way ANOVA followed by Bonferroni multiple comparison test).

Hyperglycemic mice have impaired PTGES1 induction during skin infection

PGE_2 synthesis is a tightly regulated process involving a series of specific enzymatic reactions [41,43]. In previous studies examining PGE_2 production during skin infection in hyperglycemic mice, we observed no difference in *Ptgs1* (COX-1) or *Ptgs2* (COX-2) gene

expression between control or hyperglycemic infected mice [147]. Therefore, we hypothesized that a failure of one of the two prostaglandin E2 synthases (PTGES1 and PTGES2) is likely contributing to impaired PGE_2 production in the PGE_2 synthesis pathway [43].

To test this hypothesis, protein levels of PTGES1 and PTGES2 from skin biopsies taken at day 3 post-infection in LFD and HFD fed mice were examined via immunoblot. We observed a stark and consistent failure to induce PTGES1 in the skin of mice fed the HFD (**Fig. 9A and 9B**), with little difference in PTGES2 expression (**Fig. 9A and 9C**). These data matched with previous observations [147] and our initial hypothesis. The results also correlated with the expression pattern of these enzymes as PTGES1 expression is induced during inflammation, and thought to produce the majority of PGE_2 during inflammation, while PTGES2 is constitutively expressed to maintain homeostatic levels of PGE_2 [43].

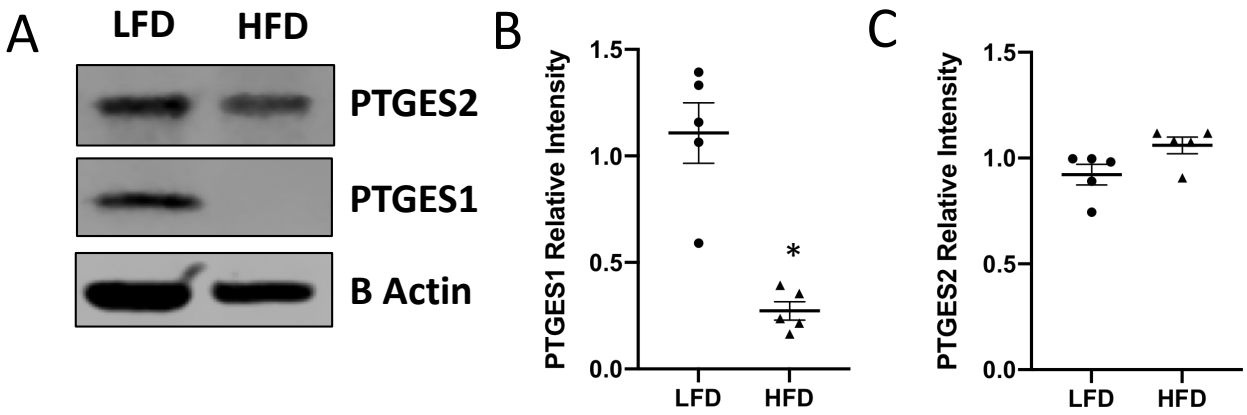

Figure 9. DIO hyperglycemic mice have impaired PTGES1 induction during infection. A.) Representative Western blot for PTGES1, PTGES2, and Beta Actin from biopsies collected at day 3 post-infection in low and high fat diet fed mice. **B.)** Quantification of densitometry values for PTGES1 taken from Western blots of skin biopsy homogenates as in **A. C.)** Quantification of densitometry values for PTGES2 taken from Western blots of skin biopsy homogenates as in **A.** Data represent the mean ± SEM from 5 mice from 2-3 independent experiments. **B** and **C.)** *p<0.05 vs. LFD (Mann-Whitney Test).

To confirm these results and examine where PGE_2 synthesis may be actively occurring within the abscess architecture within the skin, *in situ* hybridization against *Ptges1 and Ptges2* mRNA was performed. Using histology samples from LFD and HFD fed mice at day 3 post-infection, a lower percentage of *Ptges1+* cells was observed in biopsies from hyperglycemic animals (**Fig. 10A and 10B**). However, we did detect a slight increase in the percentage of *Ptges2*+ cells, possibly compensating for reduced *Ptges1* expression (**Fig. 10A and 10C**). One of the more intriguing findings from these experiments was the location of *Ptges1* and *-2* expression both at the periphery of the abscess but also within the abscess itself (**Fig. 10A**), suggesting a role for PGE_2 not only in the formation of the abscess and immune cell recruitment but also in bacterial elimination/control within the abscess. However, these data demonstrate that DIO hyperglycemic mice have impaired PTGES1 induction in response to bacterial stimuli at both the protein and mRNA level.

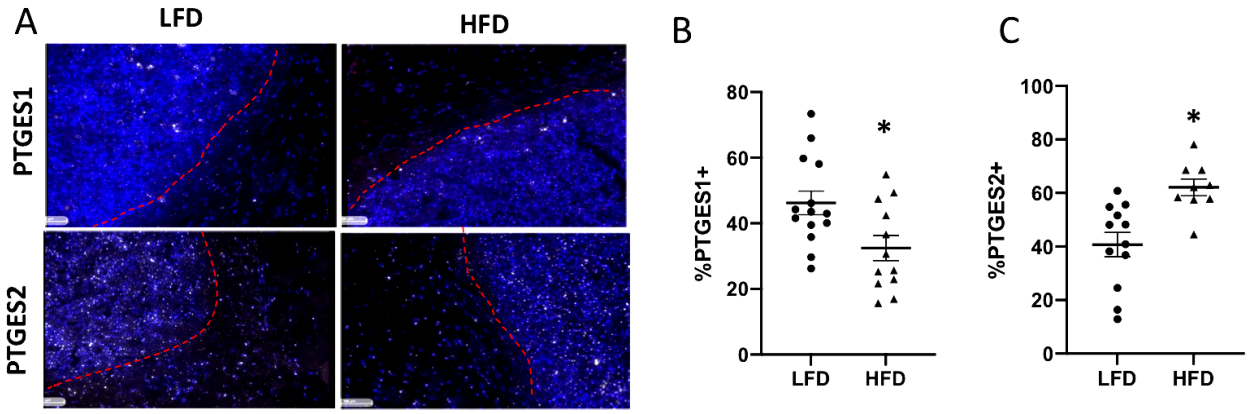

Figure 10. *In situ* hybridization against *Ptges1* and *Ptges2*. A.) Representative images of *in situ* hybridization against *Ptges1* and *Ptges2* (white specks) counterstained with DAPI from abscess biopsies collected from mice infected s.c with MRSA at day 3 post-infection. Red lines indicate edge of abscess **B.)** Quantification of the percentage of cells positive for *Ptges1* as determined via HALO software from slides stained as in **A**. Each point represents the average from 3 fields of view at 40x. **C.)** Quantification of the percentage of cells positive for *Ptges2* as determined via HALO software from slides stained as in **A**. Each point represents the average from 3 fields of view at 40x. Data represent the mean ± SEM from 7-11 mice from 2-3 independent experiments. **B** and **C.)** *p<0.05 vs. LFD (Mann-Whitney Test).

Since STZ-induced hyperglycemic mice also displayed impaired production of PGE_2 during MRSA skin infection, we wanted to examine if these mice also had a similar deficit in PTGES1 induction contributing to this phenotype. When skin biopsy homogenates from infected control and STZ-induced hyperglycemic mice were analyzed for protein levels of PTGES1 and PTGES2 via immunoblot, we again saw a stark lack of PTGES1 expression (**Fig. 11A and 11B**) as well as similar expression of PTGES2 (**Fig. 11A and 11C**) at day 3 post-infection. *In situ* hybridization against *Ptges1* and *Ptges2* mRNA on biopsy sections from these same mice revealed similar results with a lower percentage of cells positive for *Ptges1* in the skin of STZ-induced hyperglycemic mice than controls (**Fig. 11D**). However, no difference was seen in the percentage of cells positive for *Ptges2* between our two infection groups (**Fig. 11E**). While this suggests a common hyperglycemia-dependent mechanism limiting PTGES1 induction, further studies will be needed to rule out side effects of either hyperglycemia model that could contribute to this phenotype, such as obesity itself or off target effects of STZ.

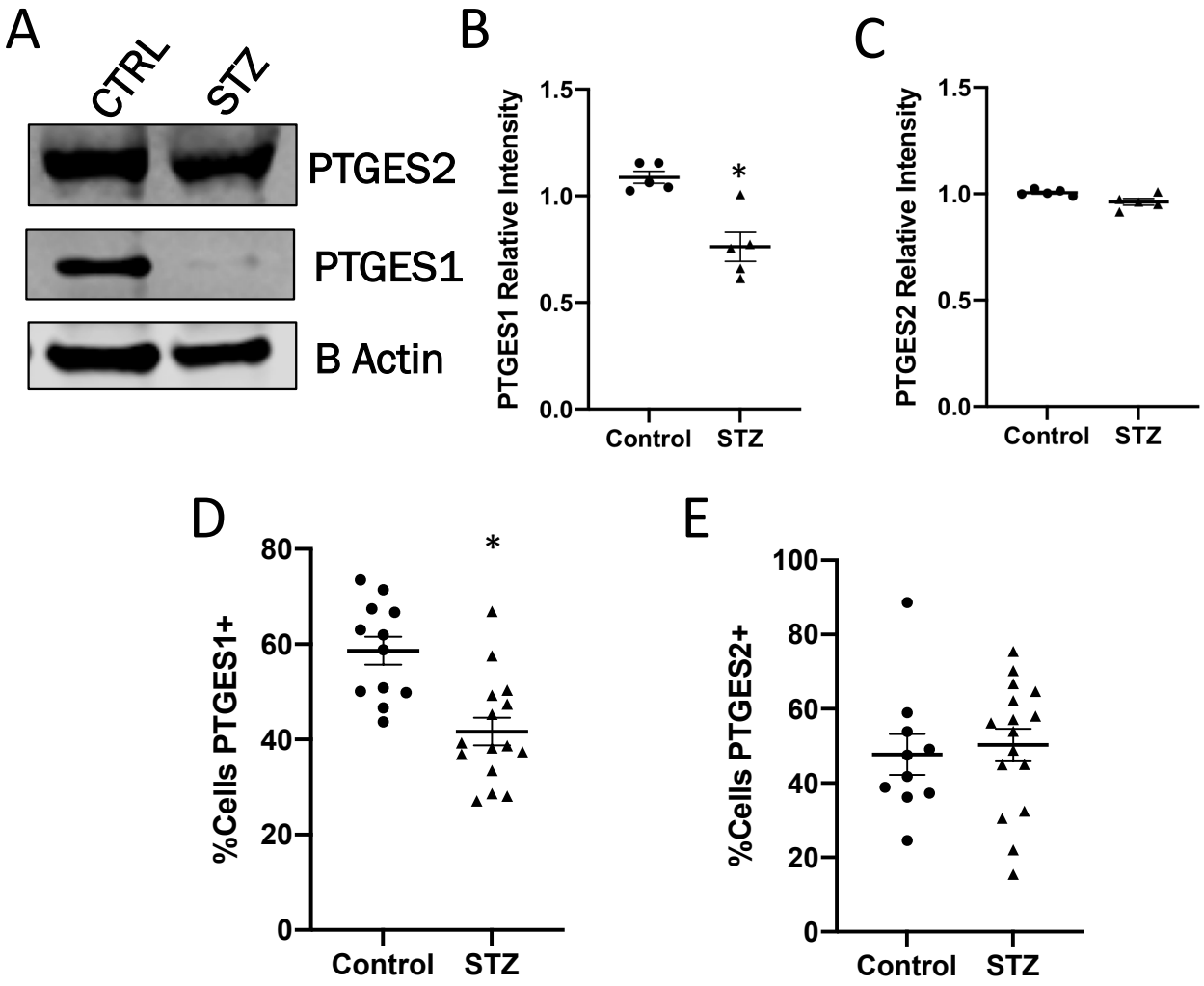

Figure 11. STZ mice have impaired PTGES1 induction during skin infection. A.) Representative Western blot for PTGES1, PTGES2, and Beta Actin from biopsies collected at day 3 post-infection in control and STZ-induced hyperglycemic mice. **B.)** Quantification of densitometry values for PTGES1 taken from Western blots of skin biopsy homogenates as in **A. C.)** Quantification of densitometry values for PTGES2 taken from Western blots of skin biopsy homogenates as in **A. D.)** Quantification of the percentage of cells positive for *Ptges1* as determined via *in situ* hybridization quantified utilizing HALO software from biopsies collected at day 3 post-infection in control and STZ-induced hyperglycemic mice. **E.)** Quantification of the percentage of cells positive for *Ptges2* from biopsies as in **D** via HALO software. Data represent the mean ± SEM from 5-12 mice from 2-3 independent experiments. *p<0.05 vs. Control (Mann-Whitney Test).

Misoprostol enhances IL-1β and CXC chemokine production

PGE_2 is produced rapidly during the process of inflammation and has been shown to both enhance and impair proinflammatory cytokine and chemokine release dependent on tissue localization and pathogen [54,56,59]. Therefore, we sought to examine possible impacts of misoprostol treatment on the inflammatory milieu in the skin of infected hyperglycemic mice. The abundance of 17 different proinflammatory cytokines and chemokines was analyzed from skin biopsy homogenates taken at day 3 post-infection in LFD and HFD mice treated with or without misoprostol via bead multiplex array. Upon analysis, we observed that misoprostol increased the levels of several of these cytokines. Of note, three chemokines known to be critical for neutrophil recruitment in response to skin infection or injury, CXCL1, CXCL2, and CXCL5 [10,13,72], were significantly increased in infected HFD mice treated with misoprostol (**Fig. 12A**). Furthermore, IL-1β, a cytokine known to promote the expression of CXCL1, -2, and -5, as well as being critical for *S. aureus* abscess formation [13,119], was also significantly enhanced with misoprostol treatment in hyperglycemic HFD mice. IL-1β has also been shown to be critical for neutrophil recruitment during *S. aureus* skin infection [117,118].

We also examined the expression of these cytokines and chemokines in the skin of control and STZ-induced hyperglycemic mice treated with or without misoprostol at day 3 post-infection. We again observed significantly increased expression of IL-1β, CXCL1, and CXCL2 in the skin of STZ-induced hyperglycemic mice treated with misoprostol (**Fig. 12B**). However, we did not observe any changes in CXCL5 production in misoprostol-treated STZ hyperglycemic mice. Overall, these data point to misoprostol treatment activating a similar

cytokine/chemokine profile to improve infection outcome in both models of hyperglycemia. These results led us to hypothesize that PGE_2 produced during infection may promote IL-1β maturation and release which in turn might promote chemokine expression (CXCL1 and CXCL2) to drive phagocyte recruitment resulting in proper abscess formation and bacterial control/clearance.

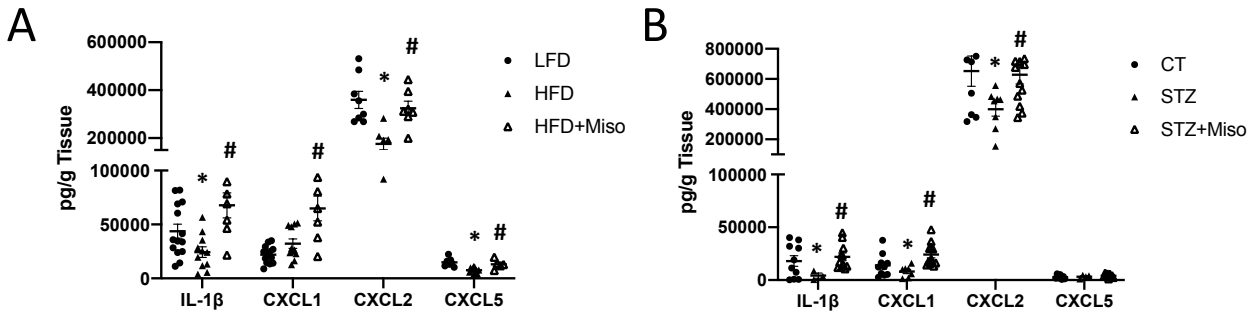

Figure 12. Misoprostol treatment enhances chemokine release during skin infection. A.) Levels of IL-1β, CXCL1, CXCL2, and CXCL5 in skin biopsy homogenates collected at day 3 post infection in LFD and HFD mice treated with or without misoprostol as measured using a bead array multiplex (Eve Technologies). **B.)** Levels of the same cytokines as measured in **A** in skin biopsy homogenates from control and STZ mice treated with or without misoprostol at day 3 post infection. Data represent the mean ± SEM from 5-14 mice from 2-3 independent experiments. *p<0.05 vs. LFD or CT. #p<0.05 vs. HFD or STZ (One-way ANOVA followed by Bonferroni multiple comparison test).

Misoprostol enhances CXCR2+ neutrophil and monocyte recruitment

The hallmark of *S. aureus* infection at multiple sites throughout the body is the formation of a neutrophilic abscess that is dependent on abundant neutrophil migration to the site of infection [122,124]. While neutrophils are the predominant cell type recruited during early infection and within the abscess, macrophages have been shown to interact with the abscess capsule and play a role in its breakdown prior to wound healing [114,125]. Based on our data that misoprostol treatment enhances the expression of chemokines known to drive

neutrophil recruitment in response to skin infection or injury, we performed flow cytometry analysis on infection biopsies from LFD and HFD infected and misoprostol treated mice. Collecting biopsies at day 3 post-infection, we first looked at the presence of monocytes (CD11b+Ly6c+), neutrophils (CD11b+Ly6g+), and macrophages (CD11b+F4/80+). Initially, no significant difference was seen in the total numbers of either monocytes (**Fig. 13A**), neutrophils (**Fig. 13B**), or macrophages (**Fig. 13C**) between infection or treatment groups. While there was a slight decrease in the overall numbers of monocytes and macrophages in HFD groups, this did not appear to be impacted by misoprostol treatment.

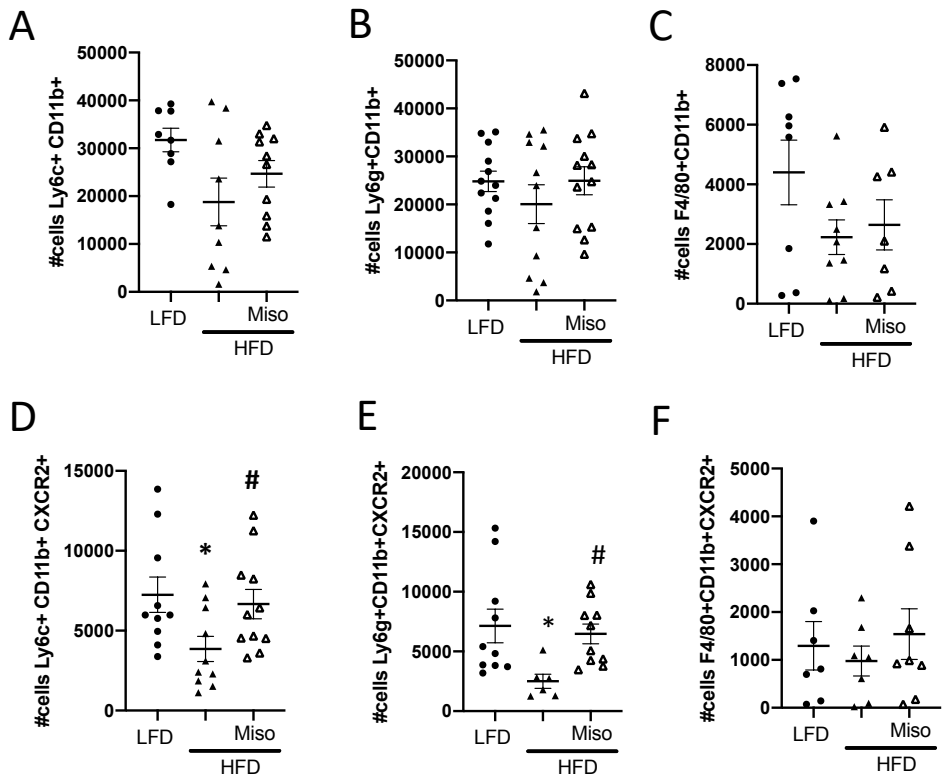

Figure 13. Misoprostol enhances CXCR2+ phagocyte recruitment during skin infection. A.) Total number of monocytes (Ly6c+CD11b+) in skin biopsies from low and high fat diet mice infected s.c. with MRSA and treated with or without misoprostol at day 3 post-infection. **B.)** Total number of neutrophils (Ly6g+CD11b+) in skin biopsies from mice treated as in **A**. **C.)** Total number of macrophages (F4/80+CD11b+) in skin biopsies from mice treated as in **A**. **D.)** Total number of CXCR2+ monocytes from skin biopsies from **A**. **E.)** Total number of CXCR2+ neutrophils from skin biopsies from **B**. **F.)** Total number of CXCR2+ macrophages from skin biopsies in **C**. Data represent the mean ± SEM from 5-10 mice from 2-3 independent experiments. *p<0.05 vs. LFD. #p<0.05 vs. HFD (One-way ANOVA followed by Bonferroni multiple comparison test).

Since CXCL1, CXCL2, and CXCL5 all bind to the same cognate receptor, CXCR2, we hypothesized that more specific cell recruitment might be occurring via this receptor. It has been well documented by several groups that CXCR2+ monocyte and neutrophil recruitment to the site of skin wounds is critical not only for initial pathogen clearance but also for wound healing and revascularization [10,13,29,72]. This could be crucial in hyperglycemic skin infection as human patients often experience impaired pathogen clearance and delayed wound healing

[74]. Previous work in the lab has also demonstrated that neutrophils in the skin of STZ-induced hyperglycemic mice lack the typical "swarming" behavior [112] that may be improved in specific CXCR2+ phagocytes which are better primed to eliminate and resolve skin infections. When the recruitment of CXCR2+ neutrophils and monocytes was examined in the skin of infected HFD hyperglycemic mice, we observed reduced numbers of both CXCR2+ monocytes and neutrophils compared to untreated LFD fed mice. Furthermore, treatment with misoprostol significantly increased the numbers of these CXCR2+ cell populations in the skin of HFD fed mice (**Fig. 13D and 13E**). However, no change was observed in CXCR2+ macrophage recruitment with misoprostol treatment (**Fig. 13F**).

Next, we examined the recruitment of the same cell populations in the skin of infected control and STZ-induced hyperglycemic mice at day 3 post-infection. While we again did not see changes in the overall numbers of monocytes, neutrophils, or macrophages with misoprostol treatment, we did observe a significant increase in the numbers of CXCR2+ monocytes and neutrophils in our STZ-induced hyperglycemic mice treated with misoprostol (**Fig. 14A** and **14B**). This correlated with the increased expression of CXCL1 and CXCL2 we had previously observed with misoprostol treatment and suggests misoprostol enhanced CXCR2+ monocyte and neutrophil recruitment is not hyperglycemia-model dependent. These data led us to hypothesize that PGE_2 synthesis may promote targeted cell recruitment to the site of infection during skin infection via enhanced secretion of CXC chemokines and these CXCR2+ phagocytes may be driving misoprostol enhanced bacterial clearance.

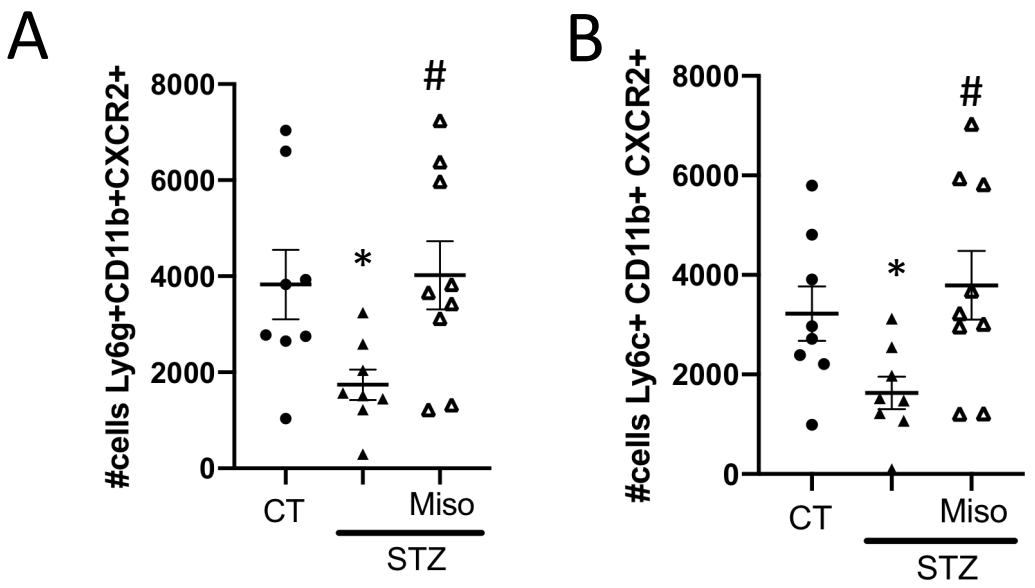

Figure 14. Enhanced CXCR2+ neutrophil and monocyte recruitment in STZ mice treated with misoprostol. A.) Total number of CXCR2+ neutrophils (Ly6g+CD11b+) in skin biopsies from control and STZ-induced hyperglycemic mice infected s.c. with MRSA and treated with or without misoprostol, at day 3 post-infection. **B.)** Total number of CXCR2+ monocytes (Ly6c+CD11b+) in skin biopsies from mice treated as in **A**. Data represent the mean ± SEM from 8-10 mice from 2-3 independent experiments. **p*<0.05 vs. CT. #*p*<0.05 vs. STZ (One-way ANOVA followed by Bonferroni multiple comparison test).

PTGER3 is necessary for the therapeutic benefit of misoprostol treatment

PGE_2 and misoprostol act by binding to four distinct GPCRs named EP1, EP2, EP3, and EP4 [51]. Since these receptors are primarily either $G_{\alpha s}$ or $G_{\alpha i}$ coupled, with cAMP being the secondary messenger, we examined cAMP levels in the skin of infected and treated mice. We hypothesized this would allow us to determine which receptor misoprostol was acting through during skin infection in hyperglycemic mice. In both LFD and HFD fed mice treated with misoprostol during MRSA skin infection lower tissue cAMP was observed compared to untreated animals (**Fig. 15A**). To confirm misoprostol treatment was lowering tissue cAMP, we also performed imaging mass spectrometry on biopsy sections from our HFD mice at day 3 post-infection. We again detected lower levels of tissue cAMP in the skin of our misoprostol-

treated mice compared to untreated animals (**Fig. 15B**). As EP3 is the sole $G_{\alpha i}$ coupled EP receptor known to lower intracellular cAMP [51], as well as the receptor for which misoprostol has the highest binding affinity *in vitro* [51,53], we hypothesized that EP3 was the primary receptor through which misoprostol was driving its therapeutic benefit during skin infection.

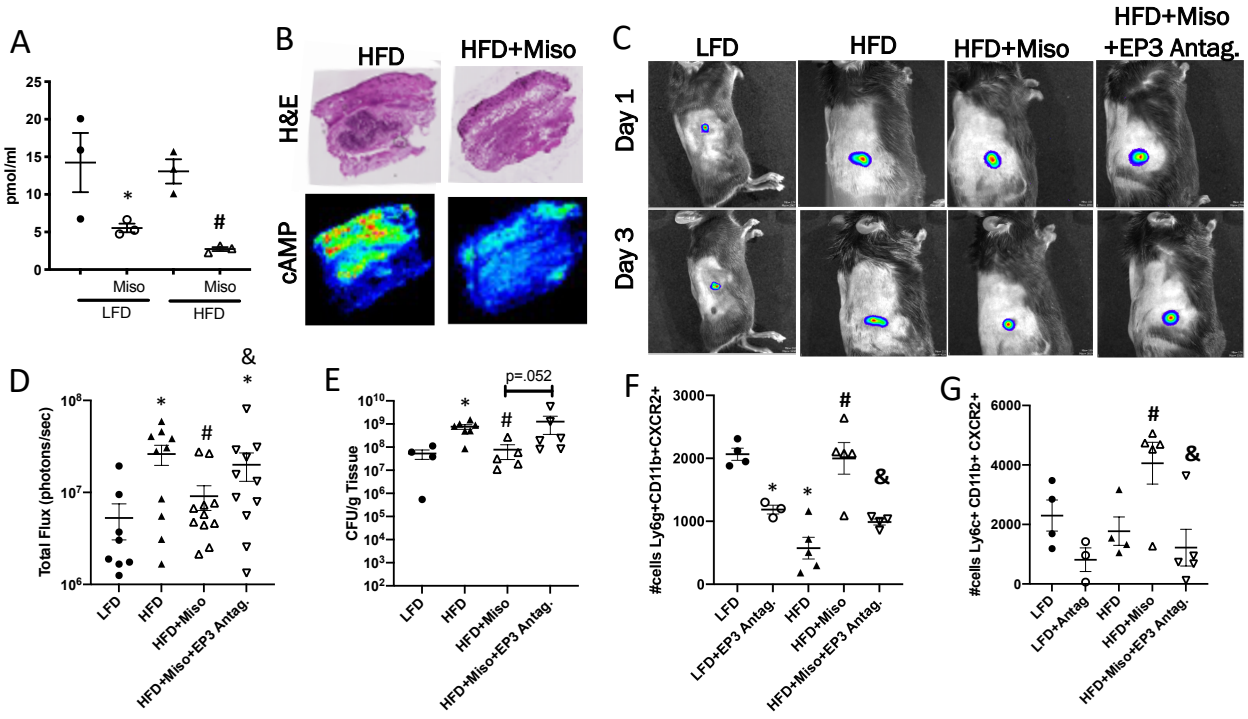

Figure 15. Examining EP3 antagonism during *S. aureus* skin infection and misoprostol treatment in HFD mice. A.) cAMP levels as measured via ELISA in skin biopsies taken at day 3 post-infection in LFD and HFD mice treated with or without misoprostol. **B.)** Representative images of Imaging Mass Spectrometry for cAMP from skin biopsies from mice treated as in **A**. **C.)** Representative images of bioluminescent MRSA in LFD and HFD mice treated with or without misoprostol plus an EP3 antagonist (L-798,106) at day 1 and day 3 post-infection using planar bioluminescent imaging. **D.)** Quantification of Total flux from mice treated as in **C** at day 3 post-infection using the IVIS Spectrum. **E.)** Bacterial burden as measured by CFU from skin biopsy homogenates from mice treated as in **C** at day 3 post-infection. **F.)** Total number of CXCR2+ neutrophils (Ly6g+CD11b+) from biopsies collected from mice treated as in **C** at day 3 post-infection. **G.)** Total number of CXCR2+ monocytes (Ly6c+CD11b+) from mice treated as in **C** collected at day 3 post-infection. Data represent the mean ± SEM from 3-6 mice from 2-3 independent experiments. *p<0.05 vs. LFD. #p<0.05 vs. HFD. &p<0.05 vs. HFD+Miso (One-way ANOVA followed by Bonferroni multiple comparison test).

To test this hypothesis, we initially performed a round of subcutaneous skin infections in which we treated hyperglycemic mice immediately after infection and twice daily during infection with either misoprostol or misoprostol combined with an EP3 antagonist (L-798,106). After a 3-day infection, we found that combined treatment with the EP3 antagonist and misoprostol did not have the same therapeutic benefit in HFD mice as misoprostol treatment alone. Mice treated with the antagonist had elevated bacterial burden as measured by both *in vivo* bioluminescent bacterial imaging (**Fig. 15C** and **15D**) and CFU (**Fig. 15E**), demonstrating increased bacterial burden despite misoprostol treatment. However, some of these mice did have reduced bacterial burden compared to untreated HFD animals, suggesting misoprostol may be acting in part through other EP receptors as it is receptor non-selective, or that our EP3 receptor antagonist was not fully inhibiting receptor signaling. Flow cytometry was also performed on infection biopsies collected from these mice to correlate EP3 activation during misoprostol treatment with improved CXCR2+ phagocyte recruitment. Hyperglycemic mice treated with the combination of the EP3 antagonist plus misoprostol had reduced numbers of both CXCR2+ neutrophils (**Fig. 15F**) and monocytes (**Fig. 15G**) compared to mice receiving misoprostol alone. Furthermore, euglycemic animals receiving the antagonist alone also had reduced numbers of these same CXCR2+ cell populations compared to untreated controls (**Fig. 15F** and **15G**). Together these data suggest a potential role for EP3 activation during skin infection in helping to promote CXCR2+ phagocyte recruitment in both hyperglycemic and euglycemic animals.

Next, we sought to investigate this phenotype of EP3 antagonism limiting the therapeutic benefit of misoprostol during skin infection in a second model of hyperglycemia.

We repeated these 3-day infections in control or STZ-induced hyperglycemic mice treated with or without misoprostol in conjunction with the EP3 antagonist (L-798,106). In this model, we found that hyperglycemic mice receiving the EP3 antagonist had significantly increased bacterial burdens than mice treated solely with misoprostol. While hyperglycemic mice treated with misoprostol had reduced bioluminescent bacterial burden as seen via *in vivo* imaging, combined treatment with the EP3 antagonist impaired misoprostol-enhanced bacterial clearance (**Fig. 16A** and **16B**). These imaging results were confirmed when infection biopsy homogenates were collected and plated for CFU at day 3 post-infection with mice receiving misoprostol treatment alone having significantly reduced bacterial burden compared to untreated hyperglycemic mice or those receiving combined treatment (**Fig. 16C**). Together these data strengthened our results from our previous HFD infection about the importance of EP3 during misoprostol treatment, however, we still wanted to confirm these data in a cleaner genetic model of EP3 deletion.

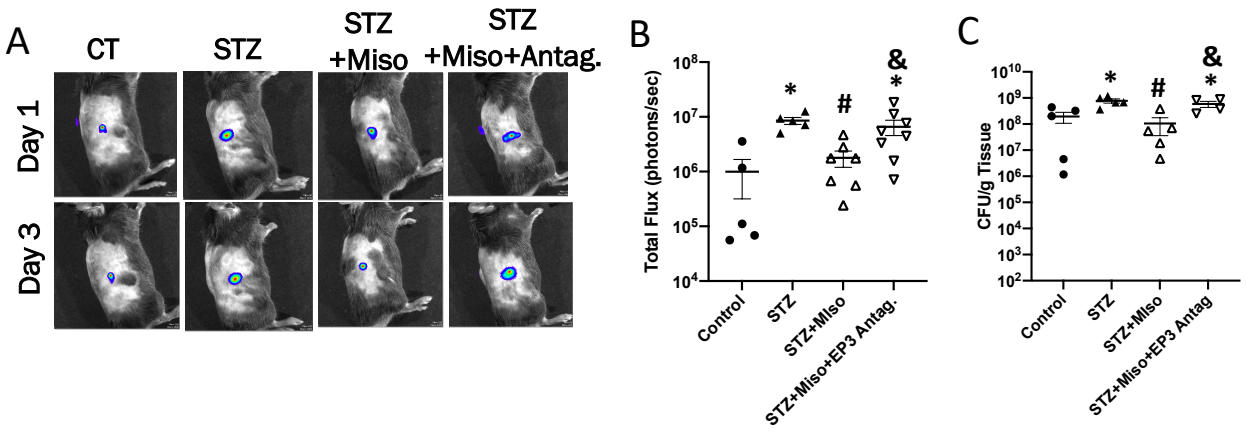

Figure 16. EP3 antagonism during *S. aureus* skin infection in STZ treated mice. A.) Representative images of bioluminescent MRSA in control and STZ-induced hyperglycemic mice treated with or without misoprostol plus an EP3 antagonist (L-798,106) at day 1 and day 3 post-infection using planar bioluminescent imaging. **B.)** Quantification of Total flux from mice treated as in **A** at day 3-post infection using the IVIS Spectrum. **C.)** Bacterial burden as measured by CFU from skin biopsy homogenates from mice treated as in **A** at day 3 post-infection. Data represent the mean ± SEM from 5-6 mice from 2-3 independent experiments. *p<0.05 vs. Control. #p<0.05 vs. STZ. &p<0.05 vs. STZ+Miso (One-way ANOVA followed by Bonferroni multiple comparison test).

To confirm these data in a genetic model of EP3 deletion, we infected control and EP3-/- mice that had been fed either the LFD or HFD for three months prior to infection with bioluminescent MRSA. Mice were treated with misoprostol or vehicle control immediately after infection and twice daily during infection as we have done previously. After 3 days of infection, we found that HFD EP3-/- mice had similar infection outcomes to wildtype HFD animals; however, HFD EP3-/- mice receiving misoprostol had worse infection outcomes compared to wildtype HFD animals receiving misoprostol. Compared to wildtype HFD mice receiving misoprostol, HFD EP3-/- mice treated with misoprostol had higher bacterial burden as measured by both *in vivo* imaging of bioluminescent MRSA (**Fig. 17A** and **17B**) and CFU (**Fig 17C**). Flow cytometry was also performed on infection biopsies from these animals to confirm our previous results demonstrating a link between EP3 activation and CXCR2+ phagocyte

recruitment during misoprostol treatment. Analysis revealed a similar phenotype in EP3-/- mice where mice lacking the EP3 receptor had reduced numbers of CXCR2+ neutrophils (**Fig. 17D**) and monocytes (**Fig. 17E**) regardless of glucose levels or misoprostol treatment. While these data do not rule out the involvement of other EP receptors, they indicate that EP3 is to some degree necessary for the full therapeutic benefit of misoprostol treatment and improved CXCR2+ phagocyte recruitment during hyperglycemic skin infection.

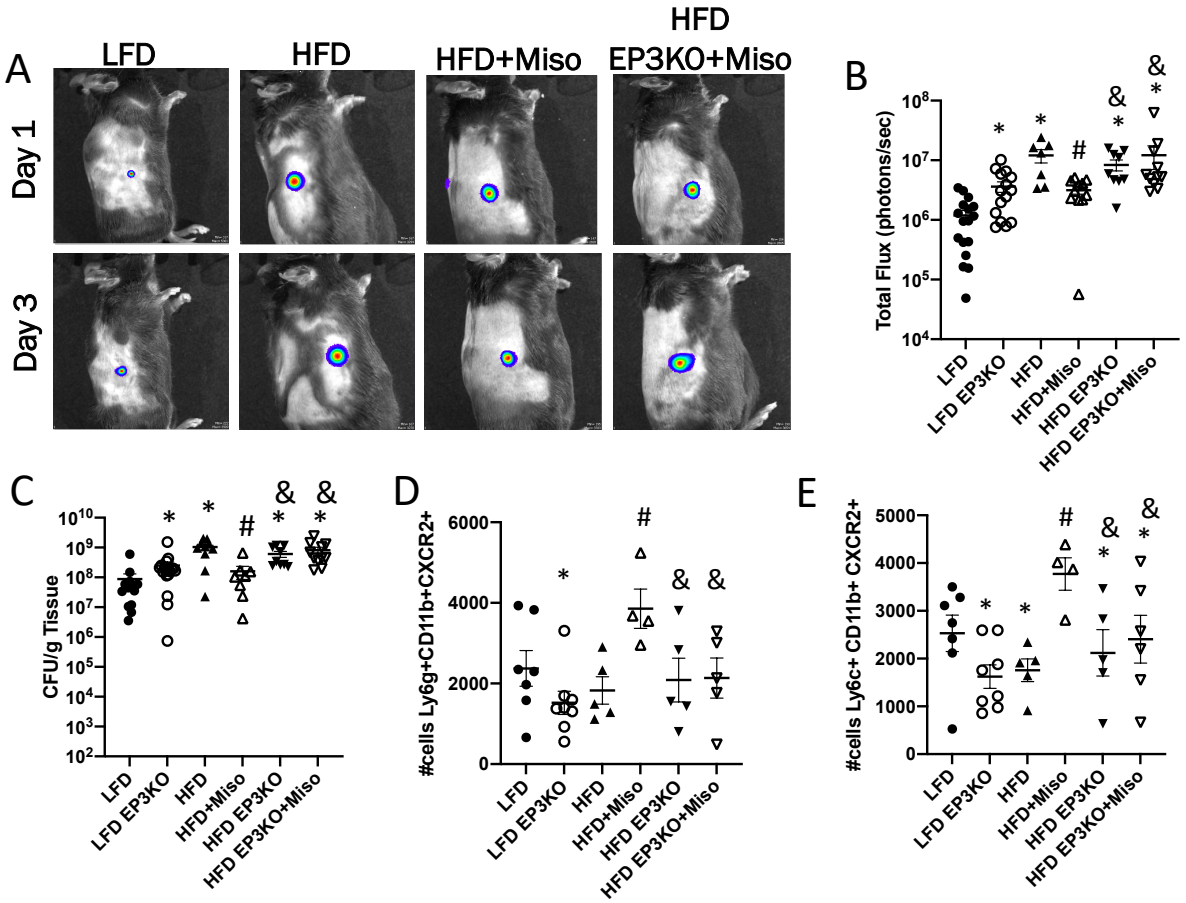

Figure 17. EP3 deletion limits effectiveness of misoprostol treatment. A.) Representative images of bioluminescent MRSA in wildtype and EP3-/- LFD and HFD fed mice treated with or without misoprostol at day 1 and day 3 post-infection using planar bioluminescent imaging. **B.)** Quantification of Total flux from mice treated as in **A** at day 3 post-infection using the IVIS Spectrum. **C.)** Bacterial burden as measured by CFU from skin biopsy homogenates from mice treated as in **A** at day 3 post-infection. **D.)** Total number of CXCR2+ neutrophils (Ly6g+CD11b+) from biopsies collected from mice treated as in **A** at day 3 post-infection. **E.)** Total number of CXCR2+ monocytes (Ly6c+CD11b+) from mice treated as in **A** collected at day 3 post-infection. Data represent the mean ± SEM from 4-6 mice from 2-3 independent experiments. *p<0.05 vs. LFD. #p<0.05 vs. HFD. &p<0.05 vs. HFD+Miso (One-way ANOVA followed by Bonferroni multiple comparison test).

CXCR2 antagonism blunts therapeutic benefit of misoprostol treatment

Based on the importance of neutrophils in *S. aureus* skin infection, both in pathogen clearance and abscess formation [114,117,119], as well as data demonstrating improved CXCR2+ neutrophil recruitment with misoprostol treatment, we hypothesized that CXCR2+ cell recruitment was a driving factor in the therapeutic benefit of misoprostol treatment. To test

this hypothesis, we performed subcutaneous infections in which we treated LFD or HFD mice 3 hours prior to infection with a CXCR2 antagonist (Navarixin) or vehicle control (corn oil). Immediately after subcutaneous MRSA infection these mice were then treated topically with either misoprostol ointment or vehicle control as we have done previously. At the end of a 3-day infection, we found that HFD fed animals treated with the CXCR2+ antagonist plus misoprostol had worse infection outcomes than those receiving misoprostol alone. This was seen *in vivo* via imaging of bioluminescent MRSA (**Fig. 18A** and **18B**) which correlated with worse bacterial burden as measured *ex vivo* via CFU plated from skin biopsy homogenates (**Fig. 18C**). Furthermore, LFD fed mice receiving the CXCR2+ antagonist alone also had worse infection outcomes by these same measures when compared to untreated controls (**Fig. 18A-C**). Together, these data demonstrate CXCR2+ antagonism negatively impacts bacterial clearance under both euglycemic and hyperglycemic conditions during MRSA skin infection and misoprostol treatment. To confirm the efficacy of the CXCR2 antagonist treatment, flow cytometry analysis was performed on infection biopsies collected from these same mice at day 3 post-infection. Analysis revealed that LFD mice receiving the CXCR2+ antagonist had reduced numbers of CXCR2+ neutrophils (**Fig. 18D**) and monocytes (**Fig. 18E**) compared to untreated animals. HFD fed mice receiving misoprostol and the antagonist also had significantly reduced numbers of CXCR2+ phagocytes compared to those mice receiving misoprostol alone (**Fig. 18D** and **18E**).

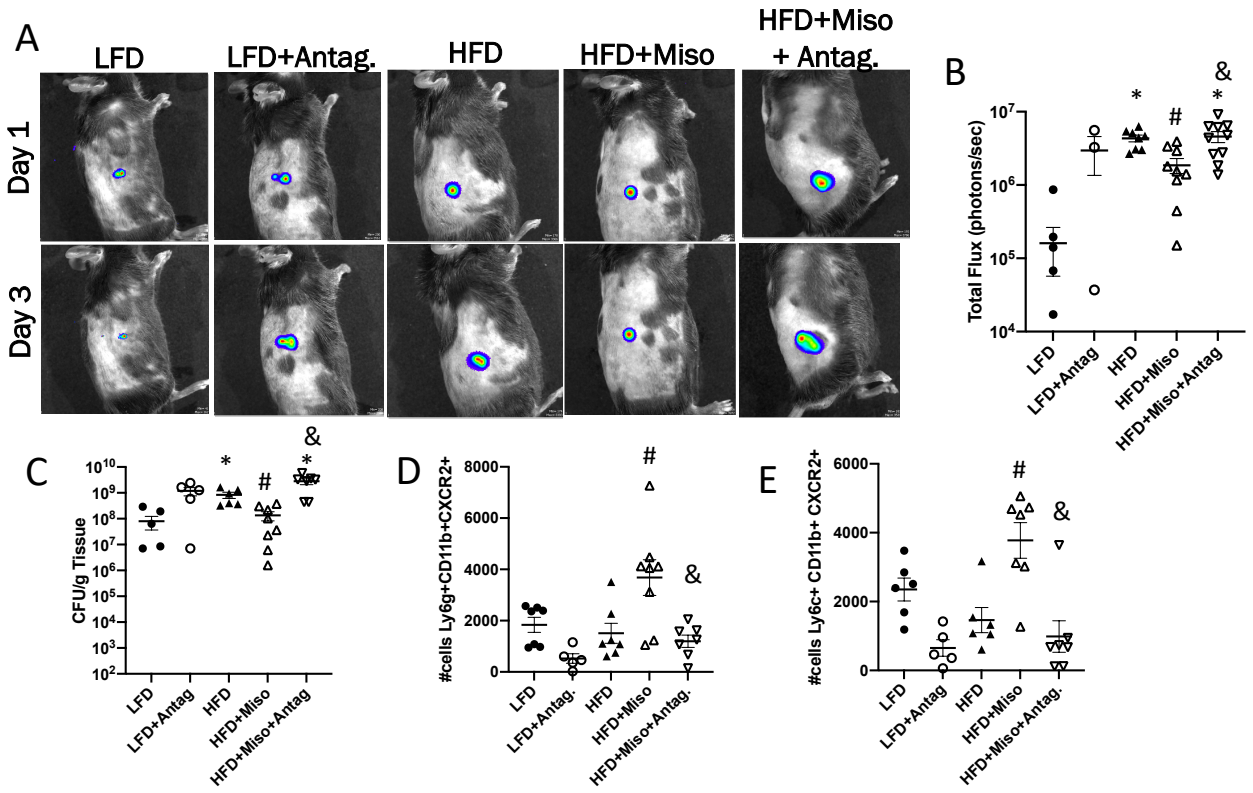

Figure 18. CXCR2 antagonism blunts therapeutic benefit of misoprostol treatment. A.) Representative images of bioluminescent MRSA in the skin of LFD and HFD animals treated with misoprostol or a CXCR2+ antagonist (Navarixin) (5mg/kg) together or individually at day 1 and day 3 post-infection using the IVIS Spectrum. **B.)** Quantification of total flux from bioluminescent MRSA at day 3 post-infection in mice treated as in **A. C.)** Bacterial burden as measured by CFU from skin biopsy homogenates from mice treated as in **A** at day 3 post-infection. **D.)** Total number of CXCR2+ neutrophils (Ly6g+CD11b+) in the skin of mice treated as in **A** at day 3 post-infection as measured by flow cytometry. **E.)** Total number of CXCR2+ monocytes (Ly6c+CD11b+) in the skin of mice infected and treated as in **A** at day 3 post-infection as measured by flow cytometry. Data represent the mean ± SEM from 3-5 mice from 2-3 independent experiments. *p<0.05 vs. LFD. #p<0.05 vs. HFD. &p<0.05 vs. HFD+Miso (One-way ANOVA followed by Bonferroni multiple comparison test).

As we had done previously, we also wanted to confirm the importance of these CXCR2+ phagocytes during misoprostol treatment in a second model of STZ-induced insulin-deficient hyperglycemia. We, therefore, repeated these infections in control and STZ-treated mice, pretreating them before infection with a CXCR2 antagonist followed by twice-daily misoprostol treatments over the course of a three-day infection. Similar to the results seen in our LFD and

HFD mice, hyperglycemic mice receiving the CXCR2 antagonist had a higher bioluminescent bacterial burden compared to mice receiving misoprostol alone (**Fig. 19A** and **19B**). Furthermore, control animals receiving the antagonist alone also had a greater bacterial burden than untreated animals, suggesting an important role for these cell populations during skin infection. Biopsies harvested from these mice at day 3 post-infection and plated for CFU matched the *in vivo* imaging data with misoprostol treatment alone resulting in decreased bacterial burden in the skin of hyperglycemic mice that was increased when treatment was combined with the CXCR2 antagonist (**Fig. 19C**). Flow cytometry of these same infection biopsies revealed that while misoprostol treatment enhanced the recruitment of CXCR2+ monocytes (**Fig. 19D**) and neutrophils (**Fig. 19E**) to the site of infection, the combined treatment with the CXCR2 antagonist reduced the number of these cell populations recruited to the skin during MRSA infection. The correlation in these data between the recruitment of CXCR2+ monocytes and neutrophils with bacterial burden indicates a role for CXCR2+ phagocytes in skin host defense against MRSA and highlights them as contributors to misoprostol enhanced skin host defense during hyperglycemic skin infection.

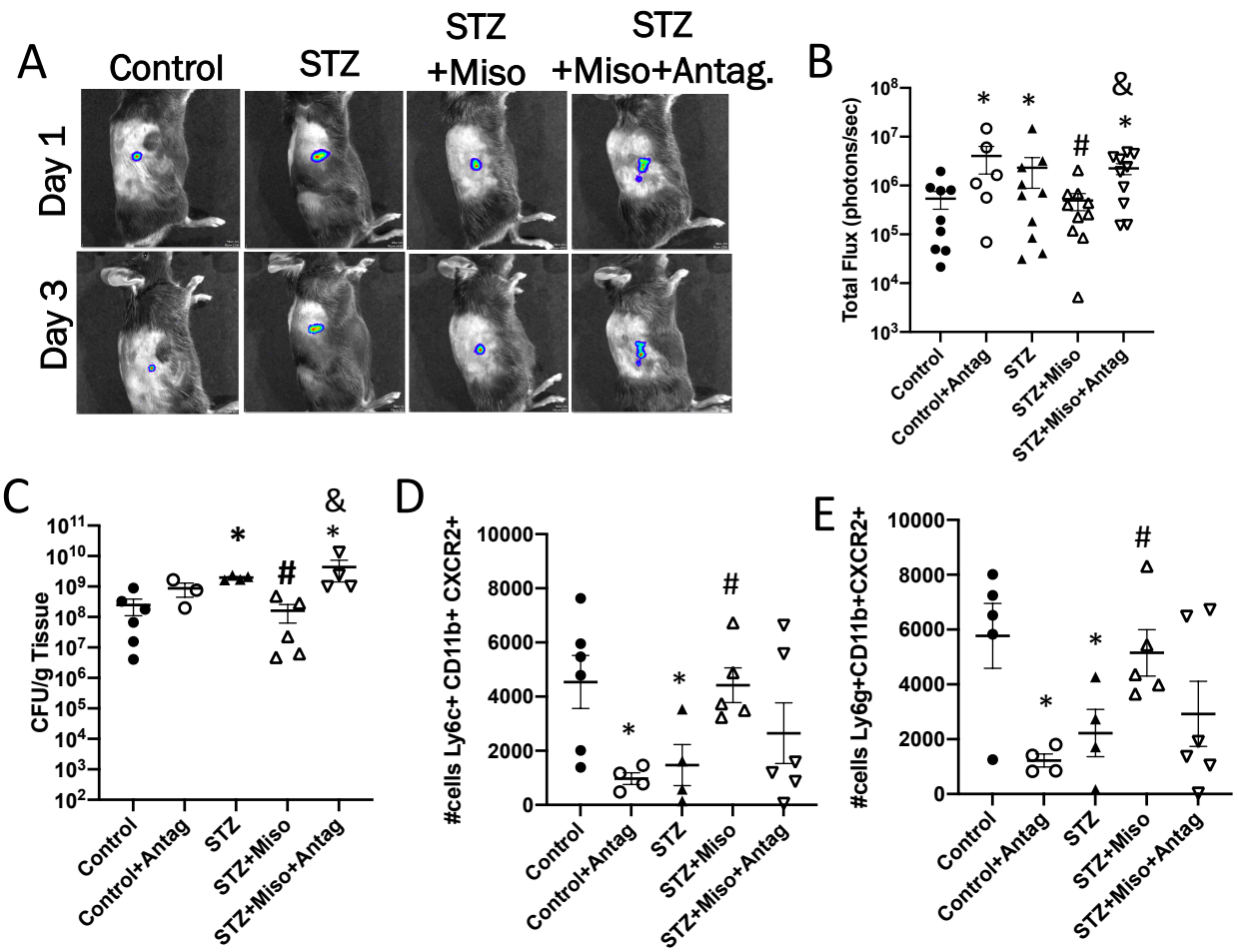

Figure 19. CXCR2 antagonism impairs skin host defense against MRSA. A.) Representative images of bioluminescent MRSA in the skin of control and STZ-induced hyperglycemic mice treated with misoprostol or a CXCR2+ antagonist (Navarixin) (5mg/kg) together or individually at day 1 and day 3 post-infection using the IVIS Spectrum. **B.)** Quantification of total flux from bioluminescent MRSA at day 3 post-infection in mice treated as in **A. C.)** Bacterial burden as measured by CFU from skin biopsy homogenates from mice treated as in **A** at day 3 post-infection. **D.)** Total number of CXCR2+ monocytes (Ly6c+CD11b+) in the skin of mice treated as in **A** at day 3 post-infection as measured by flow cytometry. **E.)** Total number of CXCR2+ neutrophils (Ly6g+CD11b+) in the skin of mice infected and treated as in **A** at day 3 post-infection as measured by flow cytometry. Data represent the mean ± SEM from 3-6 mice from 2-3 independent experiments. *p<0.05 vs. Control. #p<0.05 vs. STZ. &p<0.05 vs. STZ+Miso (One-way ANOVA followed by Bonferroni multiple comparison test).

Misoprostol treatment enhances STAT-1 phosphorylation

STAT-1 is a proinflammatory transcription factor that can promote the production of several proinflammatory cytokines and chemokines [153,154]. As several cytokines were

significantly upregulated in the skin of hyperglycemic mice treated with misoprostol, we hypothesized that enhanced STAT-1 activation could be a potential mechanism by which misoprostol treatment enhances skin host defense.

Interferon-gamma (IFNγ) is another cytokine strongly associated with STAT-1 activation. Therefore, we examined the abundance of IFNγ in the skin of infected and treated mice at day 3 post-infection. Our data show that IFNγ production was impaired in untreated, infected HFD mice and was enhanced with misoprostol treatment (**Fig. 20A**). Western blotting of these same infected and treated skin biopsy homogenates also revealed decreased total STAT-1 expression in the skin of HFD mice (**Fig. 20B**). STAT phosphorylation was also reduced in the skin of hyperglycemic mice compared to euglycemic controls but was enhanced with misoprostol treatment (**Fig. 20B** and **20C**), suggesting misoprostol treatment was enhancing STAT-1 activation and promoting downstream cytokine production. Therefore, we aimed to understand the mechanisms underlying the misoprostol/STAT-1 axis in the skin of HFD mice.

SOCS-1 is a protein whose transcription is driven by STAT-1 and is part of a classical negative feedback loop in STAT-1 activation, limiting STAT-1 phosphorylation to prevent hyper inflammation [76]. As a significant regulator of STAT-1 activation, we also examined levels of SOCS-1 in the skin of infected and treated LFD and HFD fed mice. Expression of SOCS-1 was significantly higher in the skin of hyperglycemic HFD fed mice compared to euglycemic controls (**Fig. 20D** and **20E**). Furthermore, increased expression of SOCS-1 was reduced in the skin of misoprostol treated and infected HFD animals (**Fig. 20D** and **20E**). These data suggest that increased SOCS-1 expression during hyperglycemic skin infection may be contributing to

impaired skin host defense in HFD fed mice by limiting the release of proinflammatory chemokines and cytokines. This increased SOCS-1 expression could be a compensatory mechanism to deal with the low-grade chronic inflammation associated with obesity and hyperglycemia outside of infection. Furthermore, these data led us to hypothesize that misoprostol may be acting to limit SOCS-1 expression in the skin of these mice during infection to improve skin host defense through improving STAT-1 phosphorylation and downstream cytokine release, although a direct mechanism between SOCS-1 and misoprostol has yet to be fully elucidated.

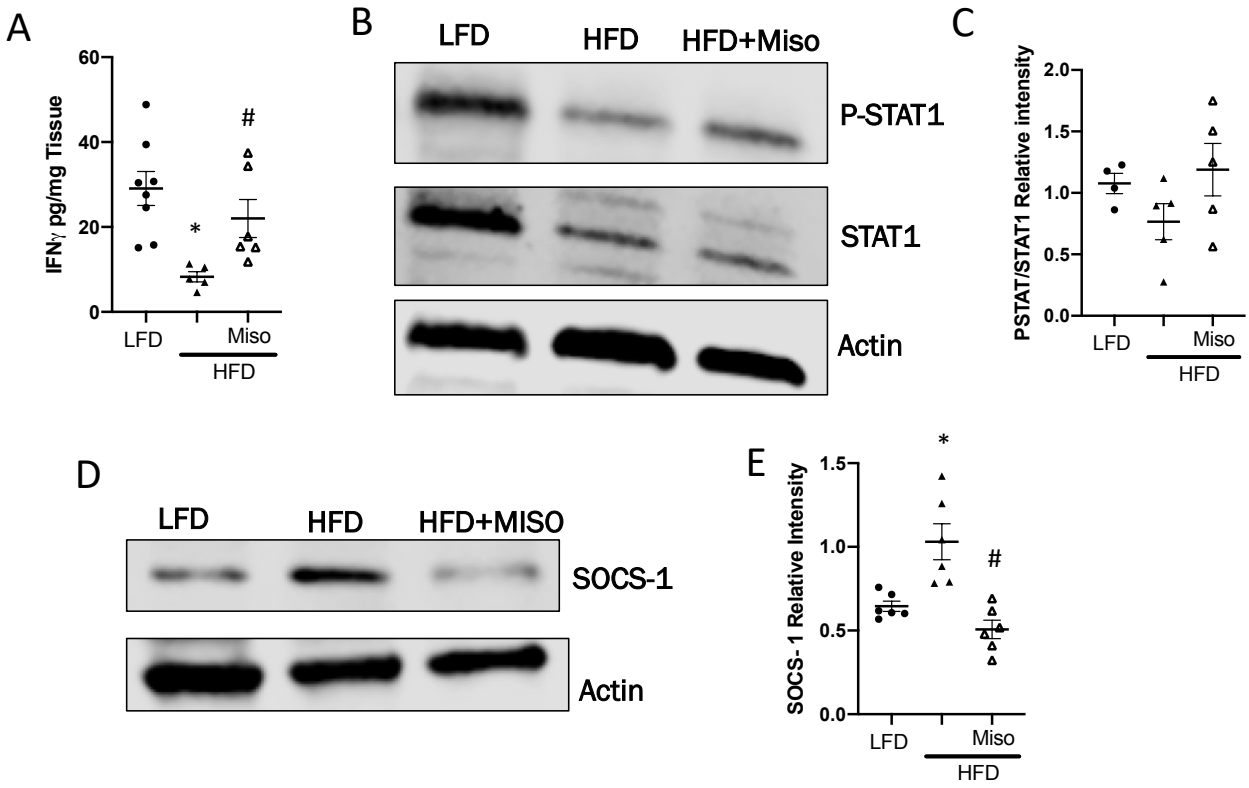

Figure 20. Misoprostol treatment enhances STAT-1 phosphorylation. A.) Levels of IFNγ as measured via ELISA from skin biopsy homogenates from LFD and HFD fed mice infected s.c. and treated immediately after and twice daily with misoprostol at day 3 post-infection. **B.)** Representative Western blots for P-STAT-1 (Y701), tSTAT-1, and Actin in biopsies collected at day 3 post-infection in mice treated as in **A. C.)** Quantification of densitometry of Western blots for P-STAT-1 and STAT-1 as shown in **B. D.)** Representative Western Blots for SOCS-1 and Actin from biopsies collected at day 3 post-infection in mice infected and treated as in **A. E.)** Quantification of Western blots as shown in **D.** Data represent the mean ± SEM from 4-5 mice from 2-3 independent experiments. *p<0.05 vs. LFD. #p<0.05 vs. HFD (One-way ANOVA followed by Bonferroni multiple comparison test).

PART II – SOCS-1 restrains skin host defense against *S. aureus*

This section is adapted from "SOCS-1 inhibition of type I interferon restrains Staphylococcus aureus skin host defense" published in PLoS Pathogens and has been reproduced with the permission of the publisher.

Klopfenstein N, Brandt SL, Castellanos S, Gunzer M, Blackman A, Serezani CH (2021) SOCS-1 inhibition of type I interferon restrains *Staphylococcus aureus* skin host defense. PLoS Pathog 17(3): e1009387. https://doi.org/10.1371/journal.ppat.1009387

SOCS-1 expression is elevated during skin infection in hyperglycemic mice

Pathogens can induce SOCS-1 expression to exploit its ability to dampen the innate immune response and allow for immune system evasion [81]. To determine if SOCS-1 expression was upregulated in response to *S. aureus* skin infection, as well as to confirm our results that indicated hyperglycemia enhanced SOCS-1 expression during skin infection, we examined the levels of *Socs1* mRNA in the skin of control and STZ-induced hyperglycemic mice prior to infection and at days 1 and 3 post-infection. *Socs1* mRNA expression was induced in response to subcutaneous MRSA infection and increased over the first three days of infection (**Fig 21A**). Furthermore, hyperglycemic mice had significantly higher levels of *Socs1* expression at both days 1 and 3 post-infection than euglycemic control mice (**Fig 21A**). Western blots from skin biopsy homogenates of mice at day 3 post-infection confirmed these results, demonstrating increased SOCS-1 expression in the skin of STZ-induced hyperglycemic mice (**Fig. 21B and 21C**). As SOCS-1 is closely associated with STAT-1 activation and phosphorylation, we also examined STAT-1 expression in the skin of these mice. When we determined levels of STAT-1 phosphorylation via immunoblot in these same biopsy samples, we observed that

increased SOCS-1 expression correlated with reduced levels of total STAT-1 as well as STAT-1 phosphorylation in the infected skin of hyperglycemic mice (**Fig. 21B and 21C**). Together these data demonstrate that enhanced levels of SOCS-1 during skin infection in hyperglycemic mice correlates with their worse infection outcomes. This led us to hypothesize that enhanced SOCS-1 expression in these mice is detrimentally impacting skin host defense, resulting in poor bacterial clearance.

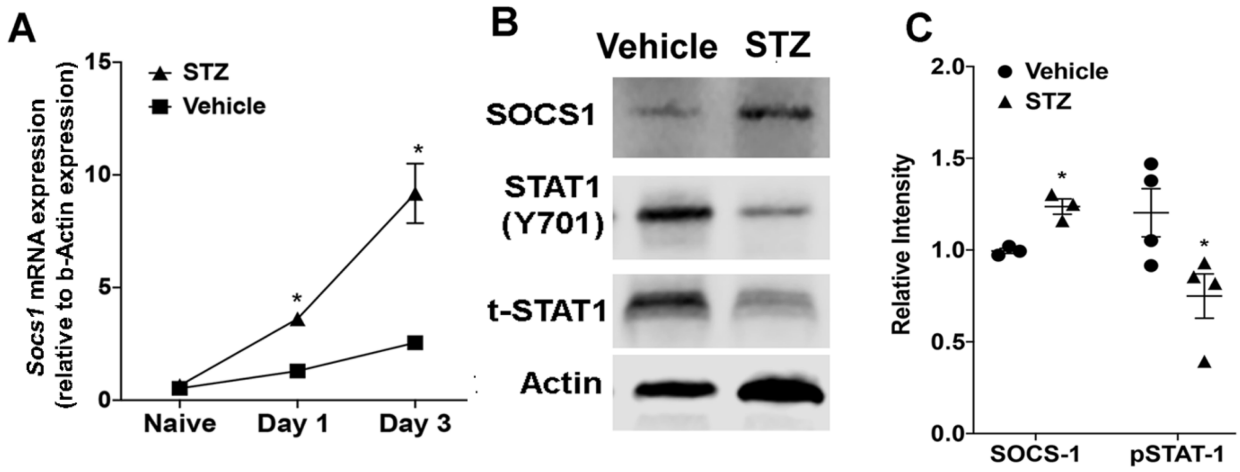

Figure 21. STZ mice have increased SOCS-1 expression during skin infection. A.) Expression of *Socs1* mRNA at day 1 and day 3 post-infection in biopsies collected from STZ-induced hyperglycemic and control mice. **B.)** Representative Western blots for SOCS-1, pSTAT-1, and tSTAT-1 from biopsies collected at day 3 post-infection in STZ-induced hyperglycemic and control mice. **C.)** Densitometry quantification of separate Western blots as shown in **B.** Data represent the mean ± SEM from 3-5 mice from 2-3 independent experiments. **A.)** **p*<0.05 vs. Vehicle (Two-way ANOVA followed by Bonferroni multiple comparison test). **C.)** **p*<0.05 vs. Vehicle (Mann-Whitney Test).

Hyperglycemic mice have impaired IFN signaling during skin infection

To investigate possible impacts of enhanced SOCS-1 expression on the innate inflammatory response, we performed a bead array multiplex gene expression analysis on mRNA collected from infected skin biopsies of both control and STZ-induced hyperglycemic

mice at day 1 post-infection. We observed an overall downregulation of genes involved in the interferon (IFN) signaling pathway, a major cytokine pathway regulated by STAT and SOCS proteins [33], in the infected skin of hyperglycemic mice (**Fig. 22A and 22B**). When specific IFN-related genes were examined, we observed decreased expression of *Ifna1, Ifnb1, Ifng,* and *Stat1* in the skin of infected hyperglycemic animals (**Fig. 22A and 22B**). Importantly, increased levels of *Socs1* were also observed (confirming our previous results [**Fig. 21**]) along with *Socs3, Irf2, Irf3,* and *Irf7,* all genes involved in the regulation of IFN signaling. Overall, these data demonstrate that STZ mice have impaired IFN signaling during MRSA skin infection. This led us to hypothesize that this pathway may be critical in skin host defense against MRSA, and its impairment in hyperglycemic mice may in part drive worse infection outcomes.

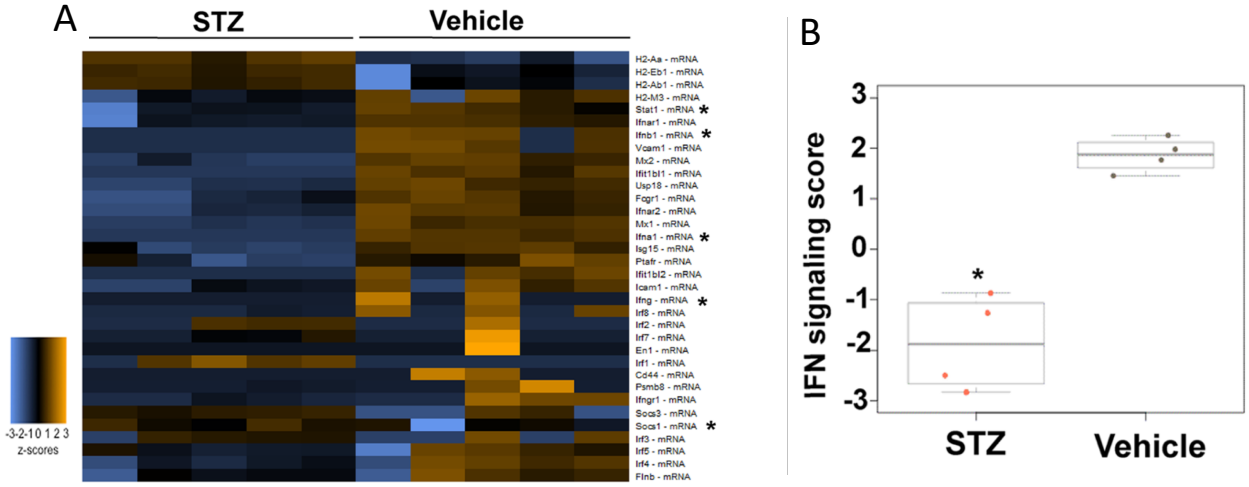

Figure 22. Hyperglycemic mice have impaired IFN signaling during skin infection. A.) Heatmap of genes analyzed via NanoString from mRNA isolated from infected skin of iKIR and SCR KIR treated mice at day 1 post-infection. **B.)** IFN signaling score determined using the NanoSolver from data shown in **A.** Data represent the mean ± SEM from 5 mice from 2 independent experiments. *$p<0.05$ vs. Vehicle (Mann-Whitney Test).

SOCS-1 inhibition improves infection outcomes in hyperglycemic mice

Next, we investigated the impact that SOCS-1 inhibition may have on infection outcomes in hyperglycemic mice using pharmacological and genetic approaches. SOCS-1 inhibits STAT-1 activation by binding to JAK receptors and preventing their kinase activity [78]. SOCS-1 binds to JAK receptors via its SH2 domain and a short motif upstream of SH2, known as the KIR (kinase inhibitory region), that directly inhibits the kinase activity of JAK tyrosine kinases [78,79]. The SOCS-1 KIR occupies the substrate-binding groove of JAK and prevents subsequent phosphorylation of target proteins [78,79]. Previously, we have utilized a SOCS-1 KIR blocking peptide termed iKIR that enhanced STAT-1 and STAT-3 phosphorylation in macrophages during sepsis to promote HIF1α-dependent cytokine release [148]. Therefore, we examined if treatment with this peptide could also influence skin host defense in hyperglycemic mice. During subcutaneous skin infection with MRSA, hyperglycemic mice were injected i.p. 1 hour prior to infection with the iKIR peptide or scrambled KIR peptide (SCR KIR) control, followed by daily treatments post-infection. Mice treated with the iKIR peptide had significantly improved infection outcomes compared to those receiving the control peptide. iKIR-treated mice had decreased infection area (**Fig. 23A**) over the course of a 9-day infection that correlated with reduced bacterial burden in the skin at day 9 post-infection (**Fig. 23B**).

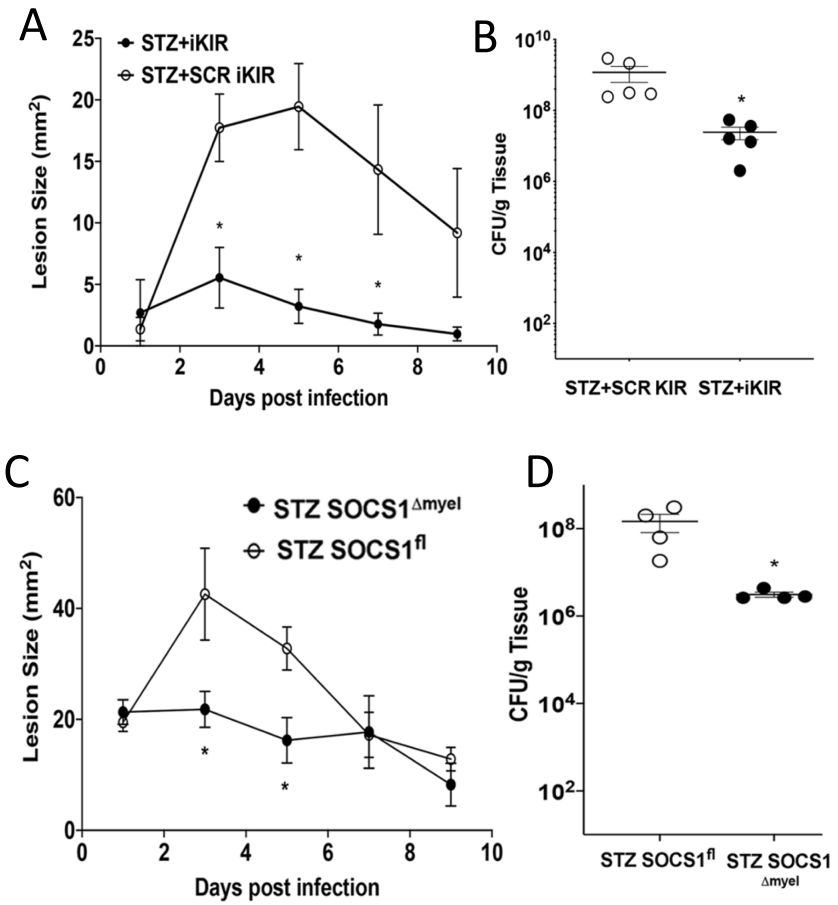

Figure 23. Inhibition of SOCS-1 improves skin infection outcome in hyperglycemic mice. A.) Surface lesion size as measured via caliper in STZ-induced hyperglycemic treated with either iKIR or SCR KIR peptide over the course of a 9-day subcutaneous MRSA skin infection. **B.)** Bacterial load as determined by CFU in skin biopsy homogenates collected from mice in **A** at day 9 post-infection. **C.)** Surface lesion size as measured via calipers in STZ-induced hyperglycemic *Socs1*^{fl} and *Socs1*$^{\Delta myel}$ mice over the course of a 9-day subcutaneous MRSA skin infection. **D.)** Bacterial burden as measured via CFU from skin biopsy homogenates in mice from **C** at day 9 post-infection. Data represent the mean ± SEM from 4-5 mice from 2 independent experiments. **A** and **C.)** *p<0.05 vs. SOCS1^{fl} or SCR KIR treated mice (Two-way ANOVA followed by Bonferroni multiple comparison test). **B** and **D.)** *p<0.05 vs. SOCS1^{fl} or SCR KIR treated mice (Mann-Whitney Test).

SOCS-1 is expressed in cells of both the innate and adaptive immune response [78]. As neutrophils and macrophages are known to be critical in bacterial control and elimination during MRSA skin infection [114,117], we further studied the role of myeloid-specific SOCS-1

actions during skin infection. For this, we generated *Socs1*$^{\Delta myel}$ mice by crossing LysM^{cre} with *Socs1*$^{fl/fl}$ mice to delete SOCS-1 in myeloid cells expressing lysozyme M (primarily neutrophils and macrophages). Infections in STZ-induced hyperglycemic *Socs1*$^{\Delta myel}$ mice had reduced lesion size (**Fig. 23C**) and bacterial load (**Fig. 23D**) when compared to hyperglycemic *Socs1*^{fl} mice over a 9-day infection. Together, this indicates that inhibiting SOCS-1 actions during hyperglycemia improves bacterial clearance and that iKIR treatment could potentially represent a host-centered immunostimulatory approach to treat antibiotic-resistant infections in the skin.

SOCS-1 inhibition improves skin host defense in euglycemic mice

As SOCS-1 expression was also induced in response to *S. aureus* skin infection in euglycemic mice, we were curious if SOCS-1 inhibition could also improve infection outcome in wildtype animals. During infection with bioluminescent MRSA, wildtype mice were treated i.p. 1 hour prior to infection with the iKIR or SCR KIR peptide followed by daily treatments throughout infection as we had done previously. Mice treated with the iKIR peptide had decreased lesion size over the course of a 9-day infection (**Fig. 24A**) that correlated with reduced bioluminescent bacterial burden at day 9 post infection (**Fig. 24B**). When biopsies were harvested at several time points post infection, reduced bacterial burden was also observed in iKIR treated animals as measured by CFU as early as 6 hours post infection that persisted until day 9 post infection (**Fig. 24C**). Histological analysis of skin biopsies of the infection site with H&E staining also revealed smaller, more compact abscesses in the skin of iKIR treated mice (**Fig. 24D**), demonstrating improved bacterial control. Next, we repeated these infections in euglycemic

Socs1^{fl} and *Socs1*$^{\Delta myel}$ mice to examine whether myeloid-specific SOCS-1 deletion would improve MRSA skin infection outcomes. Infection in *Socs1*$^{\Delta myel}$ mice resulted in smaller lesion size over the course of infection (**Fig. 24E**) and decreased bacterial burden in the skin at day 9 post-infection (**Fig. 24F**). In sum, these data demonstrate that pharmacological inhibition or myeloid cell specific deletion of SOCS-1 significantly improves MRSA skin infection outcomes in both euglycemic as well as hyperglycemic mice.

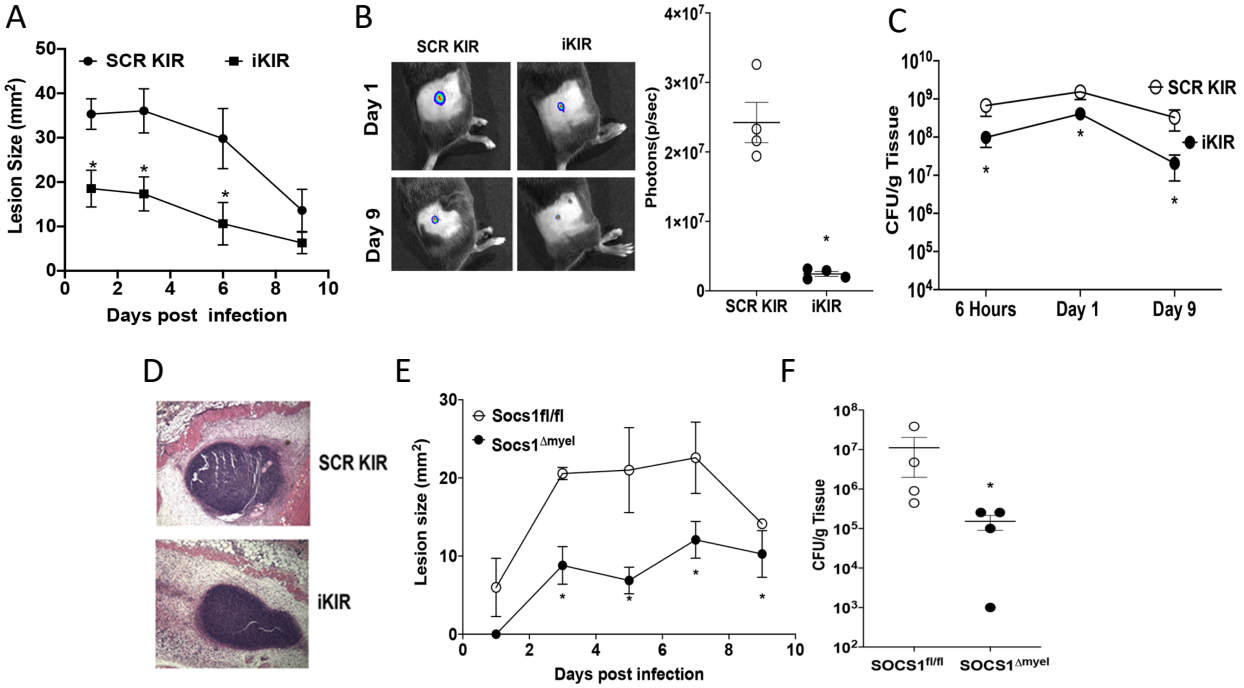

Figure 24. SOCS-1 inhibition improves skin host defense. A.) Bioluminescent infection area in mice treated with either iKIR or SCR KIR peptide using the *in vivo* animal imaging (IVIS Spectrum) detection system. **B.) Left-** Representative images of bioluminescent MRSA in the skin of mice treated as in **A. Right-** Total flux (photons/second) of bioluminescent MRSA detected in mice treated as in **A** using the IVIS Spectrum. **C.)** Bacterial load as determined by CFU from skin biopsy homogenates from mice treated as in **A** at the indicated time points post-infection. **D.)** Representative H&E stains from skin biopsy sections from mice treated as in **A** and shown at 10X magnification. **E.)** Infected area as measured via caliper every other day during the course of a 9-day infection in *Socs1*^{fl} and *Socs1*$^{\Delta myel}$ mice. **F.)** Bacterial load as determined by CFU from skin biopsy homogenates from mice infected as in **E** at day 9 post-infection. Data represent the mean ± SEM from 3-9 mice from 2 independent experiments. **A** and **E.)** **p*<0.05 vs. SOCS1^{fl} or SCR KIR treated mice (Two-way ANOVA followed by Bonferroni multiple comparison test). **C** and **F.)** **p*<0.05 vs. SOCS1^{fl} or SCR KIR treated mice (Mann-Whitney Test).

SOCS-1 inhibition improves bacterial phagocytosis and killing dependent on nitric oxide

Based on our previous data demonstrating the impact of SOCS-1 inhibition on abscess formation and bacterial control in the skin, we hypothesized that SOCS-1 inhibition might improve antimicrobial effector functions such as phagocytosis and bacterial killing in phagocytes. When Gram staining was performed on infection biopsy histology samples of wildtype mice treated with either iKIR or SCR KIR, MRSA was primarily located within cells in iKIR treated mice, while a higher abundance of extracellular bacteria was observed in the skin of SCR KIR treated animals (**Fig. 25A**). While this suggested increased bacterial phagocytosis in the skin of iKIR treated animals, we wanted to investigate the potential for increased bacterial killing *in vitro*. When bone marrow-derived macrophages (BMDMs) from both *Socs1*$^{\Delta myel}$ and wildtype mice treated with the iKIR peptide were challenged with GFP-MRSA, we observed enhanced bacterial phagocytosis when compared to *Socs1*^{fl} or SCR KIR treated BMDMs (**Fig. 25B**). Furthermore, SOCS-1 inhibition also enhanced bacterial killing of GFP-MRSA in BMDMs (**Fig. 25C**). These data led us to hypothesize that SOCS-1 inhibition may enhance macrophage antimicrobial effector functions during MRSA skin infection.

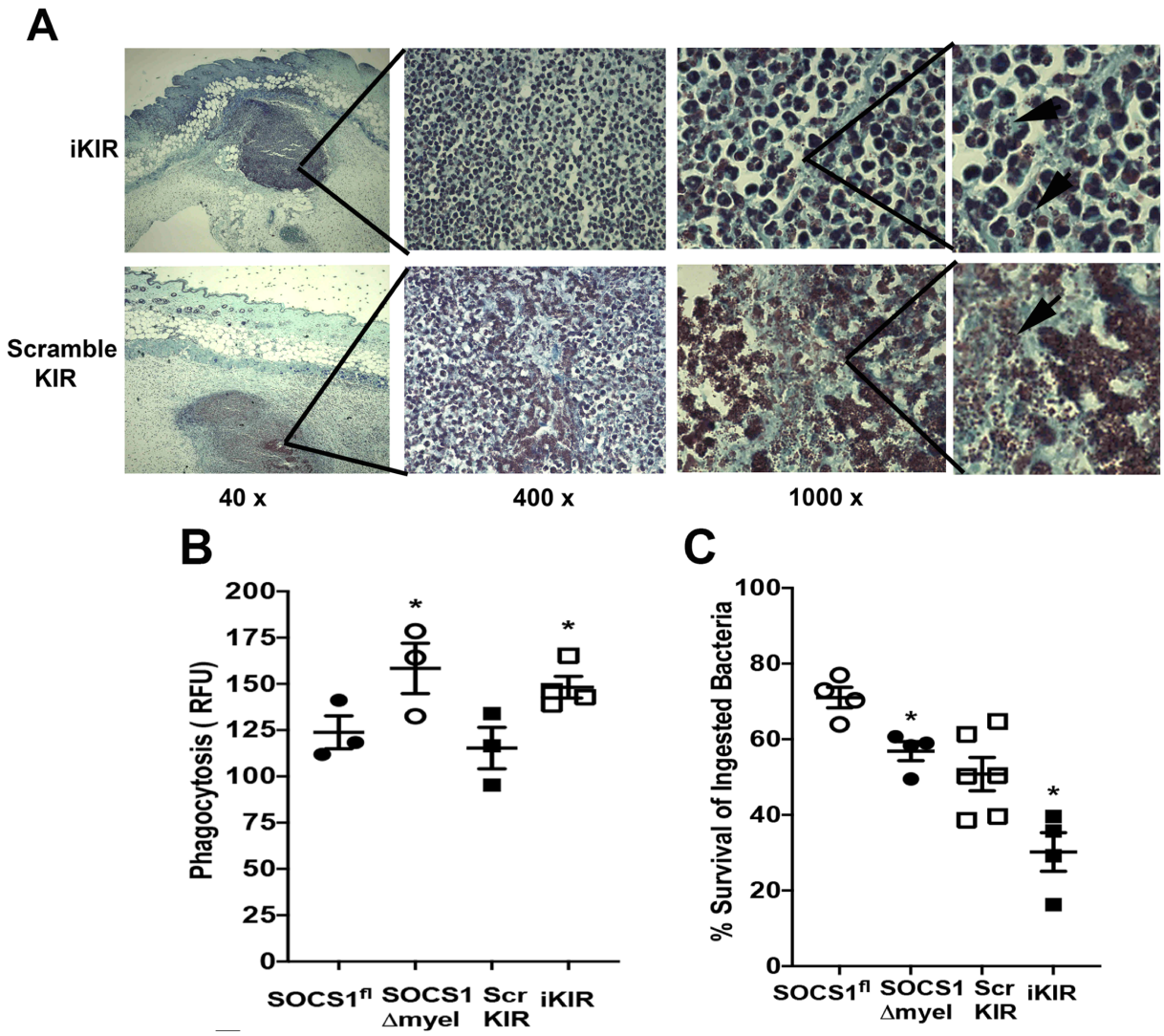

Figure 25. SOCS-1 inhibition improves bacterial phagocytosis and killing. A.) Gram staining of skin biopsy sections collected at day 1 post-infection with MRSA in mice treated with either iKIR or SCR KIR. Gram staining to label gram-positive bacteria is shown in purple/brown. Magnifications are as shown. Black arrows indicated extracellular MRSA clusters. Images are representative of 3-5 mice per group. **B.)** Phagocytosis of GFP tagged MRSA by BMDMs from *Socs1*^{fl} and *Socs1*$^{\Delta myel}$ mice or BMDMs from WT mice treated with either iKIR or the SCR KIR peptide. **C.)** Determination of bacterial killing of GFP tagged MRSA by BMDMs from **B** as described in Methods. Data represent the mean ± SEM from 3-6 mice from 2 independent experiments. *p<0.05 vs. SOCS1^{fl} or SCR KIR treated mice (One-way ANOVA followed by Bonferroni multiple comparison test).

Nitric Oxide (NO) is a potent antimicrobial molecule produced by phagocytes during infections [114,115,117]. To assess if SOCS-1 regulates NO production in macrophages, we

initially examined *Nos2* expression (the gene that encodes the inducible nitric oxide synthase protein [iNOS]) in infected mice treated with either iKIR or SCR KIR. We found significantly elevated levels of *Nos2* expression in the skin of iKIR-treated treated mice versus SCR KIR-treated animals at day 1 post-infection (**Fig. 26A**). Since increased NO release could be promoting more efficient bacterial killing *in vivo*, we examined the contributions of increased iNOS/NO in bacterial killing in iKIR treated BMDMs. BMDMs from wildtype mice were treated with either iKIR alone or iKIR plus an iNOS inhibitor (1400W dihydrochloride) before challenge with GFP-MRSA. Treatment with the iNOS inhibitor ablated the beneficial effects of SOCS-1 inhibition on bacterial killing (**Fig. 26B**). Notably, SOCS-1 inhibition did increase NO release in MRSA-challenged BMDMs, and the addition of the iNOS inhibitor reversed this trend (**Fig. 26C**). We also examined the impact of SOCS-1 inhibition on ROS production which is known to be actively involved in *S. aureus* killing [114,115,117]. When we tested levels of H_2O_2 in the skin of infected mice treated with iKIR or SCR KIR, we did not detect any significant differences between the two treatment groups (**Fig. 26D**). Together, these data suggest that SOCS-1 regulates antimicrobial programs in macrophages dependent on NO release.

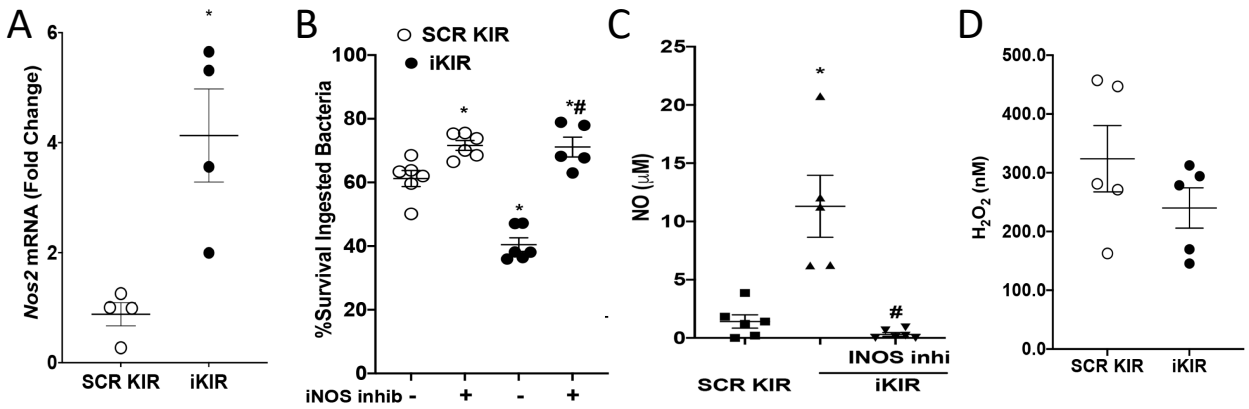

Figure 26. SOCS-1 inhibition improves bacterial killing dependent on nitric oxide. A.) mRNA expression of *Nos2* in the skin of infected mice treated with either the IKIR or SCR KIR peptide at day 1 post-infection as determined by qPCR. **B.)** Determination of bacterial killing of GFP tagged MRSA by BMDMs from wildtype mice treated with either iKIR, SCR KIR, or iKIR+iNOS inhibitor (1400W dihydrochloride). **C.)** Measurement of NO in the supernatants of BMDMs from **B. D.)** H_2O_2 levels in the skin of mice treated with either the iKIR or SCR KIR peptides at day 1 post-infection as determined by the Amplex Red assay. Data represent the mean ± SEM from 4-6 mice from 2 independent experiments. **A** and **D.)** **p*<0.05 vs. SCR KIR. #*p*<0.05 vs. iKIR (Mann-Whitney Test). **B** and **C.)** **p*<0.05 vs. SCR KIR. #*p*<0.05 vs. iKIR (One-way ANOVA followed by Bonferroni multiple comparison test).

SOCS-1 inhibition improves STAT-1 dependent production of proinflammatory cytokines

Next, we determined whether the inhibition of SOCS-1 influences STAT-1 activation during skin infection. Using biopsies from infected and peptide-treated mice at day 3 post-infection, we found that while *S. aureus* induces STAT-1 phosphorylation, iKIR treatment further enhanced STAT-1 phosphorylation compared to mice treated with the SCR KIR peptide (**Fig. 27A**). Furthermore, iKIR did not change SOCS-1 expression during infection and treatment. To confirm that this phenotype was STAT-1 specific, we also examined the activation of STAT-3 and found its phosphorylation was unchanged in response to iKIR treatment during MRSA skin infection (**Fig. 27A**). Finally, we also confirmed that *Socs1*$^{\Delta myel}$ had increased pSTAT-1 abundance during skin infection when compared to *Socs1*^{fl} control animals (data not shown).

We then sought to determine the impact increased pSTAT-1 had on the production of 17 cytokines and chemokines known to influence the skin inflammatory response and skin host defense [114,115,117]. Our data show that iKIR specifically enhanced a group of proinflammatory cytokines/chemokines known to drive proper abscess formation (IL-1β) [119] and neutrophil recruitment (CXCL1 and CXCL2) [10], but not monocyte recruitment (CCL2) [126] in response to MRSA skin infection (**Fig. 27B**). These results indicate that SOCS-1 inhibition up regulates a specific group of cytokines and chemokines known to influence neutrophil migration and functions necessary for an efficient host immune response to MRSA skin infection.

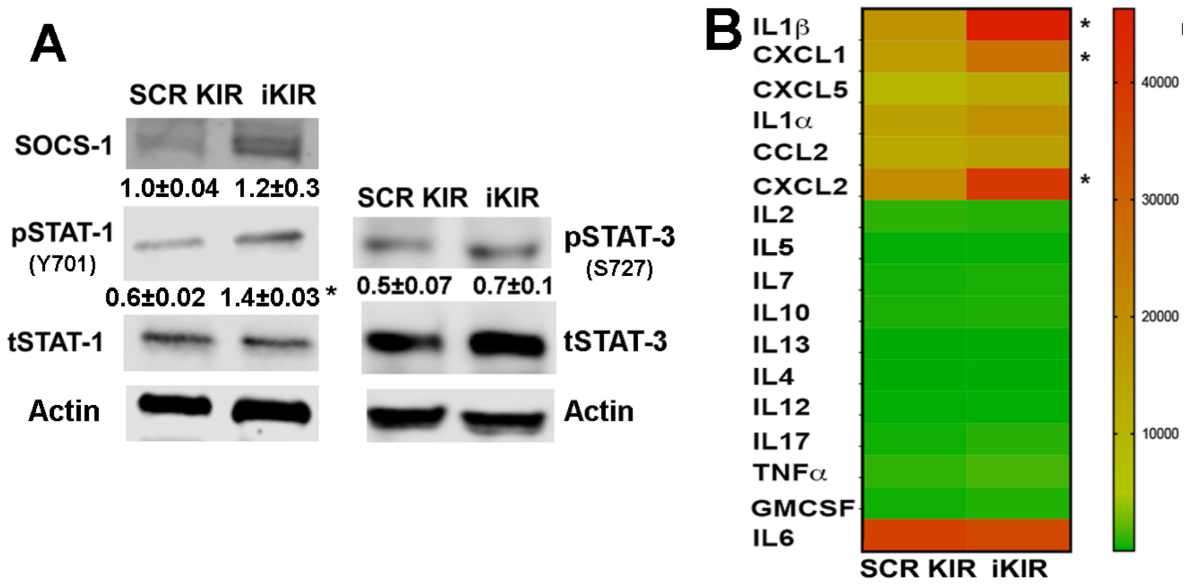

Figure 27. SOCS-1 inhibition improves STAT-1 dependent cytokine release. A.) Representative Western Blots for SOCS-1, pSTAT-1 (Y701), tSTAT-1, PSTAT-3 (S727), tSTAT-3, and Actin from biopsies collected at day 3 post-infection in SCR KIR and iKIR treated animals. The numbers represent mean densitometry analysis of the bands ± SEM (n=four to five mice/group). **B.)** Heat-map of proteins involved in the inflammatory immune response and its resolution in mice treated with either iKIR or SCR KIR at day 1 post-infection with MRSA as measured by bead array multiplex (Eve Technologies). Proteins are listed on the left-hand y-axis, group alphabetically by clades. Red indicates higher protein abundance while green represents lower abundance. (n=4-5 mice/group). Data represent the mean ± SEM from 4-5 mice from 2 independent experiments. *p<0.05 vs. SCR KIR (Mann-Whitney Test).

Since IL-1β, CXCL1, and CXCL2 have all been shown to promote phagocyte recruitment to the skin in response to infection or injury [10,115,118,126], and iKIR enhances the production of these mediators during MRSA skin infection, we investigated whether iKIR treatment also increases neutrophil or monocyte migration to the site of infection. To determine specific phagocyte recruitment, we utilized different transgenic mice that express fluorescent proteins specifically within myeloid cells, monocytes/macrophages, or neutrophils to detect the accumulation of these phagocytes in the skin using IVIS optical imaging [138,140,155]. We first infected EGFP-LysM mice (mainly neutrophils as well as monocytes and macrophages express EGFP) [155] and imaged the animals at day 3 post-infection. We detected a slight yet non-significant increase in GFP signal in the skin of iKIR-treated mice when compared to infected mice treated with the SCR KIR peptide (**Fig. 28A**). Next, to examine if iKIR treatment influences monocyte or macrophage recruitment, we infected and treated MMDTR mice (cells that are CSFR1+ express the mCherry fluorescent protein) [140] and found no difference in mCherry fluorescent signal between SCR KIR- or iKIR-treated animals at day 3 post-infection (**Fig. 28B**). Finally, to determine if iKIR treatment enhances neutrophil recruitment specifically, we infected and treated Catchup$^{IVM\text{-}red}$ mice in which cells expressing Ly6g also express the tdTomato fluorophore [138]. We found that mice treated with the iKIR peptide had significantly increased tdTomato signal in the skin during infection (**Fig. 28C**). These results were confirmed by flow cytometry of infected biopsies from Catchup$^{IVM\text{-}red}$ mice. Our data revealed no difference in total macrophage numbers but increased neutrophil abundance in iKIR treated mice compared to SCR KIR treated (**Fig. 28D**). These data led us to hypothesize that SOCS-1 may

play a role in dampening neutrophil recruitment by diminishing the secretion of chemoattractants such as CXCL1 and IL-1β that are critical in skin host defense against MRSA.

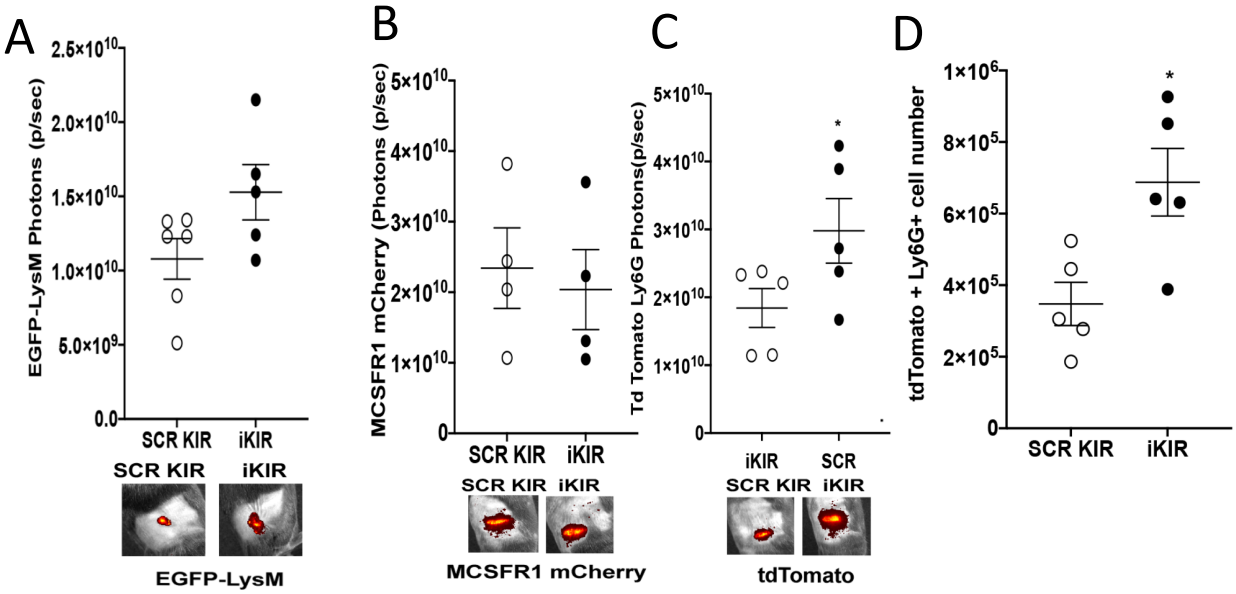

Figure 28. SOCS-1 inhibition improves neutrophil recruitment during skin infection. A.) Total Flux (photons/second) of EGFP detected in the skin of EGFP-LysM mice treated with either iKIR or SCR KIR at day 3 post-infection. Representative pictures shown below. **B.)** Total flux of mCherry signal detected in MMDTR mice treated with either iKIR or SCR KIR at day 3 post-infection, with representative pictures shown below. **C.)** Total flux of tdTomato signal detected in Cathchup$^{IVM\text{-}Red}$ mice treated with either iKIR or SCR KIR at day 3 post-infection with representative pictures shown below. **D.)** Total number of tdTomato+ cells in biopsies collected from mice in **C**. Data represent the mean ± SEM from 4-6 mice from 2 independent experiments. *p<0.05 vs. SCR KIR (Mann-Whitney Test).

Improved skin host defense with SOCS-1 inhibition is dependent on type I interferons

STAT-1 is known to drive the expression of a number of proinflammatory cytokines, the most prominent being the interferons (IFNs), both type I (IFNα and IFNβ) and type II (IFNγ), which along with STAT-1 phosphorylation, are negatively regulated by SOCS-1 in a negative feedback loop [76,78]. Whether SOCS-1 regulates the production of type I or type II IFNs during skin infection remains to be determined. When we examined the levels of both type I and type

II IFNs in the skin of infected mice treated with either iKIR or SCR KIR, we detected a higher abundance of all three interferons (IFNα, IFNβ, and IFNγ) in the skin of iKIR treated mice compared to SCR KIR treated at day 3 post-infection (**Fig. 29A**). Due to the prominent role of IFNγ in enhancing phagocyte antimicrobial effector function [33], we hypothesized it might be driving improved infection outcome in iKIR treated animals. To test this hypothesis, we blocked IFNγ action in iKIR-treated and infected mice using an anti-interferon gamma receptor (IFNGR) antibody. Mice treated with the anti-IFNGR antibody plus SCR KIR had higher bacterial burdens than mice receiving the control IgG antibody at day 1 post-infection (**Fig. 29B**). However, while iKIR plus the IgG control antibody decreased bacterial burden in the skin, treatment with the anti-IFNGR antibody did not prevent iKIR enhanced bacterial clearance (**Fig. 29B**). This led us to hypothesize that IFNγ is not solely involved in the therapeutic benefit of SOCS-1 inhibition during MRSA skin infection.

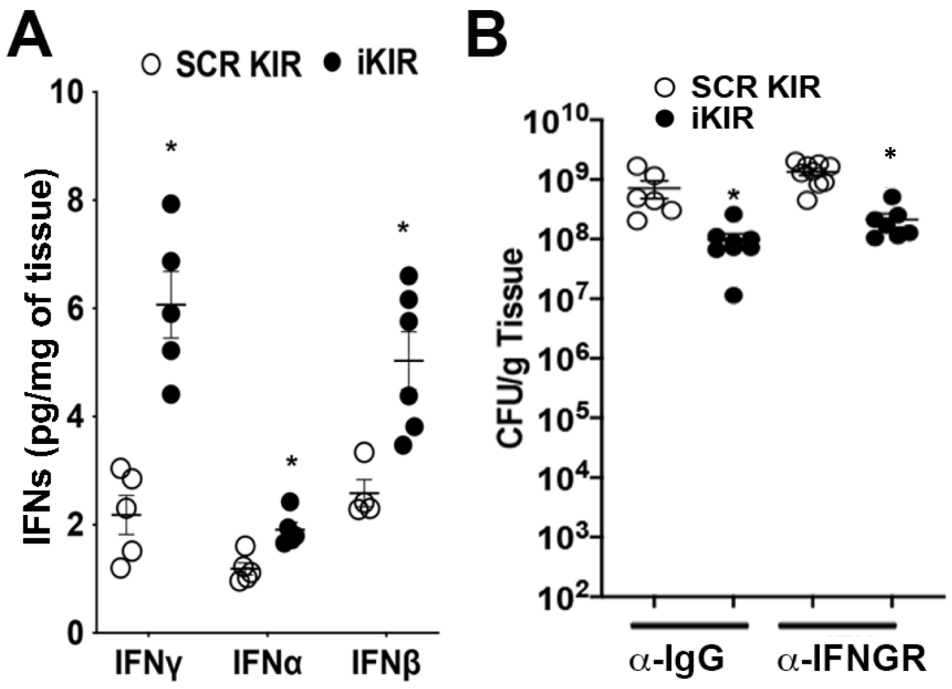

Figure 29. SOCS-1 inhibition improves type I and type II interferon release. A.) Interferon levels in the skin at day 1 post-infection in SCR KIR and iKIR treated animals as measured via ELISA. **B.)** Bacterial load as determined by CFU in skin biopsy homogenates of SCR KIR and iKIR treated mice treated with either IFNGR antibody or IgG control at day 1 post-infection. Data represent the mean ± SEM from 5-6 mice from 2 independent experiments. **A.)** *p<0.05 vs. SCR KIR (Mann-Whitney Test). **B.)** *p<0.05 vs. SCR KIR (One-way ANOVA followed by Bonferroni multiple comparison test).

Next, to determine if iKIR actions were dependent on type I interferons (IFNα/β), we utilized an antibody against their common receptor, the interferon alpha-beta receptor (IFNAR). We found that the treatment of mice with the anti-IFNAR antibody and SCR KIR peptide increased bacterial burden in the skin over mice receiving the control antibody. Furthermore, the IFNAR blocking antibody also impaired iKIR mediated decreases in lesion size (**Fig. 30A**) and bacterial burden as measured by both CFU (**Fig. 30B**) and bioluminescent bacterial imaging (**Fig. 30C**). We also utilized a genetic approach to inhibit type I interferon actions during skin infection by using IFNAR knockout mice to confirm these results. Wildtype and IFNAR-/- mice were treated with either the iKIR or SCR KIR peptides followed by MRSA skin infection as we

had done previously. After a 3-day infection, we observed that IFNAR-/- mice had worse infection outcomes when compared to wildtype mice as measured by both lesion size (**Fig. 30D**) and bioluminescent bacterial burden (**Fig. 30E** and **30F**). Furthermore, IFNAR-/- did not benefit from iKIR treatment in regards to lesion size or bacterial burden (**Fig. 30D-F**). This led us to hypothesize that iKIR mediated enhanced bacterial clearance was in part dependent on type I interferon signaling.

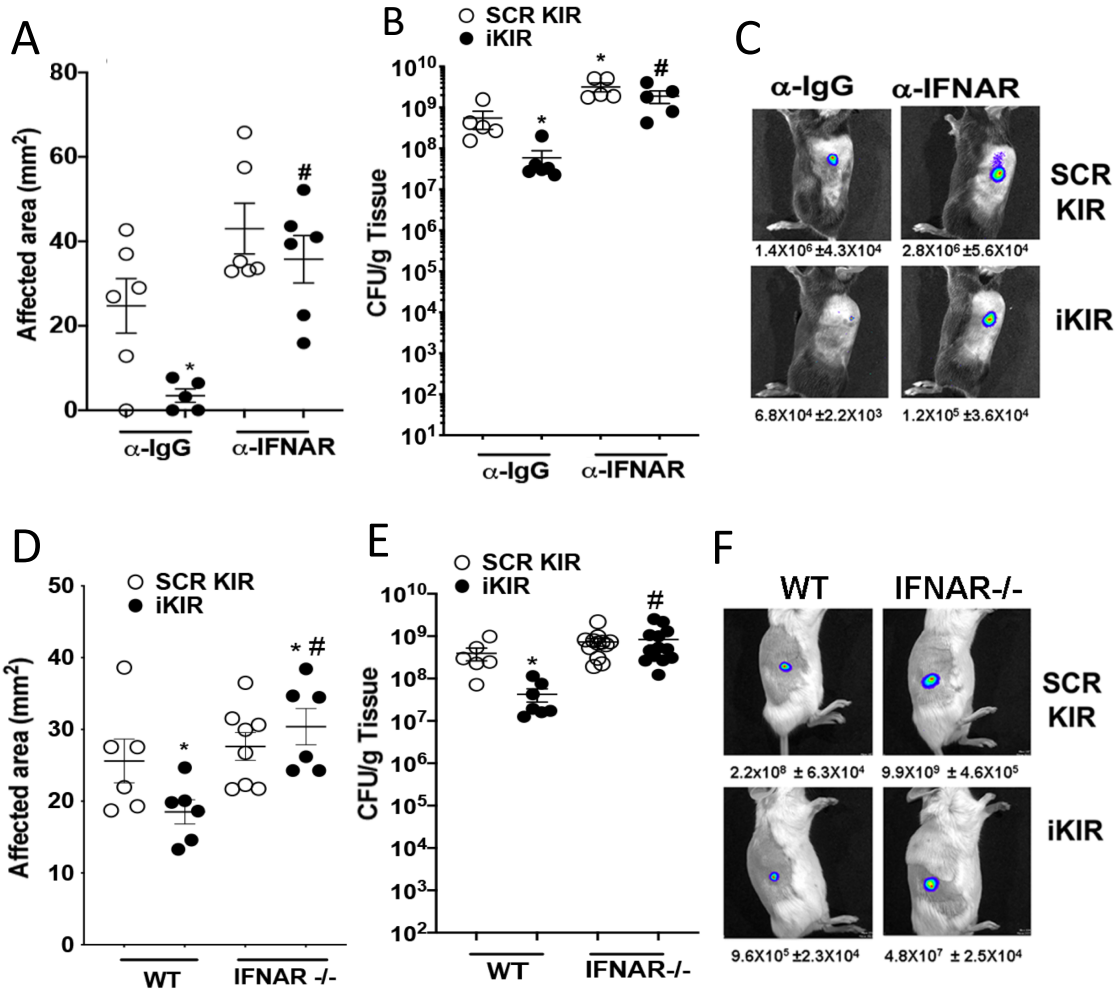

Figure 30. Improved infection outcome with SOCS-1 inhibition is dependent on type I interferon signaling. A.) Bioluminescent infection area in the skin of SCR KIR- and iKIR-treated animals treated with or without an IFNAR blocking antibody at day 1 post-infection. **B.)** Bacterial burden as determined by CFU from skin biopsy homogenates from mice treated as in **A** at day 1 post-infection. **C.)** Representative images of bioluminescent MRSA in the skin of mice treated as in **A** using planar bioluminescent imaging with total flux (photons/second) ± SEM listed below. **D.)** Surface lesion size as measured via caliper at day 3 post-infection in BALB/c or BALB/c IFNAR -/- mice treated with either iKIR or SCR KIR. **E.)** Bacterial load as measured by CFU from skin biopsy homogenates from mice treated as in **D** at day 3 post-infection. **F.)** Representative images of bioluminescent MRSA in the skin of mice treated as in **D** using planar bioluminescent imaging with total flux (photons/second) given below. Data represent the mean ± SEM from 3–9 mice from 2-3 independent experiments. *p<0.05 vs. SCR KIR+αIGG or SCR treated WT mice. #p<0.05 vs. iKIR+ αIGG or iKIR treated WT mice (One-way ANOVA followed by Bonferroni multiple comparison test).

Finally, we examined if there was a link between SOCS-1/type I IFN production and NO production during *in vivo* MRSA skin infection. When we assessed skin biopsy homogenates from mice receiving the IFNAR blocking antibody during infection, we saw that while iKIR treatment enhanced NO in the skin, mice receiving the blocking antibody had NO levels similar to those observed in SCR KIR-treated mice (**Fig. 31A**). Biopsies from infected IFNAR-/- and wildtype mice revealed a matching phenotype with inhibition of SOCS-1 and IFNAR returning NO levels to those seen in control animals, ablating enhanced NO production seen with iKIR treatment in wildtype animals (**Fig. 31B**). Together these data highlight a previously unknown axis of SOCS-1 and type I IFNs in regulating NO-mediated bacterial killing in the context of MRSA skin infection.

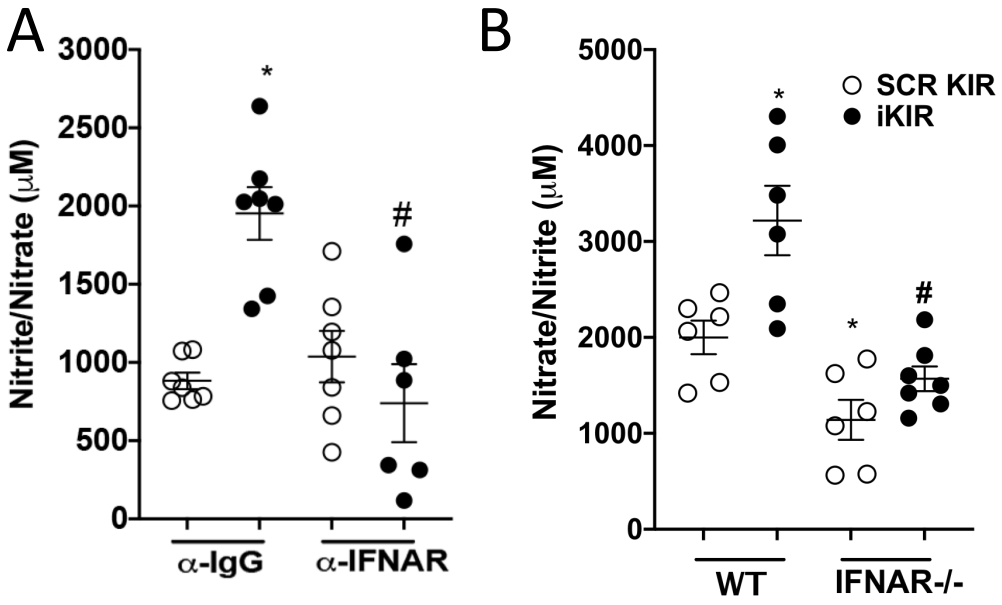

Figure 31. IFNAR blockade limits nitric oxide release. A.) Nitrite/Nitrate as measured via Griess assay from biopsies collected from mice treated with either SCR KIR or iKIR in conjunction with either an IFNAR blocking antibody or IgG control at day 1 post-infection. **B.)** Nitrite/Nitrate as measured via Griess assay from biopsies collected from BALB/c or BALB/c IFNAR -/- mice treated with either iKIR or SCR KIR at day 3 post-infection. Data represent the mean ± SEM from 5–7 mice from 2-3 independent experiments. *p<0.05 vs. SCR KIR+αIGG or SCR treated WT mice. #p<0.05 vs. iKIR+ αIGG or iKIR treated WT mice (One-way ANOVA followed by Bonferroni multiple comparison test).

CHAPTER 4

DISCUSSION AND FUTURE DIRECTIONS

Part I – PGE_2 in skin host defense

Models of diabetes

Patients with both type I and type II diabetes have increased susceptibility to skin and soft tissue infections [105–107,134]. While it has long been known that hyperglycemia is closely correlated with increased susceptibility to infection in these patients, the direct mechanism between hyperglycemia and impaired skin host defense remains elusive. In the current work, we utilized murine models of both insulin-deficient and insulin-resistant hyperglycemia to study its impact on skin host defense.

The primary model used was the diet-induced obesity (DIO) model wherein mice were fed a HFD for several months prior to infection, resulting in obesity and insulin-resistant hyperglycemia [156]. While genetic models of obesity are more commonly studied in the context of infection and immunity, the genetic nature of these models can make it difficult to discern the mechanisms contributing to impaired host defense. In particular, ob/ob and db/db mice, which lack a component of the leptin signaling pathway and develop obesity similar to DIO mice, have been frequently used to study mechanisms of impaired host defense as a result of obesity [157–159]. However, studies have demonstrated that administration of leptin can reverse many of these obesity-related impairments in host defense [157,160]. Furthermore, several studies have highlighted a role for leptin in activating components of the immune response [161,162], and we determined that a non-genetic model would allow us to more

carefully discern the impact of obesity-associated hyperglycemia on skin host defense against MRSA. Furthermore, the DIO mouse model more closely mimics human obesity, which generally does not have a single genetic component [156]. However, this model does have other co-morbidities such as increased circulating lipids and insulin resistance that have been shown to impact the immune response outside of hyperglycemia and must be considered when drawing conclusions from these mice [163].

Most of the studies utilizing a DIO mouse model aim to examine the metabolic impact of obesity with those focused on impaired host defense primarily examining the contributions of the expanded or altered adipose tissue. Several studies have found that adipose tissue processes such as adipogenesis, adipokine release, and adipose tissue expansion can negatively impact skin host defense [163–165]. In particular, it has been demonstrated that dermal adipogenesis, which becomes impaired during obesity in response to *S. aureus* skin infection, is critical for antimicrobial peptide generation to eliminate pathogens [163]. However, impaired wound healing, which is a significant problem in both obese and diabetic patient populations [72,74], is the focus of most skin studies utilizing the DIO mouse model. Most of these studies highlight the chronic inflammatory state, driven by obesity, within these wounds as the major driving factor in limiting their ability to properly heal [166,167]. Other factors such as poor revascularization, which is a major problem in diabetic skin wounds, have also been shown to limit wound healing in DIO mice [158].

PGE_2 also plays a role in impaired wound healing in obese mice, with one study demonstrating that COX-1-derived PGE_2 promoted keratinocyte proliferation and migration, while COX-2-derived PGE_2 resulted in inflammation that limited this process [73]. Therefore,

our work represents a unique context of the DIO mouse model and MRSA skin infection, in that we primarily focused on the immune response within these mice and the impact of the PGE_2 signaling pathway on skin host defense and immune cell recruitment, outside of the context of adipose tissue or wound healing.

The second model of hyperglycemia utilized in these studies was induced via low dose injections of STZ, which leads to DNA damage and death of the insulin-producing pancreatic beta cells, resulting in impaired insulin production and hyperglycemia [168]. This model is widely used due to the speed at which mice become hyperglycemic (within 10 days) compared to the DIO mouse model which requires several months of special feeding. While there are also genetic models of insulin-deficient hyperglycemia, such as the non-obese diabetic (NOD) mouse [169], we wanted to avoid confounding factors, such as the microbiota which can influence the incidence of hyperglycemia in these mice, contributing to impaired skin host defense. The STZ model is also widely used when studies are primarily focused on the impact of hyperglycemia on different processes, with blood glucose levels in STZ-treated mice being higher than obesity-related models. However, due to the toxic nature of STZ, some off-target effects are possible with higher doses of treatment, including organ damage and immunosuppression of specific immune cell populations [142,170]. Utilizing a low dose strategy for STZ administration, we did not see any elevations in markers for organ damage immediately after treatment or after 30 days before skin infection (data not shown). By waiting for 30 days after the final administration of STZ, we also avoid the immunosuppressive effects of STZ which typically occur for a short time after administration of the final dose of STZ at a high concentration [142].

The simplicity of the STZ model means there is a sizeable amount of literature using this model to study host defense and wound healing within the context of diabetes-related hyperglycemia. Impaired antimicrobial effector functions such as impaired phagocytosis and impaired ROS and RNS generation in macrophages and neutrophils have been shown to contribute to impaired host defense in multiple models of both local and systemic infection in STZ-induced hyperglycemic mice [112,141,171,172]. Similar to DIO mice, poor revascularization has also been shown to impair wound healing in STZ-treated mice, although they do not have the same level of hyper inflammation as DIO mice [173,174]. However, during wound healing in STZ-induced hyperglycemic mice, outside of the context of infection, PGE_2 has also been shown to promote vascularization and wound healing [175], demonstrating similarities to results seen in DIO mice. As the mechanisms driving impaired host defense in STZ-induced hyperglycemic mice have been more thoroughly investigated, we determined it would be an appropriate secondary model to confirm results in our DIO mice, as both models demonstrate similarities in skin immune responses to infection and wound healing that suggests a hyperglycemia-dependent mechanism limiting skin host defense in both models.

By utilizing a model of both insulin-resistant and insulin-deficient hyperglycemia, we were able to determine that the presence or lack of insulin itself did not significantly affect PGE_2 synthesis or the efficacy of misoprostol treatment in either model. Furthermore, despite the differences in the mechanisms of hyperglycemia in these models, and noted immune impairments in previous studies, we saw a high degree of parity in our studies between DIO- and STZ-induced hyperglycemic mice which strengthens the results from both models. DIO- and STZ-induced hyperglycemic mouse models both have impaired skin host defense that correlates

with reduced PGE_2 production, and infection outcomes in both groups were improved with misoprostol treatment. Furthermore, both groups displayed similar impairments in PTGES1 induction during skin infection, likely leading to impaired PGE_2 synthesis. Concerning misoprostol treatment, we demonstrated that in both models EP3 was necessary for the full therapeutic benefit of treatment and drove a similar cytokine profile in the skin of both groups. Finally, both DIO and STZ-treated mice had impaired recruitment of CXCR2+ phagocytes that was improved with misoprostol treatment and correlated with better infection outcomes. Together the similarity of these results has led us to hypothesize that a hyperglycemia-dependent mechanism is limiting the skin immune response in both mouse models that is improved during misoprostol treatment. To test this hypothesis future studies examining if treatments to restore euglycemia reverse these phenotypes will be needed.

However, we cannot discount possible unintended effects from either model as possibly impacting our results outside of the role of hyperglycemia in driving impaired skin host defense. STZ, as noted previously, can result in general organ toxicity; however, this work utilized a low-dose strategy of STZ administration [142,170] to avoid these off-target effects. As for the HFD model, other confounding effects of obesity such as increased adipogenesis or adipokine release may impact skin host defense separate from hyperglycemia [165]. Future infections in obese and STZ-treated mice that are not hyperglycemic will help delineate the role of hyperglycemia versus obesity or impaired insulin production in the context of skin host defense and the role of PGE_2 during skin infection. Finally, as both type I and type II diabetes are often associated with several co-morbidities that cannot be accurately modeled in these mouse models [106,129], exploring the role of PGE_2 in human skin infection samples with various co-

morbidities may provide insight into the exact role of hyperglycemia versus its downstream co-morbidities in contributing to impaired skin host defense.

Misoprostol vs. PGE_2

PGE_2 is a widely studied lipid mediator that has functions both in homeostasis and inflammation [42,44]. PGE_2 exerts its pleiotropic effects by binding to four distinct G protein-coupled receptors (EP1-4), which impact a wide variety of biological functions [51]. PGE_2 is quickly metabolized by dehydrogenase enzymes, which makes the use of this lipid *in vivo* challenging [41,43]. However, there are several different PGE analogs with similar EP binding properties as observed with native PGE_2. Misoprostol is an FDA-approved PGE analog that binds to these EP receptors, albeit with different affinities [51,53]. Misoprostol is prescribed to treat NSAID-induced stomach ulcers where impaired PGE_2 production results in inflammation and tissue damage within the gut [176]. In this context, misoprostol acts as replacement therapy for PGE_2 to limit inflammation and restore homeostasis to stomach tissue. However, misoprostol is also prescribed to induce labor within pregnant women by promoting vasodilation and smooth muscle contraction in the uterus [177], a reaction similar to inflammation, demonstrating the duality of misoprostol to enhance or limit inflammatory processes similar to PGE_2. Here, misoprostol was used to restore PGE_2 levels in the skin of hyperglycemic mice due to its stability and its FDA approval as a therapeutic, as well as its ability to bind the same receptors as PGE_2.

There are differences in receptor binding affinity and kinetics between PGE_2 and misoprostol, however, that must be considered in a broader context for the present work. First,

while EP3 and EP4 are considered high-affinity receptors for both PGE_2 and misoprostol, PGE_2 binds to EP4 with a slightly higher affinity, while misoprostol has a slightly higher affinity for EP3 [51–53,57]. The affinity for EP3 is likely the reason why misoprostol improves inflammatory cytokine release and skin host defense in our studies, as EP3 activation is correlated with fever and proinflammatory cytokine induction [9,54,55,64]. Interestingly, it has been shown that while PGE_2 can promote inflammation through the secretion of proinflammatory cytokines such as IL-1β, it also limits inflammation by controlling TNF-α levels [178]. This was seen in the current study with misoprostol treatment enhancing IL-1β and related chemokines with no impact on TNF-α secretion, demonstrating shared signaling pathways between PGE_2 and misoprostol.

Several research groups have demonstrated that the ability of PGE_2 to impair antimicrobial effector functions, such as phagocytosis, ROS/RNS generation, and macrophage maturation are dependent on EP2 and EP4 signaling through increasing cAMP concentrations that activate the downstream targets PKA and EPAC [57,59,66,68]. Therefore, the fact that we observe decreased cAMP with misoprostol treatment during MRSA skin infection that correlates with improved cytokine release, further supports EP3 as a critical receptor in our system and suggests misoprostol may activate different signaling programs compared to PGE_2. However, we did not investigate the impact misoprostol may have had on the effector function of recruited cells during skin infection and treatment. The potential activation of PKA or EPAC in our system and a role for the other EP receptors must not be ignored and should be investigated in future studies.

While having the highest affinity for EP3 *in vitro,* misoprostol is considered receptor non-selective and can bind to all 4 EP receptors [52]. Therefore, it is improbable that topical treatment with misoprostol is binding solely to EP3 in the skin of infected, hyperglycemic mice. When we treated infected mice topically with either an EP3 (Sulprostone) or EP4 (ONO-AE3) specific agonist individually or together, we did not see the same therapeutic benefit in lesion size or bacterial burden, as misoprostol treatment alone, again highlighting the potential involvement of other EP receptors during misoprostol treatment (data not shown). We also examined expression of the EP receptors within the skin of hyperglycemic and euglycemic mice to see if differences in receptor expression may account for the therapeutic benefit of misoprostol during hyperglycemia. However, when we examined the expression of these receptors by both ISH and qPCR from infection biopsies, we detected no significant difference between control and hyperglycemic groups (data not shown). It must also be considered that a unique binding property of misoprostol may be improving skin host defense of hyperglycemic mice, different from *de novo* PGE_2 production in response to bacterial stimuli. Relevant to this research are studies highlighting the ability of misoprostol to bind to different sites on EP3 receptor isoforms than PGE_2 that may impact its downstream signaling [51]. As this is the receptor through which our data suggests misoprostol is driving its therapeutic benefit, differences between PGE_2 and misoprostol should be considered for future therapeutic implications of misoprostol treatment.

In studies investigating the signaling pathways of PGE_2, misoprostol is often used for comparisons against cells treated with PGE_2. Several of these studies examining the immunosuppressive effects of PGE_2 demonstrate that while misoprostol can limit immune cell

effector function, migration, and maturation similar to PGE_2, it is significantly less effective at doing so [53,66]. Furthermore, misoprostol did not limit proinflammatory cytokine release from these cells as PGE_2 treatment did, demonstrating that while misoprostol can limit inflammation, it is not as immunosuppressive. Other studies have also demonstrated the diminished ability of misoprostol to induce keratinocyte migration and proliferation compared to PGE_2 [179]. The reduced cellular response to misoprostol versus PGE_2 treatment in these previous studies implies it may be a better therapeutic strategy to treat impaired PGE_2 production rather than treating with PGE_2 itself. Misoprostol likely has a wider therapeutic dosing range that would restore homeostatic signaling and avoid the extremes of hyper inflammation or immunosuppression that could result from excessive treatment with PGE_2. We hope in future studies to examine combining misoprostol treatment with topical antibiotics to further boost its therapeutic benefit during MRSA skin infection under hyperglycemic conditions.

Balance of PGE_2 in the regulation of inflammation/antimicrobial effector functions

Traditionally, PGE_2 was studied for its potent role in driving the cardinal signs of inflammation (heat, pain, redness, and swelling) [9,54,55,64]. Paradoxically, however, in certain contexts PGE_2 production has also been shown to be immunosuppressive. Its impact on the cellular immune response has been shown to limit immune cell effector functions such as ROS/RNS generation and phagocytosis [42,57,59,66]. Increased plasma PGE_2 is also associated with an immunosuppressed state in patients with certain traumas, including those with excessive burn wounds or patients recently receiving a bone marrow transplant [180]. The

immunosuppressive effect of PGE_2 is also thought to contribute to the severity of multiple diseases, including HIV infection [181] and cancer [182], in which excessive PGE_2 production limits the ability of the immune system to clear virally infected or cancerous cells. This duality of PGE_2 makes it a potential target for therapeutic intervention to restore homeostasis in diseases where dysregulation of inflammation is an underlying cause.

During infection, PGE_2 is produced in response to bacterial stimuli and stimulates the production of proinflammatory cytokines such as IL-1β, IL-17, or IL-8 while limiting inflammation by controlling TNF-α levels and inducing IL-10 secretion [178]. The unique nature of PGE_2 to induce a specific and balanced cytokine profile highlights its duality, as well as the importance of this molecule in maintaining homeostasis during inflammation. PGE_2 has been reported as having a role in promoting inflammasome activation, which is tied to its role in increasing IL-1β production. In particular, PGE_2 signaling via the EP3 receptor leads to activation of the NLRC4 inflammasome during infection with *Anaplasma phagocytophilum*, a gram-negative pathogen that primarily infects neutrophils [183]. Furthermore, IL-1β binding to the IL-1R increases COX-2 expression, creating a positive feedback loop between PGE_2 and IL-1β through the MAPK-ERK pathway [70]. Given the known importance of IL-1β in skin host defense against MRSA [114,116,119], the relationship of PGE_2 to IL-1β production and inflammasome activation during MRSA skin infection should be an area of future research.

The role of PGE_2 in skin host defense does require careful regulation, as euglycemic mice treated with misoprostol during MRSA skin infection develop significantly worse infection outcomes than untreated mice. While this may be due to impaired immune cell effector

function via EP2 and EP4 signaling in treated euglycemic animals, it may also be in part to a hyperinflammatory response caused by excessive EP3 receptor signaling in the skin of these mice during misoprostol treatment. While we did not further investigate the negative impact of misoprostol treatment in control animals, future research in this area could better help us to understand the differences between euglycemic and hyperglycemic skin and the role PGE_2 plays in skin host defense. In particular, we plan to investigate how treatments to restore euglycemia in hyperglycemic animals, via treatment with insulin or other medications, might impact the efficacy of misoprostol treatment during skin infection. These studies could have significant implications on the use of misoprostol to treat skin infections while also treating patients for hyperglycemia. A better understanding of the threshold of PGE_2 production between promoting or suppressing the immune system will also greatly benefit future efforts to utilize PGE_2 as a therapeutic intervention in inflammatory diseases.

The duality of PGE_2 makes it an interesting molecule to study in the context of hyperglycemia where impaired antimicrobial effector function in phagocytes is correlated with hyper inflammation, as opposed to immunosuppression, during infection [72,112,135,137]. The ability of PGE_2 to promote inflammation in this context should theoretically be deleterious, as it would further exacerbate the hyperinflammatory response. However, our data indicate that instead of driving damaging inflammation, via TNF-α or IL-6 secretion, PGE_2 production during skin infection may be critical to drive a specific inflammatory cascade, primarily through EP3 signaling, which decreases intracellular cAMP and enhances IL-1β production, to recruit specific CXCR2+ phagocyte populations to the skin. Recent studies on the role of PGE_2 in inflammasome activation have highlighted that while single high doses of PGE_2 can be immunosuppressive and

impair inflammasome assembly, small continuous exposure (similar to daily treatments with misoprostol) may prime the inflammatory response for inflammasome activation [55,178]. In particular, low dose repeated exposure to PGE_2 has been shown to increase IL-1β secretion by increasing pro-IL-1β transcripts prior to their processing by the inflammasome to mature IL-1β [71,184]. This is thought to occur through the activation of NF-κB and CREB, via EP3 receptor signaling lowering intracellular cAMP, which has been shown in previous studies investigating the role of PGE_2 on inflammasome activation [54,70,178]. We hypothesize this transcriptional pathway may be activated in the skin of our hyperglycemic mice treated with misoprostol resulting in the greater production of IL-1β we observe in the skin of misoprostol treated mice. Hypothetically increased IL-1β production then signals via the IL-1R to promote the enhanced production of the CXC chemokines (CXCL1, 2, and 5) that drive CXCR2+ phagocyte recruitment. While the findings here have exciting therapeutic implications, further studies to understand the role of PGE_2 production and the secondary messenger cAMP in response to injury or infection by various pathogens in multiple organs will be critical to better understand how PGE_2 synthesis and EP receptor signaling may impact inflammatory dysregulation.

While our data suggests CXC chemokine recruitment of CXCR2+ phagocytes is a driving factor behind misoprostol-enhanced skin host defense in hyperglycemic mice, we cannot rule out the potential impact misoprostol may have had on the effector functions of these recruited cells. Further studies to decipher the impact of misoprostol on inflammation and cell recruitment versus phagocyte effector functions could provide further understanding of the role PGE_2 has in skin host defense against MRSA.

PGE_2 role in wound healing

Chronic skin wounds are a major problem for both obese and diabetic patients [72,74,173,174]. Generally, skin wounds follow similar stages of inflammation, proliferation, and remodeling/maturation [126]. However, chronic wounds do not follow this well-defined healing pathway, often failing to transition from the inflammatory phase to the proliferative phase. These wounds are often characterized by persistent inflammation, excessive ROS, impaired angiogenesis, and poor reepithelization [73,127,173]. Open wounds also act as portals for bacterial colonization and infection in these patient populations and contribute to their high rates of nosocomial and recurrent infections which place an enormous burden on healthcare systems [106,134].

PGE_2 is released as part of the wound healing process [50,73,185], and its impaired production in the skin of patients with hyperglycemia could contribute to decreased wound healing during MRSA skin infection. Therefore, we hypothesize that misoprostol treatment may be contributing to the wound healing process during skin infection in hyperglycemic mice which benefits overall skin host defense. In humans, chronic wounds are characterized by elevated levels of IL-1α, TNF-α, IL-6, and CCL2, which are thought to drive deleterious phagocyte recruitment during wound healing [72,74,126]. In mice treated with misoprostol, however, we do not observe elevated levels of these inflammatory cytokines. Rather, as mentioned previously, we observe that misoprostol treatment enhances a specific cytokine/chemokine cascade that promotes specific immune cell recruitment via CXCR2. Therefore, we hypothesize it avoids the damaging hyper inflammation and tissue damage associated with chronic wounds.

Several studies examining skin wound healing in CXCR2-/- mice have also demonstrated that a failure to recruit these CXCR2+ phagocytes can impair the wound healing process [28,29].

Another primary characterization of chronic wounds is that keratinocytes within these wounds are hyperproliferative but non-migratory [166,167]. Keratinocytes express all four EP receptors and have been found to respond to PGE_2 [50]. Several groups have demonstrated PGE_2 can promote both keratinocyte proliferation and migration [50,72,73]. In these same studies, misoprostol had a similar effect on keratinocyte proliferation and migration, although to a lesser degree. Excessive PGE_2 production by cancerous skin melanomas is also associated with their excessive proliferation and migration into deeper tissues [182]. Therefore, given these known effects of PGE_2 on keratinocytes, we hypothesize that topical treatment of misoprostol in our studies could be impacting skin re-epithelization and wound healing independently of pathogen clearance. It is known that both DIO and STZ-induced hyperglycemic mice have impaired wound healing outside of infection, and future studies investigating misoprostol treatment of these "sterile" wounds could unveil novel roles for PGE_2 in the wound healing process and therapeutic strategies to treat these wounds.

Another major process that must occur for proper wound healing, especially in the context of MRSA infection, is the removal of dead/apoptotic cells and cellular debris via efferocytosis. The process of efferocytosis is a critical step in the transition from the proliferative to the remodeling phase during wound healing [186,187]. A failure to remove these apoptotic cells during wound healing can cause a secondary inflammatory response to these cells becoming necrotic and leaking intracellular contents [127,186]. This creates a chronic inflammatory state that often defines these hyperglycemic wounds that will never

properly heal and can become chronic non-healing ulcers that can require limb amputation to prevent infection of these open wounds. The process of efferocytosis is primarily handled by alternatively activated or "M2" macrophages [127,186]. As part of this process, macrophages release PGE_2 to limit inflammation and promote the switching of macrophages to an M2 or wound healing phenotype, further enhancing efferocytosis [128,187]. Limiting inflammation is also critical for initiating the remodeling phase of wound healing. It has also been demonstrated that impaired phagocytosis in macrophages from patients with diabetes also negatively impacts efferocytosis [127]. We have also seen an increase in apoptotic cell burden in the skin of hyperglycemic mice during MRSA skin infection (data not shown). Therefore, we hypothesize that misoprostol may promote efferocytosis at later stages of the infection, enhancing the wound healing process. While the primary focus of this research was on the impact of misoprostol on the initial innate inflammatory response, it is possible that at later stages of the infection, misoprostol was acting to promote efferocytosis and a switch in macrophage activation states to promote proper wound healing. This would benefit overall skin host defense by avoiding a chronic inflammatory state which can lead to immune cells becoming unresponsive to inflammatory stimuli and limiting their effector functions. Cell death and efferocytosis are both areas of interest in our work and future studies in this area could shed light on how PGE_2 deficiency and misoprostol treatment may impact dead cell clearance and wound healing during infection.

PGE_2 released during efferocytosis and wound healing has also been shown to improve the release of pro-angiogenic factors such as VEGF which promote revascularization of the tissue during repair [50,175,179]. As poor revascularization is another major problem in

diabetic and other chronic skin wounds [72,175], this represents another stage in the wound healing process in which misoprostol treatment may be improving skin host defense. Some groups have also demonstrated that misoprostol treatment can also promote the release of these angiogenic factors from macrophages *in vitro* [73,175]. We hypothesize the duality of both PGE_2 and misoprostol as both initiators and resolvers of the inflammatory response can be beneficial at multiple stages of infection and wound healing. This duality also makes misoprostol an ideal therapeutic to apply throughout infection to promote different stages of the host immune response and wound healing to improve infection outcomes.

PGE_2/cAMP/SOCS-1 axis

Induction and maintenance of the innate inflammatory response is controlled via the actions of various proinflammatory cytokines which primarily signal via the activation of receptor-bound tyrosine kinases, known as Janus Kinases (JAKs). These kinases activate a family of transcription factors, the Signal Transducers and Activators of Transcription (STATs). JAK-STAT signaling is responsible for the transcription of cytokine-inducible genes that drive innate immune cell activation and the inflammatory response during infection [153]. However, overactivation of this pathway can lead to deleterious inflammation and is therefore tightly controlled by a family of proteins, Suppressors of Cytokine Signaling (SOCS), in a negative feedback loop [78,88].

One of the more interesting findings from our current work when looking for mechanisms of misoprostol enhanced skin host defense was that SOCS-1 levels were

significantly elevated in the skin of our DIO hyperglycemic mice compared to controls and this trend was reversed with misoprostol treatment. Decreased SOCS-1 expression correlated with increased STAT-1 phosphorylation and the production of the related cytokine IFNγ. While enhanced SOCS-1 expression during hyperglycemic skin infection was likely a compensatory mechanism in response to the low-grade chronic inflammation in these mice, further studies in control and STZ-induced hyperglycemic mice demonstrated it also impairs phagocyte antimicrobial effector functions. Furthermore, its inhibition significantly improved MRSA skin infection outcomes in both control and hyperglycemic mice. Although our follow up studies highlighted this novel role of SOCS-1 in limiting the host immune response to MRSA, future studies investigating the relationship between PGE_2 secretion, the secondary messenger cAMP, and SOCS-1 could provide a novel pathway for therapeutic intervention during severe infection and diseases related to a dysregulation of the inflammatory response.

There are a few studies that do suggest a link between PGE_2 and SOCS-1 expression in different models. One group in particular found that macrophages and T cells infected with *Leishmania donovani* had significantly increased levels of SOCS-1 and SOCS-3 that correlated with infection severity [188]. They found that infected macrophages also secreted increased levels of PGE_2 and its signaling via the EP2 receptor and subsequent increasing intracellular cAMP concentrations, promoted PKA and downstream CREB activation that drove increased SOCS-1 and -3 expression [188]. Inhibition of either COX-2 or antagonism of EP2 reversed this phenotype and significantly reduced bacterial burden [188]. Furthermore, a second group examining inflammation in neurons found that *in vitro* treatment of neurons with exogenous cAMP resulted in increased SOCS-1 expression and decreased proinflammatory cytokine release

[189]. While they did not correlate this phenotype with PGE_2 production or EP receptor signaling in neurons, this work, along with the previously discussed study, point to a role of cAMP levels in dictating SOCS-1 expression. Therefore, in our system, we hypothesize that by lowering tissue cAMP via EP3 signaling during misoprostol treatment, we are decreasing SOCS-1 expression potentially by lowering PKA activation. This is an active area of study in our lab and while we have preliminarily seen that treatment of mice with topical, exogenous cAMP during MRSA skin infection results in worse infection outcomes, we are expecting to identify a connection to this phenotype with increasing SOCS-1 expression in future studies.

Limitations

While the data presented here highlights a potential pathway for therapeutic intervention during skin infection in patients with hyperglycemia, several limitations of these studies must be considered and investigated in future work. First, we only used a subcutaneous model of MRSA skin infection throughout the current work. While this model results in more reliable infection outcomes, it has been shown to elicit a slightly different immune response than more superficial models of infection. Therefore, future studies using a secondary superficial infection model (e.g. tape stripping) would further strengthen the current results on the importance of PGE_2 in skin host defense.

As mentioned previously, while the high degree of parity between our two hyperglycemia models led us to hypothesize that hyperglycemia was driving impaired skin host defense in these mice, other unintended side effect of either model must also be considered.

Obesity in particular has been shown to impair skin host defense independent of hyperglycemia due to impaired adipokine release combined with increased adipogenesis. In our current work we did not fully investigate the impact of misoprostol treatment on obese euglycemic mice. Future infections in obese mice that are not hyperglycemic will help delineate the role of hyperglycemia versus obesity during misoprostol enhanced skin host defense in DIO mice. It also has the potential to uncover new inflammatory pathways regulated by PGE_2 during obesity. Furthermore, both our models of hyperglycemia were limited to the use of male mice, as difference in the immune response between males and females have been reported, this is another biological factor that must be more fully investigated in future studies.

For the clinical implications of this work, patients with hyperglycemia are frequently treated with insulin and antibiotics during skin infection, both of which could significantly improve or impair the efficacy of misoprostol treatment. Future studies combining insulin and antibiotic treatment with misoprostol would uncover how the restoration of euglycemia in hyperglycemic mice potentially impacts the efficacy of misoprostol. In our current work euglycemic LFD mice treated with misoprostol had worse infection outcomes, however, this state of euglycemia could differ from euglycemia brought about by insulin treatment and should be more fully investigated. Combining treatment with antibiotics could also potentially uncover an enhanced impact of misoprostol with antibiotics that results in greater bacterial clearance. Finally, as mentioned previously, future studies using human samples will be critically to investigate how co-morbidities frequently associated with diabetes such as neuropathy and vascular complications, that cannot be accurately modeled in mice, impacts the efficacy of misoprostol.

Conclusion

To summarize, DIO hyperglycemic mice have impaired skin host defense characterized by poor abscess formation, increased bacterial burden, and surface lesion size compared to euglycemic controls. Poor infection outcome in DIO mice was correlated with reduced levels of PGE_2 in the skin, and treatment with the PGE analog misoprostol significantly improved bacterial clearance and abscess formation during MRSA skin infection. HFD and STZ-induced hyperglycemic mice had reduced PTGES1 expression during MRSA skin infection that likely contributed to impaired PGE_2 production. Misoprostol treatment was found to act in part through the EP3 receptor to drive increased CXCR2+ monocytes and neutrophils to the site of infection in DIO and STZ treated mice. Misoprostol treatment also regulated STAT-1 dependent SOCS-1 expression in the skin of HFD mice during infection. As impaired PGE_2 production correlated with poor infection outcome in two separate models of hyperglycemia, it highlights the importance of studying how certain disease states may impact the release of inflammatory mediators. PGE_2, and more specifically misoprostol, have therapeutic potential for other diseases in which chronic inflammation or dysregulation of the inflammatory response is an underlying cause. In the context of infection, misoprostol treatment may be combined with antibiotics to further enhance its therapeutic potential.

Part II – SOCS-1 as a negative regulator of skin host defense

Macrophage versus neutrophil SOCS-1 expression

Macrophages and neutrophils are critical in promoting skin host defense against MRSA. However, the role of each cell type during skin infection with MRSA does differ. Neutrophils are critical at multiple stages of skin infection including bacterial clearance, abscess formation, and chemokine release [115–117]. Neutrophils make up to half of the leukocytes at the site of infection 48 hours after infection and are the primary cells within the neutrophilic abscess responsible for pathogen elimination through ROS/RNS generation and NET release [114,155]. Neutrophil-derived IL-1β is critical not only for abscess formation during MRSA skin infection but also for sustained proinflammatory cytokine release and neutrophil recruitment to the site of infection [118,119]. Macrophages are typically found at the periphery of the abscess architecture and are thought to help coordinate initial pathogen recognition/control, phagocyte recruitment, cytokine release, and abscess formation during infection [112,122,150]. They are also critical for removing dead cells and cellular debris as well as abscess breakdown after pathogens have been eliminated before wound healing and revascularization [120,122,190,191]. Given this importance in skin host defense, these cell populations are often the focus of studies on the host immune response against MRSA.

To avoid damaging inflammation during infection, intracellular molecular breaks, such as SOCS-1, act in a classical negative feedback loop within immune cells such as neutrophils and macrophages to limit the perpetuation of proinflammatory signals. However, these molecular breaks can also limit immune cell effector function during infection resulting in worse infection

outcomes. Here, we highlight a negative correlation between SOCS-1 expression and infection severity during MRSA skin infection. Given the importance of macrophages and neutrophils in skin host defense against MRSA, we sought to investigate the role of SOCS-1 expression in these cells. To study the role of SOCS-1 in innate inflammatory phagocytes during MRSA skin infection, we utilized myeloid cell-specific knockout *Socs1*$^{\Delta myeloid}$ mice. These mice lacked SOCS-1 in macrophages, monocytes, and neutrophils and exhibited significantly improved infection outcomes compared to wildtype mice. However, this model did not allow us to determine the contributions of SOCS-1 deficient macrophages/monocytes versus neutrophils in improved infection outcomes in these animals. While we did see enhanced phagocytosis and killing of MRSA by SOCS-1 deficient bone marrow-derived macrophages, we did not examine the potential for improved antimicrobial effector functions in neutrophils. As neutrophils are thought to eliminate the majority of pathogen during MRSA skin infection [114,116,117], the contribution of these cells to enhanced bacterial clearance *in vivo* during SOCS-1 inhibition should be further investigated. We did, however, find increased intracellular bacteria within the abscess of iKIR treated mice *in vivo.* As neutrophils are the primary cells within the abscess, this does suggest improved antimicrobial effector functions in neutrophils with SOCS-1 inhibition.

Another area in which the contributions of neutrophils and macrophages during SOCS-1 inhibition could be critical is the secretion of proinflammatory chemokines and cytokines. Macrophages and neutrophils secrete chemokines to drive cell recruitment during skin infection [114,115]. In particular, neutrophils are critical for prolonged phagocyte recruitment during MRSA skin infection [118,119,192]. Meanwhile, early secretion of proinflammatory cytokines by skin resident macrophages is essential for initiating the host immune response to

MRSA [112,150,152]. While we observed increased production of IL-1β and the downstream chemokines CXCL1 and CXCL2 with SOCS-1 inhibition, the source of these chemokines remains to be determined. Both macrophages and neutrophils express SOCS-1, however, it is difficult to hypothesize which of these cell populations may be impacted to a greater degree by SOCS-1 inhibition. By better understanding which cell populations are impacted by SOCS-1 inhibition, we can more directly target those populations to limit the derogatory effects of SOCS-1 without broad inhibition which could lead to damaging hyper inflammation. Future studies to better delineate the contributions of SOCS-1 inhibition in neutrophils versus macrophages will allow us to better fine-tune this strategy to improve infection outcomes while maintaining a balanced immune response.

Type I vs. type II IFN signaling

Both type I and type II IFNs are well known for their roles in anti-viral immunity. However, recent work has demonstrated a role for both IFNs in promoting the host immune response against bacterial pathogens [86,193,194]. IFNγ is a potent activator of macrophages and increases the gene expression of several antimicrobial effectors such as subunits of the NADPH oxidase complex (gp91phox, p47phox), iNOS, and antimicrobial peptides [33]. It also enhances the capacity of macrophages to elicit the adaptive immune response by enhancing the expression of MHCII and antigen presentation [33]. In the current work, enhanced IFNγ signaling alone did not account for the therapeutic benefit of SOCS-1 inhibition. While we hypothesized that enhanced IFNγ production during SOCS-1 inhibition improved bacterial

phagocytosis and killing that we observed *in vitro*, blocking IFNGR did not remove the therapeutic benefit of SOCS-1 inhibition *in vivo*.

Recent work has highlighted a role for IFNβ in promoting macrophage activation and bacterial killing [86]. Under inflammatory conditions IFNβ has been shown to act in an autocrine manner to enhance iNOS expression and NO release; to drive improved bacterial killing [195,196]. Interestingly, these studies demonstrate that while IFNβ alone does not promote a significant increase in NO, IFNβ combined with TLR1/2 or 4 stimulation significantly enhances NO production [195]. As TLR1 and 2 are essential PRRs in recognizing MRSA by binding to the lipoteichoic acids that make up its cell wall [114,116], we hypothesize their activation combined with enhanced IFNβ production is promoting increased NO production and bacterial killing in our current study during SOCS-1 inhibition. We hypothesize that the autocrine nature of IFNβ signaling [194] combined with early TLR signaling is responsible for improved infection outcomes as early as 6 hours post-infection as cells producing IFNβ are quickly responding to its enhanced production. We believe that increased iKIR-dependent IFNβ production and/or actions during MRSA skin infections promote increased NO production and subsequent bacterial killing in this study.

Our current research demonstrates that increased iKIR-mediated IFNβ production and/or IFNAR signaling are sufficient to enhance bacterial killing in the absence of IFNGR signaling *in vivo*. However, due to the prominent role of IFNγ in macrophage activation [33], we cannot exclude a role for IFNγ in iKIR mediated improved skin host defense. Since we only determined bacterial burden at a single early timepoint post-infection (day 1) in IFNGR antibody-treated mice, it is possible that IFNγ could play a role in skin host defense at later time

points post-infection. Also, type I IFNs have been shown to have a suppressive effect on IFNγ signaling. Type I IFNs have been shown to downregulate IFNGR expression on macrophages during bacterial infection, making them less sensitive to IFNγ stimulation [197]. It is possible in our current study that enhanced type I interferon production early in infection was limiting the impact of increased IFNGR signaling. Further research will be needed to examine the balance of type I versus type II interferon signaling and their effects on one another that promotes an efficient host immune response to MRSA skin infection. Finally, we did not investigate whether SOCS-1 influenced IFNAR signaling directly or acted on downstream events. We speculate that SOCS-1 could play a role in limiting the activation of the IRFs downstream of IFNAR, but further studies are needed to decipher the role of SOCS-1 in type I interferon production and downstream signaling during infection.

SOCS-1 and abscess architecture

The hallmark of MRSA infections in multiple organ systems is the formation of a neutrophilic abscess. These abscesses generally have a similar structure regardless of location with a central core of live bacteria surrounded by live and dead neutrophils contained within a fibrous capsule [122,190]. However, some differences do exist in abscesses within different anatomical locations. These include the steps leading to abscess formation such as phagocyte recruitment, removal of cell debris, and capsule formation [123,124]. Furthermore, the importance of the abscess in infection outcome can vary based on the infected organ with abscesses in the lungs and kidneys being detrimental to the host while in the skin abscesses are

critical to prevent further bacterial dissemination [122,124]. While some recent work has suggested that abscess formation may benefit *S. aureus* during infection by protecting it from infiltrating phagocytes [123], the majority of literature in the field has demonstrated its necessity for bacterial control and elimination [119,150,191].

Here, we found that SOCS-1 inhibition improves abscess capsule thickness and promotes a more condensed abscess phenotype. One hypothesis for this could be that enhanced neutrophil recruitment and bacterial clearance with SOCS-1 inhibition contributed to improved abscess formation. However, recent studies have highlighted that interferons can play a role in *S. aureus* abscess formation and breakdown by influencing fibroblast actions. It has been demonstrated that IFNγ from NK cells is necessary to initiate abscess capsule breakdown by activating the fibrinolytic system, and IFNγ deficient mice form thicker abscess capsules during *S. aureus* skin infection [191]. While we did see increased type I (IFNα and IFNβ) and type II (IFNγ) interferons during SOCS-1 inhibition and skin infection, we found that the type I IFNs seemed to be the driving improved infection outcomes, rather than type II IFN. In regards to abscess formation, high levels of type I IFNs have been shown to impair the expression of the IFNγ receptor (IFNGR) [197], which in turn could result in a thicker abscess capsule as IFNGR signaling is impaired, as previous studies have demonstrated [191]. Although we did observe worse MRSA skin infection outcomes in mice treated with IFNGR blocking antibody, the impact of this treatment on abscess formation was not investigated. Future investigations into the role of SOCS-1 and type I versus type II interferons in abscess formation could provide more detail into the hierarchy of these pathways in contributing to an essential step in skin host defense against MRSA. Finally, the work here cannot rule out a role for fibroblasts or NK cells

contributing to improved skin host defense against MRSA and as mentioned previously, the impact of SOCS-1 on different cell populations should be examined in future work.

Limitations

While the data presented here highlights a potential pathway for therapeutic intervention during antibiotic-resistant skin infection, several limitations of these studies must be considered and investigated in future work. As mentioned in the previous section, limitations with our models of hyperglycemia do exist and must be investigated further for potential clinical implications. Treatments with insulin or antibiotics in conjunction with SOCS-1 inhibition could impair or enhance its therapeutic benefit and potential interactions with these drugs should be more fully investigated. Furthermore, this work was solely done in a model of insulin-deficient hyperglycemia, and future work in insulin-resistant models could further investigate the negative impact enhanced SOCS-1 expression has during skin host defense in hyperglycemic mice. Also highlighted in the previous section was our use of only a single subcutaneous infection model. It is possible that SOCS-1 expression and impact on skin host defense may vary with infection model, and future studies utilizing different infection strategies could uncover new mechanisms by which SOCS-1 regulates the host skin immune response. Finally, we did not directly quantify the level of SOCS-1 inhibition that occurred during iKIR treatment. While we did see enhanced STAT-1 activation with SOCS-1 inhibition a quantification of the degree of SOCS-1 inhibition with iKIR treatment would greatly inform future potential therapeutic strategies to limit SOCS-1 actions while avoiding overwhelming inflammation.

Conclusion

In summary, SOCS-1 expression is detrimental in both hyperglycemic and euglycemic mice during MRSA skin infection. Blocking of SOCS-1 actions, either through pharmacological inhibition or cell-specific deletion, increased bacterial clearance and decreased lesion size in both control and hyperglycemic animals. Inhibition of SOCS-1 improved proinflammatory cytokine release and bacterial killing dependent on NO release. Type I and type II IFN secretion was also improved during SOCS-1 inhibition, which was impaired in the skin of infected hyperglycemic mice. Blocking IFNAR, but not IFNGR, removed the therapeutic benefit of SOCS-1 inhibition, suggesting type I IFNs are driving improved NO release and bacterial clearance during SOCS-1 inhibition in the context of MRSA skin infection. Together these data demonstrate a potential for SOCS-1 as a target in immunostimulatory therapies to treat antibiotic-resistant infections.

REFERENCES

1. Medzhitov, R. Origin and physiological roles of inflammation. *Nature* vol. 454 428–435 (2008).

2. Takeuchi, O. & Akira, S. Pattern Recognition Receptors and Inflammation. *Cell* vol. 140 805–820 (2010).

3. Turner, M. D., Nedjai, B., Hurst, T. & Pennington, D. J. Cytokines and chemokines: At the crossroads of cell signalling and inflammatory disease. *Biochimica et Biophysica Acta - Molecular Cell Research* vol. 1843 2563–2582 (2014).

4. MC, B. & BD, L. Specialized pro-resolving mediators: endogenous regulators of infection and inflammation. *Nat. Rev. Immunol.* **16**, 51–67 (2016).

5. Kotas, M. E. & Medzhitov, R. Homeostasis, Inflammation, and Disease Susceptibility. *Cell* vol. 160 816–827 (2015).

6. Wong, C. H. Y., Heit, B. & Kubes, P. Molecular regulators of leucocyte chemotaxis during inflammation. *Cardiovascular Research* vol. 86 183–191 (2010).

7. Soehnlein, O., Steffens, S., Hidalgo, A. & Weber, C. Neutrophils as protagonists and targets in chronic inflammation. *Nature Reviews Immunology* vol. 17 248–261 (2017).

8. Shi, C. & Pamer, E. G. Monocyte recruitment during infection and inflammation. *Nature Reviews Immunology* vol. 11 762–774 (2011).

9. Tsuge, K., Inazumi, T., Shimamoto, A. & Sugimoto, Y. Molecular mechanisms underlying prostaglandin E2-exacerbated inflammation and immune diseases. *International Immunology* vol. 31 597–606 (2019).

10. Su, Y. & Richmond, A. Chemokine Regulation of Neutrophil Infiltration of Skin Wounds. *Adv. Wound Care* **4**, 631–640 (2015).

11. Abtin, A. *et al.* Perivascular macrophages mediate neutrophil recruitment during bacterial skin infection. *Nat. Immunol.* **15**, 45–53 (2014).

12. Chou, R. C. *et al.* Lipid-Cytokine-Chemokine Cascade Drives Neutrophil Recruitment in a Murine Model of Inflammatory Arthritis. *Immunity* **33**, 266–278 (2010).

13. Zaja-Milatovic, S. & Richmond, A. CXC chemokines and their receptors: A case for a significant biological role in cutaneous wound healing. *Histology and Histopathology* vol. 23 1399–1407 (2008).

14. Griffith, J. W., Sokol, C. L. & Luster, A. D. Chemokines and Chemokine Receptors: Positioning Cells for Host Defense and Immunity. (2014) doi:10.1146/annurev-immunol-032713-120145.

15. Davies, L. C., Jenkins, S. J., Allen, J. E. & Taylor, P. R. Tissue-resident macrophages. *Nature Immunology* vol. 14 986–995 (2013).

16. Epelman, S., Lavine, K. J. & Randolph, G. J. Origin and Functions of Tissue Macrophages. *Immunity* vol. 41 21–35 (2014).

17. Mosser, D. M. & Edwards, J. P. Exploring the full spectrum of macrophage activation. *Nature Reviews Immunology* vol. 8 958–969 (2008).

18. Zhang, X. & Mosser, D. M. Macrophage activation by endogenous danger signals. *Journal of Pathology* vol. 214 161–178 (2008).

19. Stocks, C. J., Schembri, M. A., Sweet, M. J. & Kapetanovic, R. For when bacterial infections persist: Toll-like receptor-inducible direct antimicrobial pathways in macrophages. *Journal of Leukocyte Biology* vol. 103 35–51 (2018).

20. Panday, A., Sahoo, M. K., Osorio, D. & Batra, S. NADPH oxidases: An overview from structure to innate immunity-associated pathologies. *Cellular and Molecular Immunology* vol. 12 5–23 (2015).

21. Gordon, S. Alternative activation of macrophages. *Nature Reviews Immunology* vol. 3 23–35 (2003).

22. Bystrom, J. *et al.* Resolution-phase macrophages possess a unique inflammatory phenotype that is controlled by cAMP. *Blood* **112**, 4117–4127 (2008).

23. RJ, S. *et al.* Macrophages: A review of their role in wound healing and their therapeutic use. *Wound Repair Regen.* **24**, 613–629 (2016).

24. Faurschou, M. & Borregaard, N. Neutrophil granules and secretory vesicles in inflammation. *Microbes and Infection* vol. 5 1317–1327 (2003).

25. Borregaard, N. & Cowland, J. B. Granules of the human neutrophilic polymorphonuclear leukocyte. *Blood* vol. 89 3503–3521 (1997).

26. Kinchen, J. M. & Ravichandran, K. S. Phagosome maturation: Going through the acid test. *Nature Reviews Molecular Cell Biology* vol. 9 781–795 (2008).

27. Brinkmann, V. *et al.* Neutrophil Extracellular Traps Kill Bacteria. *Science (80-.).* **303**, 1532–1535 (2004).

28. Milatovic, S., Nanney, L. B., Yu, Y., White, J. R. & Richmond, A. Impaired healing of nitrogen mustard wounds in CXCR2 null mice. *Wound Repair Regen.* **11**, 213–219 (2003).

29. Devalaraja, R. M. *et al.* Delayed wound healing in CXCR 2 knockout mice. *J. Invest. Dermatol.* **115**, 234–244 (2000).

30. Gordon, S. Phagocytosis: An Immunobiologic Process. *Immunity* vol. 44 463–475 (2016).

31. Areschoug, T. & Gordon, S. Scavenger receptors: Role in innate immunity and microbial pathogenesis. *Cellular Microbiology* vol. 11 1160–1169 (2009).

32. Rougerie, P., Miskolci, V. & Cox, D. Generation of membrane structures during phagocytosis and chemotaxis of macrophages: Role and regulation of the actin

cytoskeleton. *Immunol. Rev.* **256**, 222–239 (2013).

33. Schroder, K., Hertzog, P. J., Ravasi, T. & Hume, D. A. Interferon-γ: an overview of signals, mechanisms and functions. *J. Leukoc. Biol.* **75**, 163–189 (2004).

34. Von Bernuth, H. *et al.* Pyogenic bacterial infections in humans with MyD88 deficiency. *Science (80-.).* **321**, 691–696 (2008).

35. Uchiya, K. I. & Nikai, T. Salmonella enterica serovar typhimurium infection induces cyclooxygenase 2 expression in macrophages: Involvement of Salmonella pathogenicity island 2. *Infect. Immun.* **72**, 6860–6869 (2004).

36. Bogdan, C. Nitric oxide and the immune response. *Nature Immunology* vol. 2 907–916 (2001).

37. Panaro, M. A. *et al.* Nitric oxide production by Leishmania-infected macrophages and modulation by prostaglandin E2. *Clin. Exp. Med.* **1**, 137–143 (2001).

38. Nizet, V. *et al.* Innate antimicrobial peptide protects the skin from invasive bacterial infection. *Nature* **414**, 454–457 (2001).

39. Rončević, T., Puizina, J. & Tossi, A. Antimicrobial peptides as anti-infective agents in pre-post-antibiotic era? *International Journal of Molecular Sciences* vol. 20 (2019).

40. Schauber, J. & Gallo, R. L. Antimicrobial peptides and the skin immune defense system. *Journal of Allergy and Clinical Immunology* vol. 122 261–266 (2008).

41. Calde, P. C. Eicosanoids. *Essays in Biochemistry* vol. 64 423–441 (2020).

42. Kalinski, P. Regulation of Immune Responses by Prostaglandin E 2 . *J. Immunol.* **188**, 21–28 (2012).

43. Park, J. Y., Pillinger, M. H. & Abramson, S. B. Prostaglandin E2 synthesis and secretion: The role of PGE2 synthases. *Clin. Immunol.* **119**, 229–240 (2006).

44. Tilley, S. L., Coffman, T. M. & Koller, B. H. Mixed messages: modulation of inflammation and immune responses by prostaglandins and thromboxanes. *J. Clin. Invest.* **108**, 15–23 (2001).

45. Smith, W. L., Urade, Y. & Jakobsson, J. Enzymes of the Cyclooxygenase Pathways of Prostanoid Biosynthesis. *Chem. Rev* **111**, 5821–5865 (2011).

46. Morita, I. Distinct functions of COX-1 and COX-2. *Prostaglandins Other Lipid Mediat.* **68–69**, 165–175 (2002).

47. Seo, M. J. & Oh, D. K. Prostaglandin synthases: Molecular characterization and involvement in prostaglandin biosynthesis. *Progress in Lipid Research* vol. 66 50–68 (2017).

48. Murakami, M. *et al.* Cellular prostaglandin E2 production by membrane-bound prostaglandin E synthase-2 via both cyclooxygenases-1 and -2. *J. Biol. Chem.* **278**, 37937–

37947 (2003).

49. Y, L. *et al.* Age-Associated Increase in Skin Fibroblast-Derived Prostaglandin E2 Contributes to Reduced Collagen Levels in Elderly Human Skin. *J. Invest. Dermatol.* **135**, 2181–2188 (2015).

50. Sivamani, R. K. Eicosanoids and Keratinocytes in Wound Healing. *Adv. Wound Care* **3**, 476–481 (2014).

51. Sugimoto, Y. & Narumiya, S. Prostaglandin E receptors. *Journal of Biological Chemistry* vol. 282 11613–11617 (2007).

52. Biringer, R. G. A Review of Prostanoid Receptors: Expression, Characterization, Regulation, and Mechanism of Action. doi:10.1007/s12079-020-00585-0/Published.

53. Nataraj, C. *et al.* Receptors for prostaglandin E2 that regulate cellular immune responses in the mouse. *J. Clin. Invest.* **108**, 1229–1235 (2001).

54. Oka, T. Prostaglandin E2 as a mediator of fever: the role of prostaglandin E (EP) receptors. *Frontiers in bioscience : a journal and virtual library* vol. 9 3046–3057 (2004).

55. Kawahara, K., Hohjoh, H., Inazumi, T., Tsuchiya, S. & Sugimoto, Y. Prostaglandin E2-induced inflammation: Relevance of prostaglandin e receptors. *Biochimica et Biophysica Acta - Molecular and Cell Biology of Lipids* vol. 1851 414–421 (2015).

56. Martínez-Colón, G. J. & Moore, B. B. Prostaglandin E2 as a Regulator of Immunity to Pathogens. *Pharmacology and Therapeutics* vol. 185 135–146 (2018).

57. Medeiros, A., Peres-Buzalaf, C., Fortino Verdan, F. & Serezani, C. H. Prostaglandin E 2 and the suppression of phagocyte innate immune responses in different organs. *Mediators of Inflammation* vol. 2012 (2012).

58. Martínez-Colón, G. J., Taylor, Q. M., Wilke, C. A., Podsiad, A. B. & Moore, B. B. Elevated prostaglandin e 2 post-bone marrow transplant mediates interleukin-1β-related lung injury. *Mucosal Immunol.* **11**, 319–332 (2018).

59. Agard, M., Asakrah, S. & Morici, L. A. PGE2 suppression of innate immunity during mucosal bacterial infection. *Frontiers in Cellular and Infection Microbiology* vol. 4 (2013).

60. Hohjoh, H., Inazumi, T., Tsuchiya, S. & Sugimoto, Y. Prostanoid receptors and acute inflammation in skin. *Biochimie* vol. 107 78–81 (2014).

61. Hasegawa, H. *et al. Di¡erent membrane targeting of prostaglandin EP3 receptor isoforms dependent on their carboxy-terminal tail structures*.

62. Ceddia, R. P. *et al.* The PGE2 EP3 receptor regulates diet-induced adiposity in male Mice. *Endocrinology* **157**, 220–232 (2016).

63. Irie, A. *et al. Third isoform of the prostaglandin-E-receptor EP, subtype with different C-terminal tail coupling to both stimulation and inhibition of adenylate cyclase*. *Eur. J. Biochem* vol. 217 (1993).

64. Ushikubi, F. *et al.* Impaired febrile response in mice lacking the prostaglandin E receptor subtype EP3. *Nature* **395**, 281–284 (1998).

65. Levy, B. D., Clish, C. B., Schmidt, B., Gronert, K. & Serhan, C. N. Lipid mediator class switching during acute inflammation: Signals in resolution. *Nat. Immunol.* **2**, 612–619 (2001).

66. Zasłona, Z., Serezani, C. H., Okunishi, K., Aronoff, D. M. & Peters-Golden, M. Prostaglandin E 2 restrains macrophage maturation via E prostanoid receptor 2/protein kinase A signaling. *Blood* **119**, 2358–2367 (2012).

67. Cockeran, R., Steel, H. C., Mitchell, T. J., Feldman, C. & Anderson, R. Pneumolysin potentiates production of prostaglandin E2 and leukotriene B4 by human neutrophils. *Infect. Immun.* **69**, 3494–3496 (2001).

68. Sadikot, R. T. *et al.* Bacterial clearance of Pseudomonas aeruginosa is enhanced by the inhibtion of COX-2. *Eur. J. Immunol.* **37**, 1001–1009 (2007).

69. Mortimer, L., Moreau, F., MacDonald, J. A. & Chadee, K. NLRP3 inflammasome inhibition is disrupted in a group of auto-inflammatory disease CAPS mutations. *Nat. Immunol.* **17**, 1176–1186 (2016).

70. Hua, K. F. *et al.* Cyclooxygenase-2 regulates NLRP3 inflammasome-derived IL-1β production. *J. Cell. Physiol.* **230**, 863–874 (2015).

71. Zoccal, K. F. *et al.* Opposing roles of LTB4 and PGE2 in regulating the inflammasome-dependent scorpion venom-induced mortality. *Nat. Commun.* **7**, (2016).

72. Galkowska, H., Wojewodzka, U. & Olszewski, W. L. Chemokines, cytokines, and growth factors in keratinocytes and dermal endothelial cells in the margin of chronic diabetic foot ulcers. *Wound Repair Regen.* **14**, 558–565 (2006).

73. Kämpfer, H., Schmidt, R., Geisslinger, G., Pfeilschifter, J. & Frank, S. Wound inflammation in diabetic ob/ob mice: Functional coupling of prostaglandin biosynthesis to cyclooxygenase-1 activity in diabetes-impaired wound healing. *Diabetes* **54**, 1543–1551 (2005).

74. Brem, H. & Tomic-Canic, M. Cellular and molecular basis of wound healing in diabetes. *Journal of Clinical Investigation* vol. 117 1219–1222 (2007).

75. Yoshimura, A., Naka, T. & Kubo, M. SOCS proteins, cytokine signalling and immune regulation. *Nature Reviews Immunology* vol. 7 454–465 (2007).

76. Naka, T. & Fujimoto, M. SOCS1, a negative regulator of cytokine signals and TLR responses, in human liver diseases. *Gastroenterology Research and Practice* vol. 2010 (2010).

77. Kazi, J. U., Kabir, N. N., Flores-Morales, A. & Rönnstrand, L. SOCS proteins in regulation of receptor tyrosine kinase signaling. *Cellular and Molecular Life Sciences* vol. 71 3297–3310 (2014).

78. Liau, N. P. D. *et al.* The molecular basis of JAK/STAT inhibition by SOCS1. *Nat. Commun.* **9**, 1–14 (2018).

79. Waiboci, L. W. *et al.* Both the Suppressor of Cytokine Signaling 1 (SOCS-1) Kinase Inhibitory Region and SOCS-1 Mimetic Bind to JAK2 Autophosphorylation Site: Implications for the Development of a SOCS-1 Antagonist. *J. Immunol.* **178**, 5058–5068 (2007).

80. Ahmed, C. M. I., Larkin, J. & Johnson, H. M. SOCS1 mimetics and antagonists: A complementary approach to positive and negative regulation of immune function. *Frontiers in Immunology* vol. 6 183 (2015).

81. Duncan, S. A., Baganizi, D. R., Sahu, R., Singh, S. R. & Dennis, V. A. SOCS proteins as regulators of inflammatory responses induced by bacterial infections: A review. *Frontiers in Microbiology* vol. 8 2431 (2017).

82. Serezani, C. H., Lewis, C., Jancar, S. & Peters-Golden, M. Leukotriene B4 amplifies NF-κB activation in mouse macrophages by reducing SOCS1 inhibition of MyD88 expression. *J. Clin. Invest.* **121**, 671–682 (2011).

83. Mansell, A. *et al.* Suppressor of cytokine signaling 1 negatively regulates Toll-like receptor signaling by mediating Mal degradation. *Nat. Immunol.* **7**, 148–155 (2006).

84. Decker, T., Müller, M. & Stockinger, S. The Yin and Yang of type I interferon activity in bacterial infection. *Nature Reviews Immunology* vol. 5 675–687 (2005).

85. Carrero, J. A., Calderon, B. & Unanue, E. R. Type I interferon sensitizes lymphocytes to apoptosis and reduces resistance to Listeria infection. *J. Exp. Med.* **200**, 535–540 (2004).

86. McNab, F., Mayer-Barber, K., Sher, A., Wack, A. & O'Garra, A. Type I interferons in infectious disease. *Nature Reviews Immunology* vol. 15 87–103 (2015).

87. Mancuso, G. *et al.* Type I IFN Signaling Is Crucial for Host Resistance against Different Species of Pathogenic Bacteria. *J. Immunol.* **178**, 3126–3133 (2007).

88. Wu, J. *et al.* A MyD88-JAK1-STAT1 complex directly induces SOCS-1 expression in macrophages infected with Group A Streptococcus. *Cell. Mol. Immunol.* **12**, 373–383 (2015).

89. Manca, C. *et al.* Hypervirulent M. tuberculosis W/Beijing strains upregulate Type I IFNs and increase expression of negative regulators of the jak-stat pathway. *J. Interf. Cytokine Res.* **25**, 694–701 (2005).

90. Bullen, D. V. R., Baldwin, T. M., Curtis, J. M., Alexander, W. S. & Handman, E. Persistence of Lesions in Suppressor of Cytokine Signaling-1-Deficient Mice Infected with Leishmania major . *J. Immunol.* **170**, 4267–4272 (2003).

91. Shi, D. *et al.* Silencing SOCS1 in dendritic cells promote survival of mice with systemic Candida albicans infection via inducing Th1-cell differentiation. *Immunol. Lett.* **197**, 53–62 (2018).

92. Wang *et al.* SOCS1/JAK2/STAT3 axis regulates early brain injury induced by subarachnoid hemorrhage via inflammatory responses. *Neural Regen. Res.* **16**, 2453 (2021).

93. I, J. *et al.* Helicobacter pylori Subdues Cytokine Signaling to Alter Mucosal Inflammation via Hypermethylation of Suppressor of Cytokine Signaling 1 Gene During Gastric Carcinogenesis. *Front. Oncol.* **10**, (2021).

94. Chinen, T. *et al.* Prostaglandin E2 and SOCS1 have a role in intestinal immune tolerance. *Nat. Commun.* **2**, 1–11 (2011).

95. YR, N. *et al.* Prostaglandin E 2 receptor PTGER4-expressing macrophages promote intestinal epithelial barrier regeneration upon inflammation. *Gut* (2021) doi:10.1136/GUTJNL-2020-322146.

96. Tong, S. Y. C., Chen, L. F. & Fowler, V. G. Colonization, pathogenicity, host susceptibility, and therapeutics for Staphylococcus aureus: What is the clinical relevance? *Seminars in Immunopathology* vol. 34 185–200 (2012).

97. Lowy, F. D. Staphylococcus aureus Infections . *N. Engl. J. Med.* **339**, 520–532 (1998).

98. Hahn, B. L. & Sohnle, P. G. Direct translocation of staphylococci from the skin surface to deep organs. *Microb. Pathog.* **63**, 24–29 (2013).

99. Chastain, C. A., Klopfenstein, N., Serezani, C. H. & Aronoff, D. M. A Clinical Review of Diabetic Foot Infections. *Clinics in Podiatric Medicine and Surgery* vol. 36 381–395 (2019).

100. Suaya, J. A. *et al.* Incidence and cost of hospitalizations associated with Staphylococcus aureus skin and soft tissue infections in the United States from 2001 through 2009. *BMC Infect. Dis.* **14**, 296 (2014).

101. Edelsberg, J. *et al.* Trends in US hospital admissions for skin and soft tissue infections. *Emerg. Infect. Dis.* **15**, 1516–8 (2009).

102. Watkins, R. R., Holubar, M. & David, M. Z. Antimicrobial Resistance in Methicillin-Resistant Staphylococcus aureus to Newer Antimicrobial Agents. *Antimicrob. Agents Chemother.* **63**, (2019).

103. Singer, A. J. & Talan, D. A. Management of skin abscesses in the era of methicillin-resistant Staphylococcus aureus. *New England Journal of Medicine* vol. 370 1039–1047 (2014).

104. Khan, A., Wilson, B. & Gould, I. M. Current and future treatment options for community-associated MRSA infection. *Expert Opin. Pharmacother.* **19**, 457–470 (2018).

105. Muller, L. M. A. J. *et al.* Increased Risk of Common Infections in Patients with Type 1 and Type 2 Diabetes Mellitus. *Clin. Infect. Dis.* **41**, 281–288 (2005).

106. Dryden, M. *et al.* Pathophysiology and burden of infection in patients with diabetes mellitus and peripheral vascular disease: Focus on skin and soft-tissue infections. *Clin. Microbiol. Infect.* **21**, S27–S32 (2015).

107. Menne, E. N. *et al.* Staphylococcus aureus infections in pediatric patients with diabetes mellitus. *J. Infect.* **65**, 135–141 (2012).

108. Deleo, F. R., Otto, M., Kreiswirth, B. N. & Chambers, H. F. Community-associated methicillin-resistant Staphylococcus aureus. doi:10.1016/S0140-6736(09)61999-1.

109. Li, M. *et al.* Evolution of virulence in epidemic community-associated methicillin-resistant Staphylococcus aureus. *Proc. Natl. Acad. Sci. U. S. A.* **106**, 5883–5888 (2009).

110. Thurlow, L. R., Joshi, G. S. & Richardson, A. R. Virulence strategies of the dominant USA300 lineage of community-associated methicillin-resistant Staphylococcus aureus (CA-MRSA). *FEMS Immunology and Medical Microbiology* vol. 65 5–22 (2012).

111. Grunenwald, C. M., Bennett, M. R. & Skaar, E. P. Nonconventional Therapeutics against Staphylococcus aureus. *Microbiol. Spectr.* **6**, (2018).

112. Brandt, S. L. *et al.* Excessive localized leukotriene B4 levels dictate poor skin host defense in diabetic mice. *JCI insight* **3**, (2018).

113. Bitschar, K., Wolz, C., Krismer, B., Peschel, A. & Schittek, B. Keratinocytes as sensors and central players in the immune defense against Staphylococcus aureus in the skin. *J. Dermatol. Sci.* **87**, 215–220 (2017).

114. Brandt, S. L., Putnam, N. E., Cassat, J. E. & Serezani, C. H. Innate Immunity to Staphylococcus aureus : Evolving Paradigms in Soft Tissue and Invasive Infections . *J. Immunol.* **200**, 3871–3880 (2018).

115. Krishna, S. & Miller, L. S. Innate and adaptive immune responses against Staphylococcus aureus skin infections. *Seminars in Immunopathology* vol. 34 261–280 (2012).

116. Miller, L. S. & Cho, J. S. Immunity against Staphylococcus aureus cutaneous infections. doi:10.1038/nri3010.

117. Liu, Q., Mazhar, M., Miller, L. S. & Hopkins, J. Immune and Inflammatory Reponses to Staphylococcus aureus Skin Infections HHS Public Access. *Curr Dermatol Rep* **7**, 338–349 (2018).

118. Miller, L. S. *et al.* MyD88 mediates neutrophil recruitment initiated by IL-1R but not TLR2 activation in immunity against Staphylococcus aureus. *Immunity* **24**, 79–91 (2006).

119. Cho, J. S., Guo, Y., Ramos, R. I., Hebroni, F. & Plaisier, S. B. Neutrophil-derived IL-1b Is Sufficient for Abscess Formation in Immunity against Staphylococcus aureus in Mice. *PLoS Pathog* **8**, 1003047 (2012).

120. Feuerstein, R., Seidl, M., Prinz, M. & Henneke, P. MyD88 in Macrophages Is Critical for Abscess Resolution in Staphylococcal Skin Infection. *J. Immunol.* **194**, 2735–2745 (2015).

121. Greenlee-Wacker, M. C. *et al.* Phagocytosis of Staphylococcus aureus by Human Neutrophils Prevents Macrophage Efferocytosis and Induces Programmed Necrosis . *J. Immunol.* **192**, 4709–4717 (2014).

122. Kobayashi, S. D., Malachowa, N. & Deleo, F. R. Pathogenesis of Staphylococcus aureus abscesses. *American Journal of Pathology* vol. 185 1518–1527 (2015).

123. Cheng, A. G., DeDent, A. C., Schneewind, O. & Missiakas, D. A play in four acts: Staphylococcus aureus abscess formation. *Trends in Microbiology* vol. 19 225–232 (2011).

124. Cheng, A. G. *et al.* Genetic requirements for Staphylococcus aureus abscess formation and persistence in host tissues. *FASEB J.* **23**, 3393–3404 (2009).

125. Santus, W. *et al.* Skin infections are eliminated by cooperation of the fibrinolytic and innate immune systems. *Sci. Immunol.* **2**, (2017).

126. Gillitzer, R. & Goebeler, M. Chemokines in cutaneous wound healing. *J. Leukoc. Biol.* **69**, 513–21 (2001).

127. Khanna, S. *et al.* Macrophage dysfunction impairs resolution of inflammation in the wounds of diabetic mice. *PLoS One* **5**, e9539 (2010).

128. C, Y. & B, H. Cellular Responses to the Efferocytosis of Apoptotic Cells. *Front. Immunol.* **12**, (2021).

129. Association, A. D. Classification and diagnosis of diabetes: Standards of Medical Care in Diabetes-2020. *Diabetes Care* **43**, S14–S31 (2020).

130. Leto, D. & Saltiel, A. R. Regulation of glucose transport by insulin: Traffic control of GLUT4. *Nature Reviews Molecular Cell Biology* vol. 13 383–396 (2012).

131. Classification and diagnosis of diabetes: Standards of Medical Care in Diabetes-2020. *Diabetes Care* **43**, S14–S31 (2020).

132. Bluestone, J. A., Herold, K. & Eisenbarth, G. Genetics, pathogenesis and clinical interventions in type 1 diabetes. *Nature* vol. 464 1293–1300 (2010).

133. Zheng, Y., Ley, S. H. & Hu, F. B. Global aetiology and epidemiology of type 2 diabetes mellitus and its complications. *Nature Reviews Endocrinology* vol. 14 88–98 (2018).

134. Lipsky, B. A. *et al.* Skin and soft tissue infections in hospitalised patients with diabetes: Culture isolates and risk factors associated with mortality, length of stay and cost. *Diabetologia* **53**, 914–923 (2010).

135. Alba-Loureiro, T. C. *et al.* Neutrophil function and metabolism in individuals with diabetes mellitus. *Brazilian J. Med. Biol. Res.* **40**, 1037–1044 (2007).

136. Rendra, E. *et al.* Reactive oxygen species (ROS) in macrophage activation and function in diabetes. *Immunobiology* vol. 224 242–253 (2019).

137. Foss, N. T. *et al.* Impaired cytokine production by peripheral blood mononuclear cells in type 1 diabetic patients. *Diabetes Metab.* **33**, 439–443 (2007).

138. Hasenberg, A. *et al.* Catchup: A mouse model for imaging-based tracking and modulation

of neutrophil granulocytes. *Nat. Methods* **12**, 445–452 (2015).

139. Chong, M. M. W. *et al.* Suppressor of cytokine signaling-1 is a critical regulator of interleukin-7-dependent CD8+ T cell differentiation. *Immunity* **18**, 475–487 (2003).

140. Schreiber, H. A. *et al.* Intestinal monocytes and macrophages are required for T cell polarization in response to Citrobacter rodentium. *J. Exp. Med.* **210**, 2025–2039 (2013).

141. Filgueiras, L. R. *et al.* Leukotriene B4-mediated sterile inflammation promotes susceptibility to sepsis in a mouse model of Type 1 diabetes. *Sci. Signal.* **8**, (2015).

142. Deeds, M. C. *et al.* Single dose streptozotocin-induced diabetes: Considerations for study design in islet transplantation models. *Laboratory Animals* vol. 45 131–140 (2011).

143. Domingo-Gonzalez, R. *et al.* Prostaglandin E 2 –Induced Changes in Alveolar Macrophage Scavenger Receptor Profiles Differentially Alter Phagocytosis of Pseudomonas aeruginosa and Staphylococcus aureus Post–Bone Marrow Transplant . *J. Immunol.* **190**, 5809–5817 (2013).

144. Plaut, R. D., Mocca, C. P., Prabhakara, R., Merkel, T. J. & Stibitz, S. Stably Luminescent Staphylococcus aureus Clinical Strains for Use in Bioluminescent Imaging. *PLoS One* **8**, (2013).

145. Klopfenstein, N. *et al.* Murine Models for Staphylococcal Infection. *Curr. Protoc.* **1**, (2021).

146. Becker, R. E. N., Berube, B. J., Sampedro, G. R., Dedent, A. C. & Bubeck Wardenburg, J. Tissue-specific patterning of host innate immune responses by staphylococcus aureus α-Toxin. *J. Innate Immun.* **6**, 619–631 (2014).

147. Dejani, N. N. *et al.* Topical Prostaglandin e analog restores defective dendritic cell-mediated Th17 host defense against methicillin-resistant staphylococcus aureus in the skin of diabetic mice. *Diabetes* **65**, 3718–3729 (2016).

148. Piñeros Alvarez, A. R. *et al.* SOCS1 is a negative regulator of metabolic reprogramming during sepsis. *JCI insight* **2**, (2017).

149. Klopfenstein, N. *et al.* SOCS-1 inhibition of type I interferon restrains Staphylococcus aureus skin host defense. *PLOS Pathog.* **17**, e1009387 (2021).

150. Brandt, S. L. *et al.* Macrophage-derived LTB4promotes abscess formation and clearance of Staphylococcus aureus skin infection in mice. *PLoS Pathog.* **14**, (2018).

151. Serezani, C. H. C., Aronoff, D. M., Jancar, S., Mancuso, P. & Peters-Golden, M. Leukotrienes enhance the bactericidal activity of alveolar macrophages against Klebsiella pneumoniae through the activation of NADPH oxidase. *Blood* **106**, 1067–75 (2005).

152. Salina, A. C. G. *et al.* Leukotriene B4 licenses inflammasome activation to enhance skin host defense. *Proc. Natl. Acad. Sci. U. S. A.* **117**, 30619–30627 (2020).

153. Yu, H., Pardoll, D. & Jove, R. STATs in cancer inflammation and immunity: A leading role

for STAT3. *Nature Reviews Cancer* vol. 9 798–809 (2009).

154. A, G., M, H. & T, A. The Role of STAT Signaling Pathways in the Pathogenesis of Systemic Lupus Erythematosus. *Clin. Rev. Allergy Immunol.* **52**, 164–181 (2017).

155. Guo, Y. *et al.* In vivo bioluminescence imaging to evaluate systemic and topical antibiotics against community-acquired methicillin-resistant staphylococcus aureus-infected skin wounds in mice. *Antimicrob. Agents Chemother.* **57**, 855–863 (2013).

156. AJ, K., KL, E., VL, K. & AH, H. Mouse models of the metabolic syndrome. *Dis. Model. Mech.* **3**, 156–166 (2010).

157. Su, X., Cheng, Y. & Chang, D. The Important Role of Leptin in Modulating the Risk of Dermatological Diseases. *Frontiers in Immunology* vol. 11 (2021).

158. Clark, R. M., Coffman, B., McGuire, P. G. & Howdieshell, T. R. Myocutaneous revascularization following graded ischemia in lean and obese mice. *Diabetes, Metab. Syndr. Obes. Targets Ther.* **9**, 325–336 (2016).

159. S, P., J, R., F, H. & JC, L. Defects in innate immunity predispose C57BL/6J-Leprdb/Leprdb mice to infection by Staphylococcus aureus. *Infect. Immun.* **77**, 1008–1014 (2009).

160. E, P. *et al.* Leptin receptor expression and signaling in lymphocytes: kinetics during lymphocyte activation, role in lymphocyte survival, and response to high fat diet in mice. *J. Immunol.* **176**, 7745–7752 (2006).

161. Caldefie-Chezet, F., Poulin, A., Tridon, A., Sion, B. & Vasson, M.-P. Leptin: a potential regulator of polymorphonuclear neutrophil bactericidal action? *J. Leukoc. Biol.* **69**, 414–418 (2001).

162. A, L. C. & G, M. The weight of leptin in immunity. *Nat. Rev. Immunol.* **4**, 371–379 (2004).

163. Zhang, L. J. *et al.* Diet-induced obesity promotes infection by impairment ofthe innate antimicrobial defense function of dermal adipocyte progenitors. *Sci. Transl. Med.* **13**, 5280 (2021).

164. LJ, Z. *et al.* Innate immunity. Dermal adipocytes protect against invasive Staphylococcus aureus skin infection. *Science* **347**, 67–71 (2015).

165. H, T. & AR, M. Adipocytokines: mediators linking adipose tissue, inflammation and immunity. *Nat. Rev. Immunol.* **6**, 772–783 (2006).

166. Kopcewicz, M. *et al.* Cutaneous wound healing in aged, high fat diet-induced obese female or male C57BL/6 mice. *Aging (Albany. NY).* **12**, 7066–7111 (2020).

167. Paulino Do Nascimento, A. & Monte-Alto-Costa, A. Both obesity-prone and obesity-resistant rats present delayed cutaneous wound healing. *Br. J. Nutr.* **106**, 603–611 (2011).

168. S, L. The mechanisms of alloxan- and streptozotocin-induced diabetes. *Diabetologia* **51**, 216–226 (2008).

169. MS, A. & JA, B. The NOD mouse: a model of immune dysregulation. *Annu. Rev. Immunol.* **23**, 447–485 (2005).

170. Goyal, S. N. *et al.* Challenges and issues with streptozotocin-induced diabetes - A clinically relevant animal model to understand the diabetes pathogenesis and evaluate therapeutics. *Chem. Biol. Interact.* **244**, 49–63 (2016).

171. C, H. *et al.* Mice with type 1 diabetes exhibit increased susceptibility to influenza A virus. *Microb. Pathog.* **113**, 233–241 (2017).

172. Z, L. *et al.* Kinetics of immune cell responses in the multiple low-dose streptozotocin mouse model of type 1 diabetes. *FASEB bioAdvances* **1**, 538–549 (2019).

173. PM, S. *et al.* Lack of lymphocytes impairs macrophage polarization and angiogenesis in diabetic wound healing. *Life Sci.* **254**, (2020).

174. AP, S. *et al.* Deregulated immune cell recruitment orchestrated by FOXM1 impairs human diabetic wound healing. *Nat. Commun.* **11**, (2020).

175. Liu, Z., Benard, O., Syeda, M. M., Schuster, V. L. & Chi, Y. Inhibition of Prostaglandin Transporter (PGT) Promotes Perfusion and Vascularization and Accelerates Wound Healing in Non-Diabetic and Diabetic Rats. *PLoS One* **10**, e0133615 (2015).

176. MH, K. *et al.* Misoprostol Heals Small Bowel Ulcers in Aspirin Users With Small Bowel Bleeding. *Gastroenterology* **155**, 1090-1097.e1 (2018).

177. ML, S. & DA, W. Misoprostol for induction of labor. *Semin. Perinatol.* **39**, 459–462 (2015).

178. Sheppe, A. E. F. & Edelmann, M. J. Roles of eicosanoids in regulating inflammation and neutrophil migration as an innate host response to bacterial infections 2 3. 352–846 (2021) doi:10.1128/IAI.00095-21.

179. Gilman, K. E. & Limesand, K. H. The complex role of prostaglandin E 2-EP receptor signaling in wound healing. *Physiology* (2021) doi:10.1152/ajpregu.00185.2020.

180. Serezani, C. H., Ballinger, M. N., Aronoff, D. M. & Peters-Golden, M. Cyclic AMP. *http://dx.doi.org/10.1165/rcmb.2008-0091TR* **39**, 127–132 (2012).

181. JH, C. *et al.* Prostaglandin E2 and programmed cell death 1 signaling coordinately impair CTL function and survival during chronic viral infection. *Nat. Med.* **21**, 327–334 (2015).

182. Jara-Gutiérrez, Á. & Baladrón, V. The Role of Prostaglandins in Different Types of Cancer. *Cells* (2021) doi:10.3390/cells10061487.

183. X, W. *et al.* The Prostaglandin E2-EP3 Receptor Axis Regulates Anaplasma phagocytophilum-Mediated NLRC4 Inflammasome Activation. *PLoS Pathog.* **12**, (2016).

184. Z, Z. *et al.* The Induction of Pro-IL-1β by Lipopolysaccharide Requires Endogenous Prostaglandin E 2 Production. *J. Immunol.* **198**, 3558–3564 (2017).

185. Davis, F. M. *et al.* Epigenetic regulation of the PGE2 pathway modulates macrophage

phenotype in normal and pathologic wound repair. *JCI Insight* **5**, (2020).

186. S, E., EJ, L. & D, T. Immunology of Wound Healing. *Curr. Dermatol. Rep.* **7**, 350–358 (2018).

187. AL, L. & B, H. Having an Old Friend for Dinner: The Interplay between Apoptotic Cells and Efferocytes. *Cells* **10**, (2021).

188. Chandrakar, P., Parmar, N., Descoteaux, A. & Kar, S. Differential Induction of SOCS Isoforms by Leishmania donovani Impairs Macrophage–T Cell Cross-Talk and Host Defense . *J. Immunol.* **204**, 596–610 (2020).

189. Paco, S., Hummel, M., Plá, V., Sumoy, L. & Aguado, F. Cyclic AMP signaling restricts activation and promotes maturation and antioxidant defenses in astrocytes. *BMC Genomics 2016 171* **17**, 1–11 (2016).

190. Horn, J., Stelzner, K., Rudel, T. & Fraunholz, M. Inside job: Staphylococcus aureus host-pathogen interactions. *International Journal of Medical Microbiology* vol. 308 607–624 (2018).

191. Santus, W. *et al.* Skin infections are eliminated by cooperation of the fibrinolytic and innate immune systems. *Sci. Immunol.* **2**, (2017).

192. Granick, J. L. *et al.* Staphylococcus aureus recognition by hematopoietic stem and progenitor cells via TLR2/MyD88/PGE2 stimulates granulopoiesis in wounds. *Blood* **122**, 1770–1778 (2013).

193. Müller, E. *et al.* Both type I and type II interferons can activate antitumor M1 macrophages when combined with TLR stimulation. *Front. Immunol.* **9**, (2018).

194. Gao, J. J. *et al. Autocrine/Paracrine IFN-Mediates the Lipopolysaccharide-Induced Activation of Transcription Factor Stat1 in Mouse Macrophages: Pivotal Role of Stat1 in Induction of the Inducible Nitric Oxide Synthase Gene 1*. *The Journal of Immunology* vol. 161 http://www.jimmunol.org/ (1998).

195. Kaplan, A. *et al.* Failure To Induce IFN-β Production during Staphylococcus aureus Infection Contributes to Pathogenicity . *J. Immunol.* **189**, 4537–4545 (2012).

196. Zhang, X., Alley, E. W., Russell, S. W. & Morrison, D. C. Necessity and sufficiency of beta interferon for nitric oxide production in mouse peritoneal macrophages. *Infect. Immun.* **62**, 33–40 (1994).

197. SJ, K. *et al.* Type I IFNs downregulate myeloid cell IFN-γ receptor by inducing recruitment of an early growth response 3/NGFI-A binding protein 1 complex that silences ifngr1 transcription. *J. Immunol.* **191**, 3384–3392 (2013).